Targeting canonical BMP signaling: SMAD4 in limb patterning and differentiation

Inauguraldissertation

zur

Erlangung der Würde eines Doktors der Philosophie

vorgelegt der

Philosophisch-Naturwissenschaftlichen Fakultät

der Universität Basel

von

Emanuele Pignatti

Aus Brescia, Italien

Basel, 2014

Genehmigt von der Philosophisch-Naturwissenschaftlichen Fakultät
auf Antrag von
Prof. Dr. Rolf Zeller (Dissertationsleiter), Prof. Dr. Markus Affolter
(Fakultätsverantwortlicher) und Prof. Dr. Verdon Taylor (Korreferent).

Basel, den 18. Februar 2014

Prof. Dr. Jörg Schibler
Dekan

1. TABLE OF CONTENTS

2. LIST OF ABBREVIATIONS

A-P	Antero-Posterior
ACTR	Activin Receptor
AER	Apical Ectodermal Ridge
ALK	Activin Receptor-like Kinase
BABB	Benzyl Alcohol, Benzyl Benzoate
BAC	Bacterial Artificial Chromosome
BMP	Bone Morphogenetic Protein
BMPR	Bone Morphogenetic Protein Receptor
BRE	BMP-responsive element
BSA	Bovine Serum Albumin
cDNA	complementary DNA
CDS	Coding Sequence
co-SMAD	common-SMAD
COL	Collagen
Cq	Quantification cycle
Cstd	Cathepsin D
D-V	Dorso-Ventral
DIC	Differential Interference Contrast
dRMCE	dual RMCE
E	days-post-coitum
e-m	epithelial-mesenchymal
EB	Embryoid Body
EMFI	Embryonic Murine Fibroblasts
ES cell	Embryonic Stem cell
FGF	Fibroblast Growth Factor
Fjx	Four-jointed
GCR	Global Control Region
GDF5	Growth and Differentiation Factor 5
GFP	Green Fluorescent Protein
HBSS	Hank's Balanced Salt Solution
hCG	human Chorionic Gonadotropin
HH	Hamilton-Hamburger
HLH	Helix-loop-Helix
i-SMAD	Inhibitory-SMAD

Id	Inhibitor of differentiation
J.D.B.	Jean Denis Bénazet
LIF	Leukemia Inhibitory Factor
MAPK	Mitogen-activated Protein Kinase
MCS	Multiple Cloning Site
MH	MAD homology domain
MKK	Mitogen-activated Protein Kinase Kinase
Ncam	Neural Cell Adhesion Molecule
NEB	New-England Biolabs
NeoR	Neomycin Resistance
NLS	Nuclear Localization Signal
ON	Overnight
OPT	Optical Projection Tomography
P-D	Proximo-Distal
PBS	Phosphate Buffer Saline
PBT	PBS with 0.1% Tween 20
PFA	Paraformaldehyde
PFR	PBS with 4% PFA
PK	Proteinase K
polyA	Poly-Adenine Tail
pSMAD	phosphorylated SMAD
R-SMAD	Receptor SMAD
RA	Retinoic Acid
RMCE	Recombinase-mediated Cassette Exchange
RPL19	Ribosomal Protein L19
RT	Room-Temperature
RT-qPCR	Real-time quantitative PCR
SBE	SMAD Binding Element
SCX	Scleraxis
SD	Standard Deviation
SHH	Sonic Hedgehog
SMAD	Small Mothers Against Decapentaplegic
TAK1	TGFβ-activated Kinase 1
TGFβ	Transforming Growth Factor β
TSS	Transcriptional Start Site
TβR	TGFβ Receptor

WISH	Whole-Mount *In Situ*
Wt	Wild-Type
ZPA	Zone of Polarizing Activity

3. ABSTRACT

The developing limb is an ideal genetic model to investigate basic developmental mechanisms and signaling networks. The Bone Morphogenetic Protein (BMP) signaling pathway has been associated with a number of context-specific functions during limb development, including establishment of the limb signalling domains, regulation of cell proliferation and cell death, digit patterning, differentiation of the endochondral skeleton and the soft tissue.

The present work aimed at providing insights into the roles of canonical BMP signaling in mouse limb bud patterning and tissue differentiation. The canonical BMP pathway includes numerous components, which are often functionally redundant. Conversely, the non-redundant intracellular transducer SMAD4 is essential for gastrulation, such that its inactivation results in an early lethal phenotype and prevents the analysis of its functions during limb development. For the purpose of our investigation, we used the conditional inactivation of the *Smad4* gene to generate time- and space-restricted loss-of-function models during limb development.

This approach allowed us to show that mesenchymal SMAD4 is dispensable for establishment of the Apical Ectodermal Ridge (AER), which is an ectodermal source of the Fibroblast Growth Factor (FGF) signalling factors that contribute to proximo-distal (P-D) limb axis extension. However, mesenchymal SMAD4 contributes to the establishment of the SHH/GREM1/AER-FGFs feedback loop that controls limb outgrowth and patterning.

Most importantly, we observed a discrete temporal requirement of SMAD4 for the specification of digit primordia during a developmental period, when high BMP activity is essential to initiate chondrogenesis. Specific inactivation of SMAD4 in the limb mesenchyme at this stage is sufficient to inhibit the initiation of mesenchymal condensations, which represent the first structures committed to endochondral bone formation. In fact, the *Smad4* deficiency results in the absence of any limb skeletal elements. Molecular evidence indicates that the discrete pattern of genes that normally specify the chondrogenic fate is replaced by wide-spread up-regulation of genes relevant to tendon and joint development in *Smad4* deficient limb bud, but no ectopic tendons or joints are formed. These observations suggest a role for SMAD4 in cell fate restriction and differentiation of lateral plate mesoderm-derived tissues in the limb.

To further analyze the rapid changes in BMP activity during limb development, we sought to generate a mouse model which senses BMP activity in a specific and dynamic fashion. For the purpose of this project, I have established the aggregation chimera

technique to allow for the rapid investigation of *cis*-regulatory elements in the context of the *Gt(ROSA)26Sor* locus.

4. INTRODUCTION

Parts of this introduction were used to write a review:

Emanuele Pignatti, Rolf Zeller, Aimée Zuniga. **To BMP or not to BMP during vertebrate limb bud development.** Seminars in Cell & Developmental Biology, 2014. *Submitted.*

Limb development

The tetrapod limb emerges from the lateral plate mesoderm as a pocket of mesenchymal cells wrapped in a ectoderm monolayer. Three limb axes are specified during the earliest phases of limb outgrowth. The proximo-distal (P-D) axis defines the axis running from the flank of the embryo to the tip of the limb bud; the antero-posterior (A-P) axis goes from the 1st digit (the thumb in humans) to the 5th digit (the pinkie); the dorso-ventral (D-V) axis defines the prospective back and the palm of the hand (Fig. 1a). Limb patterning and outgrowth are regulated by two signaling centers: the Apical Ectodermal Ridge (AER), an ectodermal structure of the limb bud running along the D-V interface (Fernandez-Teran and Ros, 2008; Saunders, 1948); and the Zone of Polarizing Activity (ZPA), composed of a group of mesenchymal cells located in the posterior limb bud mesenchyme (Saunders, 1968; Zwilling, 1956). The instructive role of the AER along the P-D axis is mediated by FGFs (Niswander et al., 1993), and the A-P patterning activity of the ZPA is mediated by the expression of the Sonic Hedgehog (SHH) morphogen (Fig. 3B; Riddle et al., 1993).

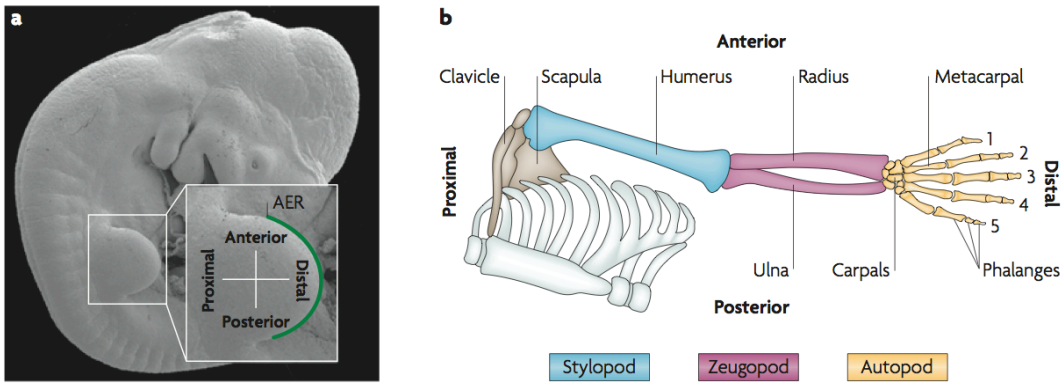

Fig. 1 Limb bud axes. a) Micrograph of a mouse embryo at gestational day 10.5. The enlarged inset shows the forelimb bud which arises from the flank of the embryo at the level of the heart.

Two axes (proximal-to-distal and anterior-to-posterior) are indicated. The green line denotes the apical ectodermal ridge (AER). b) Schematic of the skeleton of a human arm. In blue, the proximal structures of the limb, the stylopod, is here indicated as the humerus. The middle elements are indicated in purple. The zeugopod, i.e. the radius (anterior), and the ulna (posterior) are showed. The distal elements depicted in yellow are the carpals, metacarpals and phalanges, which are the skeletal elements of the autopod domain. Clavicle and scapula do not originate from the limb bud. (adapted from Zeller et al., 2009).

Limb bud outcrop from the embryo flank and specification of the axes

Limb budding from the flank mesenchyme occurs at precise levels and is controlled by the Hox gene expression code along the primary body axis (Burke et al., 1995; Molven et al., 1990). In the mouse, forelimbs are formed at around 8.75 days post coitum (E8.75), whereas hindlimb development is delayed by about 16 hours (see e.g. Saito et al., 2002). The early limb bud is characterized by a positive epithelial/mesenchymal (e-m) feedback loop that is fundamental to initiate limb outgrowth and for the establishment of the AER. *Fgf10*, which is strongly expressed in the limb mesenchyme, triggers the expression of *Wnt3* in the ectoderm, which in turn up-regulates *Fgf8* in the ventral ectoderm in a domain destined to form the AER (Kawakami et al., 2001). Inactivation of *Fgf10* results in limb agenesis (Min et al., 1998). Conversely, ectopic expression of FGF ligands in the embryonic flank mesenchyme results in localized budding and formation of limb structures (Cohn et al., 1995; Crossley et al., 1996; Ohuchi et al., 1997; Ohuchi et al., 1995). Conditional inactivation of *Wnt3* before the AER is established results in a variety of phenotypes, ranging from completely normal limb skeletal structures to limb agenesis. In agreement, the expression and maintenance of *Fgf8* are affected to a variable extent (Barrow et al., 2003). In contrast, inactivation of *Fgf8* in the ectoderm results in the loss of proximal limb skeletal elements (Lewandoski et al., 2000). This relatively mild phenotype, which is an effect of a patterning defect, is likely due to the compensation of the *Fgf8* deficiency by other FGF ligands (FGF4, FGF9, FGF17), which are expressed at later stages by the AER (Moon and Capecchi, 2000).

Specification of the D-V axis and formation of the AER

The D-V axis is specified during initiation of limb outgrowth by factors expressed by the ectoderm. *En1*, expressed by the ventral ectoderm, restricts *Wnt7a* expression to the dorsal ectoderm. *Wnt7a* in turn up-regulates and co-localizes with the LIM-homeodomain transcription factor *Lmx1b* (see e.g. Loomis et al., 1998). Inactivation of WNT7a or LMX1b

produces bi-ventral limbs. Conversely, inactivation of EN1 results in bi-dorsal limbs (Cygan et al., 1997; Dreyer et al., 1998; Parr and McMahon, 1995).

During embryonic day 9 (E9) in mouse embryos, the ectodermal cells at the distal-dorso-ventral interface form a partially stratified epithelium in mouse limb buds and a pseudostratified epithelium in the chick, the AER (reviewed by Fernandez-Teran and Ros, 2008). Ectopic AERs can be induced by juxtaposition of embryonic tissues with dorsal and ventral identities, stressing the importance of early D-V axis specification for AER positioning and formation (Tanaka et al., 1997). Expression of *Fgf8* hallmarks AER induction, such that *Fgf8* expression reveals AER morphology and intensity of FGF signalling (see e.g., Benazet and Zeller, 2013; Lewandoski et al., 2000).

Specification of the P-D axis

The P-D axis is specified during the earliest phases of limb outgrowth and its polarization is traceable with specific molecular markers. *Meis1* and *Meis2* mark the proximal limb bud mesenchyme correspondent to the prospective stylopod (the region defined by the humerus in the forelimb), *Hoxa11* is expressed by the prospective zeugopod (radius and ulna) and *Hoxa13* marks the distal limb domain corresponding to the autopod which gives rise to carpals, metacarpals and phalanges (Fig. 1b, for review see Zeller et al., 2009).

A gradient of retinoic acid (RA) seems to originate from the lateral plate mesoderm and RA production is controlled by the enzyme Retinaldehyde Dehydrogenase 2 (RALDH2). This RA gradient seems responsible for specification of proximal limb identity, but the involvement of RA is still debated due to conflicting evidence (Zhao et al., 2009). Mercader and colleagues performed gain-of-function studies to demonstrate that RA induces *Meis1* and *Meis2* in the proximal limb while FGF8 from the AER inhibits expression of these markers in the distal mesenchyme (Mercader et al., 2000). In addition, ectopic expression of retinoic acid and MEIS1 in the distal limb induces distal-to-proximal transformations (Mercader et al., 2000; Rosello-Diez and Torres, 2011). More recent evidence from loss-of-function studies show that expression of *Meis1* and *Meis2* is independent of RALDH2 (Cunningham et al., 2013). In addition, limb inactivation of *Meis1* alone results in no P-D axis defects (Hisa et al., 2004). *Aldh1a2*, which encodes RALDH2, is necessary to initiate limb bud outgrowth but dispensable for P-D axis patterning (Cunningham et al., 2013; Niederreither et al., 1999; Niederreither et al., 2002; Zhao et al., 2009). On the other hand, it is clear that FGF-mediated inhibition of proximal limb markers is exerted by the FGF-dependent RA degrading enzyme CYP26b1 and that

Cyp26b1 inactivation impairs distal progression of limb development (Probst et al., 2011; Yashiro et al., 2004; Zhou and Kochhar, 2004).

Experimental manipulation of the AER in chicken limb buds together with conditional genetic inactivation of single or more FGF ligands in the AER of mouse hindlimbs revealed the instructive role of these ectodermal signalling centers. In 1948, Saunders experimentally removed the AER from chicken wing buds at several progressively later stages of development, which resulted in loss of progressively more distal wing skeletal structures (Rowe and Fallon, 1982; Saunders, 1948). These results were interpreted as the AER influencing the underlying mesenchyme in a time-dependent manner, giving rise to the 'progress zone'. Indeed, older progress zones, but not older AERs, were able to induce more distal structures when grafted to younger wing buds (Summerbell and Lewis, 1975). FGF ligands were found to mediate the instructive role of the AER on the underlying mesenchyme. In particular AER-FGFs can rescue the massive cell death and growth arrest following experimental removal of the AER (Fallon et al., 1994; Niswander et al., 1993). In particular, FGF8 expression is sufficient to sustain the formation of wild-type limb structures in the absence of other AER-FGFs (Mariani et al., 2008). FGF8 is necessary only during AER compaction and temporally correct activation of *Shh* in the mesenchyme (Lewandoski et al., 2000). FGFs inactivation at these early stages delays activation of *Shh* and results in loss of the femur together with mild digit phenotypes. FGF8 also restrains FGF4 expression in time and space together with BMP signaling (Lewandoski et al., 2000; Selever et al., 2004). Among the AER-FGFs, FGF8 and FGF4 are essential for limb bud formation as their combined inactivation in the AER causes limb agenesis as a consequence of massive cell death (Moon and Capecchi, 2000).

The analysis of AER-FGFs during mouse limb bud development indicates that the cell survival activity is sufficient to promote maintenance and expansion of mesenchymal progenitors that give rise to the P-D axis (Mariani et al., 2008). In fact, lineage tracing of wing bud cells and transplantation experiments revealed that the progenitors that contribute to different wing compartments are specified early during limb bud development, and that the mesenchymal cells under the influence of FGF signals by the AER are regionalized in a manner that mirrors the prospective contribution to P-D limb structures (Dudley et al., 2002; Pearse et al., 2007; Sato et al., 2007; Suzuki et al., 2008; Tabin and Wolpert, 2007). Moreover, it was reported that Gli3 and Plzf transcription factors interact to specify proximal limb structures during initiation of limb bud development (Barna et al., 2005), pointing to the existence of a transcriptional mechanism that specifies discrete P-D domains during limb bud initiation. However, an

instructive role of AER-FGFs on P-D axis development is still debated (Fernandez-Teran and Ros, 2008).

Specification of the A-P axis

The A-P axis is specified by the mutual antagonistic interaction of *Gli3* and *Hand2* gene products in the early limb bud mesenchyme (Galli et al., 2010; Ros et al., 1996; Tarchini et al., 2006; te Welscher et al., 2002; Zuniga and Zeller, 1999). *Hand2* is initially expressed throughout the early limb bud mesenchyme but is then restricted to the posterior mesenchyme by *Gli3* transcriptional repressor (*Gli3R*), which is constitutively produced prior to activation of SHH signaling (Charite et al., 2000; te Welscher et al., 2002). HAND2 and GLI3R, together with several HOX transcriptional regulators impact on the limb bud *cis*-regulatory module that restricts activation of *Shh* expression to the posterior-proximal mesenchyme (Lettice et al., 2003; Sagai et al., 2005).

Limb bud patterning

At about E9.5, the BMP antagonist *Grem1* is activated by BMP signaling in the posterior limb mesenchyme to create permissive conditions (low BMP activity, see Fig. 3B) for the activation of FGF4, FGF9 and FGF17 in the AER, which in turn promote the expression of *Shh* in the underlying limb bud mesenchyme (Fig. 2; Bastida et al., 2009; Khokha et al., 2003; Lewandoski et al., 2000; Mariani et al., 2008; Michos et al., 2004; Nissim et al., 2006; Sun et al., 2002; Zuniga and Zeller, 1999). *Grem1* encodes an extracellular BMP antagonist and its inactivation results in fusion of the zeugopod elements and reduction in digit numbers, as a consequence of impaired AER compaction, down-regulation of *Fgf8* and *Shh* expression and massive mesenchymal cell death (Michos et al., 2004). Similarly, inactivation of *Shh* results in skeletal reductions that result in the loss of posterior zeugopodal elements and digits (Chiang et al., 2001). *Shh* activation by the ZPA requires several signals in addition to *Hand2* (see above), such as *Hox* genes (Kmita et al., 2005; Knezevic et al., 1997; Tarchini et al., 2006), *Bmp4* (Benazet et al., 2009; Michos et al., 2004; Nissim et al., 2006), *Fgf8* (Lewandoski et al., 2000), *Tbx2* (Nissim et al., 2007). SHH behaves as a morphogen, creating a concentration gradient along the A-P axis (Li et al., 2006; Zeng et al., 2001). Post-translational modifications result in addition of cholesterol and palmitoyl acid moieties to SHH, which modulate its long-range signaling properties, thus ensuring the proper instruction of A-P axis and digit patterning (Chen et al., 2004; Li et al., 2006).

The positive SHH/GREM1/AER-FGF feedback loop established by *Grem1* up-regulation coordinates limb bud outgrowth and patterning. During limb bud outgrowth the initially posterior AER-*Fgfs* and *Grem1* expression domains expand progressively anterior (Michos et al., 2004; Panman et al., 2006). The SHH/GREM1/AER-FGF feedback loop is terminated by high levels of FGF signaling, which inhibits *Grem1* expression, and by the increasing displacement of the *Grem1* expression domain with respect to the posterior mesenchyme as a consequence of Shh descendants being refractory to *Grem1* expression (Fig. 3C; Scherz et al., 2007; Verheyden and Sun, 2008). Furthermore, *Tbx2* is also involved in active termination of *Grem1* expression in the distal limb bud mesenchyme (Farin et al., 2013).

Ectopic expression of SHH in the anterior chick wing bud mesenchyme induces mirror-image duplication of digits (Riddle et al., 1993). In the wild-type autopod primordia, the two posterior-most digits and part of the third digit are derived from progenitors that belonged to the ZPA (Shh-descendants), while anterior digit 2 is likely specified by long-range SHH signaling (Harfe et al., 2004; Sagai et al., 2005). In contrast, the anterior-most digit 1 (thumb) is specified independent of SHH (for review, see Oberg, 2013). The instructive role of SHH provides a temporal distinct order for digit specification and determination, whereby the 4th digit is specified and forms first, while the thumb is the last one to appear (Zhu et al., 2008). The patterning activity of SHH signalling is genetically linked to *Hox* genes (Galli et al., 2010; Tarchini et al., 2006). During limb development, *Hox* genes are activated in a collinear fashion, such that *5'Hox* genes are activated later than *3'Hox* genes and in a more restricted fashion, overlapping with the ZPA in the posterior part of the limb bud. As discussed above, *5'HoxD* genes participate in activating *Shh* and restricting its expression. In turn, *Shh* promotes the anterior reverse-collinear expansion of the *Hoxd10-13* expression domains through a global control region with enhancer activity (Andrey et al., 2013; Spitz et al., 2003; Spitz et al., 2005). While almost all *HoxA* and *HoxD* paralogous group genes are expressed in developing limb buds, only the posterior ones (located at the 5' end of the *Hox* cluster – named *5'Hox* genes -) are required for specification of specific limb skeletal structures. For instance, compound inactivation of *Hoxa13* and *Hoxd13* results in loss of the autopod (Wellik and Capecchi, 2003). In contrast, deletion of either the *HoxA* or *HoxD* gene clusters alone results in only mild autopod malformations, whereas deletion of both clusters causes forelimb agenesis with exception of the scapula and the proximal-most part of the humerus (Kmita et al., 2005). Since *Hox* genes function in the context of the cluster the instructive roles of single *Hox* genes with respect to the formation of specific skeletal elements is debated (Kmita et al., 2002). However, misexpression studies and genetic manipulation revealed that

distalized *Hoxd11* expression induces polydactyly and increases digit length in the absence of more posterior genes (Goff and Tabin, 1997; Kmita et al., 2002; Sheth et al., 2012).

The BMP signaling pathway (see Fig. 2)

BMP ligands were first identified by their ability to induce ectopic bone upon subcutaneous administration *in vivo* (Urist, 1965). Since, a wealth of studies have established that BMP ligands belong to the TGFβ superfamily and fulfill a multitude of functions during embryonic and postnatal development, homeostasis and disease (see e.g. Miyazono et al., 2010). In mammals, twelve BMP ligands have been identified, which can form homo- and heterodimers with different affinities for their cognate receptors (reviewed in Butler and Dodd, 2003). Upon secretion and activation by cleavage, the extra-cellular BMP ligands can be sequestered by BMP antagonists to prevent binding the receptors and activation of signal transduction. In higher vertebrates, twelve BMP antagonists have been identified, small cysteine-knot proteins with striking structural similarities to BMP ligands (reviewed by Walsh et al., 2010). BMP antagonists modulate BMP activity in a spatio-temporally controlled manner and genetic inactivation or alteration of their expression results in congenital malformations and various diseases such as nephropathies, fibrosis, osteoarthritis and cancer (Walsh et al., 2010).

BMPs activate signal transduction by interacting with their cognate serine/threonine kinase receptors. BMP ligand dimers interact with two distinct types of trans-membrane receptors, which form hetero-tetrameric complexes that activate intracellular signal transduction (Marom et al., 2011). Type I BMP receptors include three of the seven known activin-like receptors (ALK) that belong to the TGFβ superfamily: BMPRIA (or ALK3); BMPRIB (or ALK6) and ALK-2. Type II BMP receptors include BMPRII, activin receptor II (ActRII) and ActRIIB (Murakami et al., 2009). Upon ligand binding and receptor complex formation, type II BMP receptors phosphorylate type I BMP receptors, which activate their cytoplasmic kinase activity and trigger signal transduction by phosphorylation of the receptor associated SMAD proteins (R-SMADs). BMP signal transduction is mediated by association of phosphorylated R-SMADs (SMAD1, SMAD5 and SMAD8) with the common SMAD (co-SMAD: SMAD4); the resulting complex translocates to the nucleus and activates the transcription of BMP target genes (reviewed in Massague et al., 2005). SMAD6 and SMAD7 are inhibitory SMAD (i-SMAD), which interfere with BMP signaling at different levels of the pathway (Afrakhte et al., 1998).

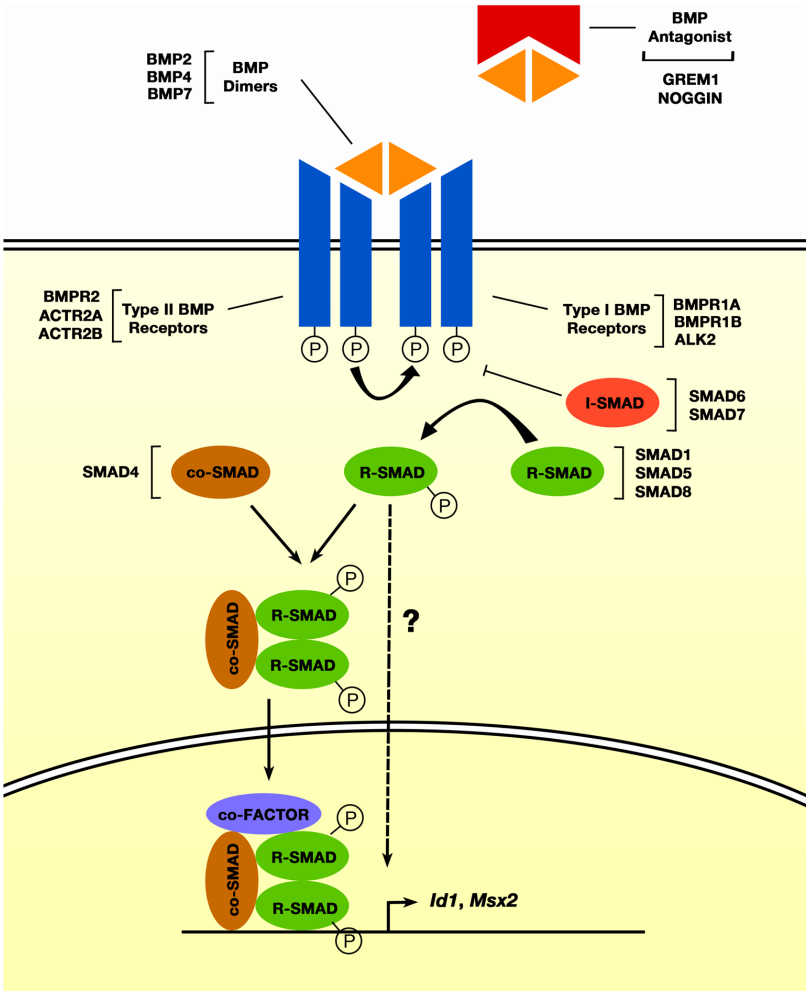

Fig. 2 The canonical BMP signalling pathway. The schematic illustrates the canonical BMP signalling pathway as relevant for limb bud development, from establishment of the AER to long bone formation. BMP homo or heterodimers act as morphogenetic ligands. Extracellular antagonists modulate BMP activity by sequestering BMP ligands and blocking their binding to the receptors. The most relevant BMP antagonists to limb bud development field are GREM1 and NOGGIN, with essential functions in limb bud outgrowth and patterning. BMP receptors are single-transmembrane glycoproteins endowed with a prevalent serine-threonine kinase activity. Type II BMP receptors (BMPR2, ACTR2A, ACTR2B) bind the ligands, recruit and trans-phosphorylate type I BMP receptors (BMPR1A, BMPR1B, ALK2) which in turn activate receptor SMADs (R-SMADs) in the cytoplasm. R-SMADs (SMAD1, -5 and -8) promote BMP signalling. Inhibitory SMADs (i-SMADs) SMAD6 and -7 inhibit BMP signalling at different levels of signal transduction. Canonical BMP signalling transduction involves heteromerization of R-SMADs with the common, non-redundant SMAD transducer SMAD4 (co-SMAD). The resulting heterotrimeric complexes translocate to the nucleus. Together with additional co-factors, these transcriptional complexes activate expression of target genes (*Id1* and *Msx2* are among the direct targets of the BMP signalling pathway). Genetic experiments provided evidence for SMAD4-independent R-SMAD signal transduction during endochondral bone formation (broken arrow in the graphic).

The intracellular BMP signalling transducer SMAD4

SMAD4 is the non-redundant mediator of the transcriptional response to both the BMP and TGFβ signaling pathways (Massague et al., 2005). Genetic inactivation of SMAD4 results in embryonic lethality during gastrulation due to reduced epiblast proliferation and impaired mesoderm formation (Yang et al., 1998a). SMAD4 is highly homologous to the mammalian R-SMAD proteins and the protein MEDEA in *D. melanogaster* (Wisotzkey et al., 1998). *Smad4* encodes two alternatively spliced protein-coding transcripts, with 11 or 12 exons. Murine SMAD4 is a protein with 551 amino acids, characterized by a N-terminal MAD homology domain 1 (MH1) and a C-terminal MH2 domain; both domains are evolutionary highly conserved and separated by a central linker sequence. The MH1 domain is globular, binds to DNA and several SMAD binding elements (SBE) have been identified (see e.g. Morikawa et al., 2011). In addition, MH1 interacts with other DNA-binding proteins, is responsible for nuclear translocation and inhibits MH2 function by physical interaction in the absence of protein phosphorylation (Jones and Kern, 2000; Shi et al., 1998). The MH2 domain is phosphorylated by receptors, mediates oligomerization with R-SMAD proteins and with other DNA-binding proteins, and is required for transcriptional activation (Massague et al., 2005). SMAD4 activity is regulated through phosphorylation and mono-ubiquitination of the linker domain (Dupont et al., 2009). Poly-ubiquitination triggers proteosomal degradation of SMAD proteins (Zhang et al., 2001).

BMP target genes

Few direct transcriptional targets of BMP signal transduction during embryonic development are known. The currently best-characterized and widely expressed BMP signalling targets are the i-SMADs, together with the *Id* and *Msx* transcriptional regulators (de Jong et al., 2004; Hollnagel et al., 1999; Pizette and Niswander, 1999). *Id* genes (*Id1-4*) are dominant negative helix-loop-helix (HLH) proteins that lack a basic DNA-binding domain, and are able to oligomerize with and sequester tissue-specific basic HLH transcription factors (e.g. MyoD, see Lingbeck et al., 2008). Single knock-out models of *Id1*, *Id2* and *Id3* are viable and exhibit minor defects. However, compound inactivation of *Id1* and *Id3* results in premature differentiation of neuroblasts and ineffective compaction of endothelial cells and sprouting of vessels (Lyden et al., 1999). BMP2 was shown to trigger the expression of *Id1* and *Id3* in neuroepithelial cells (Nakashima et al., 2001), and BMP antagonists promote formation of neural tissue in *X. laevis* (Lamb et al., 1993). These findings are consistent with a role of BMP2 as gatekeeper in neurogenesis,

with *Id1* and *Id3* as transcriptional targets and downstream effectors of BMP signal transduction (Nakashima et al., 2001). Furthermore, defects in endothelium exhibited by *Id1*;*Id3* double knock-out mouse embryos resemble the phenotype associated with the inactivation of either *Smad1* or *Smad5* (Chang et al., 1999; Lechleider et al., 2001; Lyden et al., 1999; Yang et al., 1999), suggesting that *Id* genes respond to canonical BMP signal transduction.

In addition, SMAD1/5 BMP-responsive *cis*-regulatory element (BRE; Korchynskyi and ten Dijke, 2002) was identified in the *Id1* proximal promoter. This element or the expression of *Id1* has been used as transcriptional sensor of BMP signal transduction *in vivo* (Blank et al., 2008; Monteiro et al., 2008). *Msx* genes encode basic HLH transcriptional regulators and *Msx2* is regulated specifically by BMP signal transduction. A BMP *cis*-regulatory element is located in the *Msx2* proximal promoter (Brugger et al., 2004) and its expression has been used to sense BMP activity during limb bud development (see e.g. Benazet et al., 2009). In contrast, *Msx1* expression is also regulated by pathways other than BMPs during embryonic development (Medio et al., 2012; Menezes et al., 2012; Pizette and Niswander, 1999).

The BMP signalling pathway during limb bud development

Three BMP ligands, BMP2, BMP4 and BMP7 are expressed in spatio-temporally restricted patterns in the mesenchyme and ectoderm from limb bud initiation onwards and fulfill multiple roles during limb bud initiation, outgrowth and pattern and formation of the cartilage primordia of the limb skeletal elements. While *Bmp2* expression is posteriorly restricted, *Bmp4* and *Bmp7* are expressed more widespread and restricted to the distal mesenchyme during progression of limb bud development (Fig. 3; see e.g. Michos et al., 2004). The activity of BMP ligands is modulated by the extra-cellular BMP antagonists, among them GREM1, NOGGIN, Follistatin-like 1 (Fstl1), whose genetic inactivation results in limb phenotypes. In particular, *Grem1* is expressed in the posterior mesenchyme that responds to SHH signaling, but its initially posterior-restricted expression expands distal-anterior during progression of limb bud outgrowth and becomes restricted to the interdigital domains during formation of the digit primordia (Zuniga et al., 2012). The expression of *Noggin* is only activated during formation of the digit primordia, concurrent with down-regulation of *Grem1* (Brunet et al., 1998; Danesh et al., 2009; Zuniga et al., 2012). *Bmpr1a* and *Bmpr2* are expressed at high levels by the limb bud mesenchyme (Danesh et al., 2009). As *Bmpr1a* is required to transduce mesenchymal BMP activity in the AER (see below), it must be expressed in the ectoderm; but its

ectodermal expression has not been described. *Bmpr1b* is expressed uniformly in both limb bud compartments. *Smad4* is co-expressed with *Smad1*, *Smad5* and *Smad8* in both mesenchyme and ectoderm from early limb bud stages onward (Wong et al., 2012). In chicken limb buds, Smad6 and Smad7 are co-expressed in two proximal domains during early stages, while expression shifts to the sub-AER mesenchyme at later stages (Vargesson and Laufer, 2009). Finally, the direct transcriptional targets of BMP signaling *Id1, Id3, Msx1* and *Msx2* are expressed in spatio-temporally dynamic patterns, which reflect the changes in BMP activity during limb bud development (Hollnagel et al., 1999; Pizette and Niswander, 2001). The main limb phenotypes resulting from loss-of-function studies in mouse embryos are summarized in Table 1 and the functional relevance of the dynamics of BMP signaling interactions is discussed below.

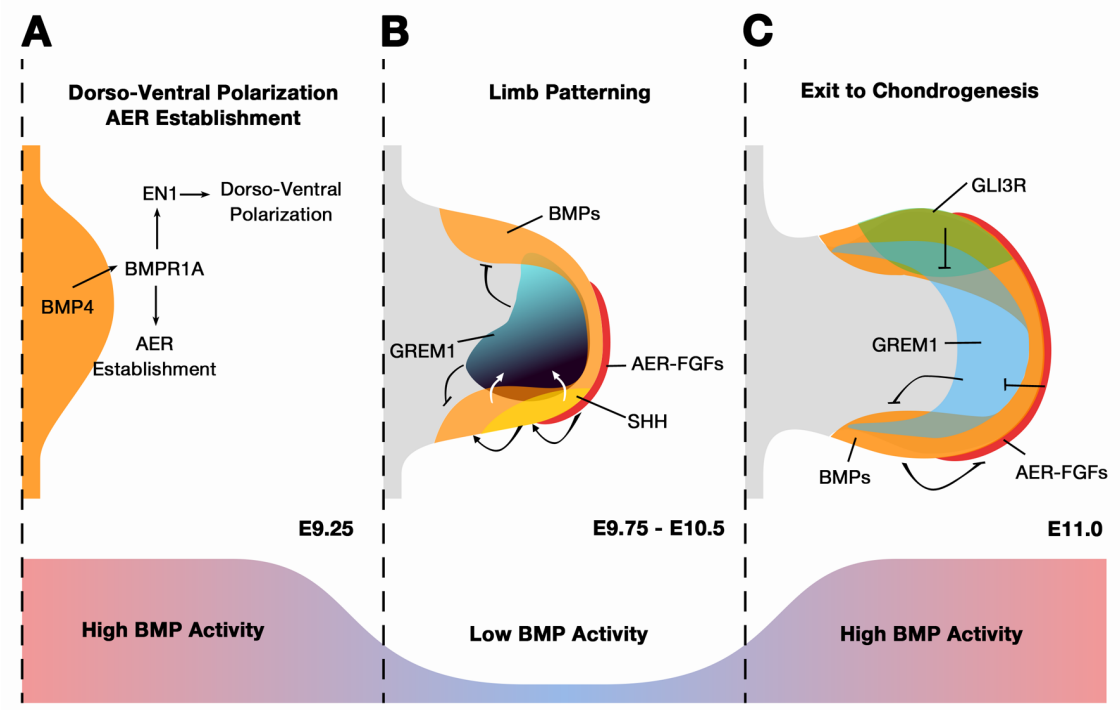

Fig. 3 Expression pattern of BMP ligands and genetic interactions of BMP activity during limb bud development. (A) Early polarization of the dorso-ventral (D-V) axis and establishment of AER require high BMP activity. Genetic evidence suggests that mesenchymal BMP4 signals through BMPR1A receptors in the ventral ectoderm to: 1) polarize the D-V axis through EN1 and 2) establish the AER. (B) During initiation of limb patterning, BMPs trigger the expression of the BMP antagonist *Grem1* in the posterior mesenchyme. This creates conditions permissive to activation of FGF4, FGF9 and FGF17 in the posterior AER (low BMP activity), which in turn results in up-regulation of *Shh* in the posterior mesenchyme. In addition, SHH sustains *Grem1* expression

and drives its distal-anterior expansion. (C) To initiate chondrogenesis, high BMP activity is required. This is achieved by 1) down-regulation of *Grem1* by AER-FGFs and GLI3R and 2) the refractoriness of Shh descendants to *Grem1* expression. Timely down-regulation of AER-*Fgf* expression by BMP activity restricts the limb bud to pentadactyly. Color code for the upper panels. Orange: BMP ligand expression; Blue: *Grem1*; Red: AER-FGF; Yellow: *Shh*; Green: GLI3R.

Table 1. Limb phenotypes associated with inactivation/aberration in BMP pathway components

Gene	Type of inactivation	Phenotype	Ref
Bmp2	Early limb mesenchyme	dysplastic scapula; syndactyly between digit 3 and 4 with incomplete penetrance	(Bandyopadhyay et al., 2006)
	Chondrocytes	impaired chondrocyte differentiation and apoptosis; severe chondro-dysplasia	(Shu et al., 2011)
Bmp4	Early limb mesenchyme	Occasional limb agenesis due to impairment in AER establishment; milder phenotype exhibits delay in AER induction and delayed termination of *Fgf8* expression; AER is flatter and less compact than in the wild-type; variable degree of anterior and posterior polydactylies	(Benazet et al., 2009; Selever et al., 2004)
	Chondrocytes	Minor skeletal defects over gross morphological observation	(Shu et al., 2011)
Bmp7	Constitutive null	Anterior polydactyly with incomplete penetrance in the hindlimb	(Luo et al., 1995)
	Early limb mesenchyme	normal limb	(Tsuji et al., 2010)
Bmp2;Bmp4	Limb ventral ectoderm and AER	Limb dorsalization; up-regulation and delayed inactivation of AER-*Fgfs;* increased cell proliferation and reduced cell death during tissue differentiation; polydactyly, digit bifurcation, interdigital webbing	(Maatouk et al., 2009)
	Early limb mesenchyme	Severe chondrodysplasia, one zeugopod element and two posterior-most digits missing in the forelimb; interdigital webbing	(Bandyopadhyay et al., 2006)
	Chondrocytes	impaired chondrocyte differentiation and apoptosis; severe chondrodysplasia	(Shu et al., 2011)
Bmp4;Bmp7	Early limb mesenchyme (*Bmp4*); Constitutive null (*Bmp7*)	dysplastic scapula, shortened fibula; absence of distal-most phalange of the 3rd digit	(Bandyopadhyay et al., 2006)
Bmp2;Bmp4;Bmp7	Limb ventral ectoderm	Down-regulated and patched AER-*Fgf8* expression domain; broad, flat, short-lived AER; polydactyly, digit bifurcation, ectrodactyly; interdigital webbing	(Choi et al., 2012)
	AER	down-regulated AER-Fgf8; polydactyly, digit bifurcation; interdigital webbing	(Choi et al., 2012)
Grem1	Constitutive null	Disruption of AER morphology; failure to induce AER-*Fgf4,9,17*; Massive cell death by E11.0; zeugopod is reduced to one element and three digits form	(Khokha et al., 2003; Michos et al., 2004)

Noggin	Constitutive null	skeletal hyperplasia; joints are not formed	(Brunet et al., 1998)
	Overexpression in the AER	limb dorsalization; delayed termination of AER-*Fgf;* syndactyly, post-axial polydactyly; prolonged interdigital webbing (until E16.5)	(Wang et al., 2004)
BmpR1b	Constitutive null	Impaired formation of the proximal phalanges	(Baur et al., 2000)
BmpR1a	Limb ventral ectoderm	Limb agenesis; AER does not form	(Pajni-Underwood et al., 2007)
	Limb ventral ectoderm during AER formation	Variable phenotype: occasional limb agenesis; variably impaired AER-*Fgf8* expression; oligodactyly, syndactyly, rare polydactyly, occasional additional phalanges	(Ahn et al., 2001)
	AER	soft tissue syndactyly, occasional polydactyly, occasional additional phalanges; interdigital webbing	(Ahn et al., 2001; Pajni-Underwood et al., 2007)
	Early limb mesenchyme	minor D-V and A-P axes defects; shortened skeletal structures, almost complete agenesis of the autopod	(Ovchinnikov et al., 2006)
	Chondrocytes	mild generalized chondrodysplasia; delay in ossification	(Yoon et al., 2005)
BmpR1a; BmpR1b	Chondrocytes (*BmpR1a*); Constitutive null (*BmpR1b*)	increased apoptosis and reduced proliferation during endochondral bone formation; impaired *Sox9* expression; severe generalized chondrodysplasia	(Yoon et al., 2005)
BmpR2	No limb phenotype		(Gamer et al., 2011)
ActRIIA	No limb phenotype		(Matzuk et al., 1995)
ActRIIB	No limb phenotype		(Oh and Li, 1997)
Tak1	Early limb mesenchyme	delayed onset and progression of chondrocyte maturation	(Gunnell et al., 2010)
	Chondrocytes	reduced proliferation, increased cell death during endochondral bone formation; late onset of hypertrophic differentiation; shortened skeletal element; humero-radial joint fusion	(Gunnell et al., 2010)
Smad4	Limb ventral ectoderm	up-regulated, broad and patchy AER-*Fgfs* domain; delayed inactivation of *Fgf4*, *Fgf8*, *Shh* expression; occasional one-element zeugopod, common ectopic outgrowths and ectrodactyly in the autopod; interdigital webbing	(Benazet and Zeller, 2013)
	AER	normal skeletal structure; interdigital webbing	(Benazet and Zeller, 2013)

	Early limb mesenchyme	up-regulated AER-*Fgf8* expression; delayed inactivation of *Fgf4, Fgf8, Shh* expression; impaired expression of *Sox9* and *Col type II*; no skeletal elements are formed	(Benazet et al., 2012)
	Handplate before tissue differentiation	failed specification of anterior-most digit primordia by *Sox9*; no skeletal elements are formed in the autopod	(Benazet et al., 2012)
	Chondrocytes	dwarfism	(Zhang et al., 2005)
Smad1	Chondrocytes	normal limb	(Retting et al., 2009)
	Limb ventral ectoderm during AER formation	normal limb	(Wong et al., 2012)
Smad5	Chondrocytes	normal limb	(Retting et al., 2009)
	Limb ventral ectoderm during AER formation	normal limb	(Wong et al., 2012)
Smad8	Chondrocytes	normal limb	(Retting et al., 2009)
Smad1; Smad5	Chondrocytes	reduced proliferation, increased cell death during endochondral bone formation; impaired hypertrophic differentiation; severe chondrodysplasia with remnants of limb skeleton	(Retting et al., 2009)
	Limb ventral ectoderm during AER formation	delayed inactivation of AER-*Fgf8*; interdigital webbing	(Wong et al., 2012)
Smad1; Smad5; Smad8	Chondrocytes (*Smad1; Smad5*); Constitutive null (*Smad8*)	reduced proliferation, increased cell death during endochondral bone formation; impaired hypertrophic differentiation; severe chondrodysplasia with remnants of limb skeleton	(Retting et al., 2009)
Smad6	Constitutive null	Delayed hypertrophic differentiation; no alteration of limb skeleton over gross morphological analysis	(Estrada et al., 2011)
	Overexpression in chondrocytes	delayed chondrocyte hypertrophy, dwarfism, osteopenia	(Horiki et al., 2004)
Smad7	Constitutive null	Increased cell death, reduced cell proliferation during endochondral bone formation; delayed hypertrophic differentiation; dwarfism	(Estrada et al., 2013)
	Overexpression in the early limb mesenchyme	impairment in *Sox9* expression and formation of mesenchymal condensations	(Iwai et al., 2008)
Id1; Id3	Constitutive null	No limb phenotype reported	(Lyden et al., 1999)
Msx2	Constitutive null	reduced thickness of growth plate and hypertrophic zone; osteopenia; interdigital webbing	(Satokata et al., 2000)
Msx1; Msx2	Constitutive null	limb dorsalization; broadened AER; loss of anterior skeletal elements (in the forelimb: radius, anterior carpals, 1st digit); lost of distal phalanges; occasional normodactyly; rare polydactyly; interdigital webbing	(Lallemand et al., 2005)

BMP activity during D-V axis specification and AER establishment

In early mouse limb buds, BMP2 is expressed by the ventral ectoderm and mesenchyme, while BMP4 and BMP7 are more widely expressed (Fig. 3A; Danesh et al., 2009; Yi et al., 2000). In chicken limb buds, BMP ligands, *Msx1* and *Msx2* target genes are expressed by the ventral ectoderm and mesenchyme before AER formation (Pizette and Niswander, 2001).

Misexpression of the BMP antagonist Noggin in the limb bud ectoderm abolishes *En1* expression, results in ectopic *Wnt7a* and *Lmx1b* expression in the ventral ectoderm and may result in induction of ectopic AER-like structure expressing *Fgf8* (Pizette and Niswander, 2001; Wang et al., 2004). In contrast, misexpression of constitutive active BMP receptors (BMPR1A and BMPR1B) results in dorsalization of AER, ectopic dorsal expression of *En1* and reduction of the *Wnt7a* and *Lmx1b* expression domains (Pizette and Niswander, 2001). These studies indicate that high BMP activity in the ventral ectoderm is required for definition of the D-V boundary and AER establishment.

En1, which functions in dorsal restriction of *Wnt7a* and *Lmx1b*, does not act downstream BMP signaling to specify the D-V axis and the AER, because *En1* deficient mouse limb buds still form an AER and *Fgf8* is activated correctly, although the AER structure fails to compact subsequently (Loomis et al., 1998; Pizette and Niswander, 2001). Conversely, MSX1, which is a BMP target in the early limb bud mesenchyme acts downstream BMP signaling to mediate its ventralization effect. This was shown as ectodermal misexpression of *Msx1* results in formation of ectopic dorsal AER (Pizette and Niswander, 2001). However, D-V axis specification is not affected in *Msx1* deficient limb buds, suggesting that the *Msx1* deficiency is compensated (Satokata and Maas, 1994).

Genetic inactivation of BMP signaling pathway at different levels has provided new insights into its early functions during limb field and AER formation. The *Prx1-Cre* transgene (Logan et al., 2002) drives Cre recombinase expression into the forelimb mesenchyme around the time when the AER is established. Inactivation of *Bmp4* in the forelimb bud using the *Prx1-Cre* transgene results in severe truncations of the forelimb and AER agenesis (Benazet et al., 2009). The same phenotype is observed when BMP4 is inactivated using a tamoxifen-inducible Cre prior to AER formation, whereas inactivation after AER formation results in polydactyly (Benazet et al., 2009; Selever et al., 2004). These results reveal the transient requirement of BMP4 for AER formation and its subsequent role in restricting the autopod to pentadactyly (Benazet et al., 2009). Inactivation of either *BmpR1a*, *BmpR1b*, *BmpR2*, *Bmp2* or *Bmp7* does not impair AER formation (Bandyopadhyay et al., 2006; Gamer et al., 2011; Yoon et al., 2005). These results suggest that BMP4 signals to the ectoderm to establish the AER.

Brn4-Cre-driven early inactivation of *Bmpr1a* in the ventral limb bud ectoderm results in partial limb agenesis and/or severe skeletal truncations due to impaired AER formation. This phenotype phenocopies the mesenchymal deletion of *Bmp4*, suggesting that BMP4 signals through ectodermal BMPR1A to instruct AER establishment (Fig. 3A). Conversely, the mutant forelimb only displays subtle malformations (Ahn et al., 2001). *Msx2-Cre*-driven inactivation of *BmpR1a* in the ventral limb bud ectoderm and AER disrupts AER induction and results in limb agenesis (Pajni-Underwood et al., 2007). As delayed inactivation results in normal development, these results point to a time-restricted requirement of *BmpR1a* in the ventral ectoderm during AER establishment. Msx2-*Cre*-driven conditional deletion of *Smad4* in the limb bud ectoderm at early stages disrupts AER formation and results in dysmorphisms and bifurcation of the phalanges, ectrodactyly and occasional loss of zeugopod elements (Benazet and Zeller, 2013). Similarly, inactivation of *Bmp2* and *Bmp4* in the ectoderm results in dysmorphism and bifurcation of phalanges (Maatouk et al., 2009). Interestingly, all cases of diminished ectodermal BMP signaling still permissive to AER formation, resulted in impaired AER compaction, elongation along the A-P axis and failure in correct formation of AER-FGF signalling. In particular, AER-*Fgf8* expression was increased and prolonged, which is likely the cause of the alterations in autopod development (Ahn et al., 2001; Choi et al., 2012; Maatouk et al., 2009; Pajni-Underwood et al., 2007; Selever et al., 2004; Wang et al., 2004). These results indicate that: 1) ectodermal *Smad4* is required for AER formation downstream of BMP2 and BMP4 ligands, to restrain AER-FGF signaling and prohibit excessive autopod outgrowth; 2) after AER establishment, ectodermal BMP2 and BMP4 act independently of SMAD4 to modulate AER-FGF activity and restrict the autopod to pentadactyly. In all cases, reduction of BMP-signaling activity in the ectoderm impairs interdigital cell death, which results in interdigital webbing. This webbing is due to increased and delayed shutdown of AER-FGF signalling: indeed, the combined inactivation of *BmpR1a*, *Fgf4* and *Fgf8* in the limb ectoderm rescues interdigital cell death (Pajni-Underwood et al., 2007).

BMP activity during limb patterning and outgrowth

As mentioned above, GREM1-mediated antagonism of BMP activity is necessary for the establishment of the positive e-m feedback loop that in turn sustains the expression of *Shh* and *AER-Fgf* during distal progression of limb bud development (Fig. 3B). *Grem1* inactivation disrupts A-P polarity, induces cell death and reduces the mesenchymal progenitors. Heterozygosity for the *Bmp4* gene partially rescues *Grem1* deficiency and

further genetic reduction of *Bmp4* rescues cell death and limb skeletal elements (Benazet et al., 2009). This study also revealed the higher genetic relevance of *Bmp4* with respect to the other BMP ligands during limb bud development.

During limb bud outgrowth and patterning, the posterior localization of the *Grem1* domain together with the anterior expression of GLI3R, which down-regulates *Grem1*, likely produces an anterior limb domain characterized by high BMP activity (Khokha et al., 2003; Lopez-Rios et al., 2012). Indeed, genetic analysis shows that BMP ligands cooperate with GLI3 to reduce the size of the anterior limb domain and restrict the autopod to pentadactyly (Bandyopadhyay et al., 2006; Hui and Joyner, 1993; Selever et al., 2004).

Tissue differentiation and initiation of chondrogenesis in the limb

Between E11.5 and E12, mesenchymal condensations in the limb bud core begin to form and outline the future skeletal elements that form subsequently by endochondral bone formation (for review see Long and Ornitz, 2013). In parallel, the connective tissue differentiates to give rise to tendons, ligaments, perichondrium, loose connective tissue, dermis, muscle and endothelium (see ten Berge et al., 2008). While most of the limb structures derive from the lateral plate mesoderm, muscle and endothelium precursor cells originate from progenitors that migrate from the somites into the limb bud, where they expand and commit to their respective fates (Buckingham et al., 2003; Chevallier et al., 1977; Yvernogeau et al., 2012).

The specification of these tissues is revealed by the activation of molecular markers, such as *Sox9* for osteo/chondroprogenitors, *Scleraxis (Scx)* for tendons, *Growth and differentiation factor 5* (*Gdf5)* and *Four-jointed (Fjx)* for joints, *MyoD* and *Myf5* for muscle precursors (Francis-West et al., 1999; Francis-West et al., 2003; Rock et al., 2005; Schweitzer et al., 2001; Wright et al., 1995). Molecular cues from the ectoderm (in particular the AER) orchestrate tissue differentiation such that e.g. condensations occur predominantly in the limb core mesenchyme. In particular, WNT signaling by the ectoderm inhibits chondrogenesis and promotes cell proliferation in the underlying mesenchyme (Hartmann and Tabin, 2001; Rudnicki and Brown, 1997; Solursh, 1984; ten Berge et al., 2008). WNT3a commits mesenchymal cells to different connective tissue fates, depending on the time of exposure. Conversely, combined exposure to WNT3a and FGF8 preserves the chondrogenic potential of mesenchymal progenitors (ten Berge et al., 2008).

FGF signaling, by the AER and mesenchyme, promotes cell survival and proliferation, which ultimately control the length of skeletal primordia and number of digit ray primordia (Davidson et al., 2005; Yu and Ornitz, 2008; Yu et al., 2003). FGF and BMP signaling up-regulate the expression of the *Sry*-related SOX9 transcription factor (Bi et al., 1999; Murakami et al., 2000; Pan et al., 2008; Wright et al., 1995). The *Sox9* haploinsufficiency is associated with severe forms of chondrodysplasia in mice and results in campomelic dysplasia in humans (OMIM Entry # 114290; Bi et al., 1999). Complete inactivation of *Sox9* in the limb bud mesenchyme results in skeletal agenesis (Akiyama et al., 2002). Furthermore, *Sox9* drives the expression of *Sox5* and *Sox6*, and interacts with them to control chondrogenesis (Akiyama et al., 2002; Lefebvre et al., 2001). *Sox9* also interacts genetically with *Scx* to control the cartilage-tendon interface (Blitz et al., 2013; Sugimoto et al., 2013). *In vitro* analysis using high-density micromass cultures provided evidence that *Sox9* is dispensable for cell compaction during condensation of mesenchymal progenitors. Rather, SOX9 is necessary to maintain the cellular aggregates, possibly by promoting their chondrogenic differentiation. In contrast, BMP signaling is required for compaction of mesenchymal progenitors (Barna and Niswander, 2007). The molecular interactions initiating cell aggregation and compaction of mesenchymal progenitors are not known. Moreover, several signaling pathways inhibit aggregation and/or chondrogenic differentiation, such as the WNT, NOTCH and RA signaling pathways (for review see Long and Ornitz, 2013). However, limb mesenchymal progenitors exhibit an inherent property to initiate chondrogenic differentiation in high-density cultures under the influence of BMP and TGFβ signaling (Barna and Niswander, 2007).

BMP activity during initiation of chondrogenic differentiation

During initiation of chondrogenic differentiation *Bmp2* and *Bmp7* become expressed by the prospective interdigital cells, while the *Bmp4* expression domain gets restricted to the distal-most mesenchyme at E12.0 (Benazet et al., 2009; Dunn et al., 1997; Dupe et al., 1999; Laufer et al., 1994; Yang et al., 1998b). In parallel, phosphorylated forms of SMAD1, -5 and -8 are strongly expressed in the distal-most mesenchyme and, to a lesser extent, in the prospective interdigital mesenchyme and at the tip of digit condensations (Suzuki et al., 2008; Witte et al., 2010). *BmpR1b* is expressed by the digit condensations, while *BmpR1a* remains diffuse throughout the mesenchyme, with higher levels in the distal-most mesenchyme (Degenkolbe et al., 2013; Zou et al., 1997). The *Msx2* and *Id1* target genes are also expressed by the interdigital mesenchyme (Evans and O'Brien, 1993;

Montero et al., 2001).

In general, BMP signaling promotes outgrowth of skeletal elements to the detriment of joint formation. For instance, genetic inactivation of the BMP antagonist *Noggin* results in fewer and larger cartilage elements and failure of joint formation (Brunet et al., 1998). In contrast, compound mesenchymal inactivation of both *Bmp2* and *Bmp4* induces a severe chondrodysplastic phenotype (Bandyopadhyay et al., 2006).

Mesenchymal condensation is characterized by the transient up-regulation of proteoglycans such as tenascin, syndecan and versican and of adhesion molecules like N-CAM and N-cadherin. During chondrogenic differentiation, molecular evidence indicates that BMP signaling up-regulates *Sox9*, which in turn functions by activating Collagen type II (COL type II), COL type IX, COL type XI and aggrecan in chondrocytes (Bell et al., 1997; Gao et al., 2013; Lefebvre et al., 2001; Sekiya et al., 2000; Yoon et al., 2005). N-cadherin mediates calcium-dependent homotypic cell-cell interactions. In an *in vitro* system, BMP2-stimulated condensation results in N-cadherin re-distribution to adherens junctions (Haas and Tuan, 1999). Moreover, N-cadherin at adherens junctions modulates the nuclear activity of the transcription factor β-catenin (Fischer et al., 2002; Modarresi et al., 2005).

What is known about contribution of BMP signaling inducing chondrogenic differentiation steps mainly comes from *in vivo* limb manipulation and gene misexpression experiments or from the used of micromass cultures. Pizette and Niswander (2000) showed a dual role for BMP ligands in mesenchymal aggregation and induction of chondrogenesis (Pizette and Niswander, 2000). When BMP ligands are sequestered by misexpression of NOGGIN, the prospective chondrogenic progenitors undergo a cell fate switch towards loose connective tissue. When NOGGIN is misexpressed over condensing tissue, *Gdf5* expression domain is expanded.

GDF5 belongs to the TGFβ superfamily, is structurally related to BMP2 and BMP4 ligands and shares the same receptors (Mueller and Nickel, 2012). GDF5 is expressed by joint primordia and its genetic inactivation results in brachypodia characterized by loss of joints, and hypoplasia of metacarpal and carpal bones in mouse embryos (Storm and Kingsley, 1999; Yi et al., 2000).

Conditional inactivation of *BmpR1a* in chondrocytes (using the *Col2-Cre* transgene), results in overall shorter limb skeletal elements with a major dysplasia of the scapula. Instead, inactivation of *BmpR1b* results in loss of the proximal-most phalanges. The compound inactivation of the type I BMP receptors results in agenesis of limb skeleton, whereas a single functional allele of *BmpR1b* rescues all the skeletal elements, which are however shorter with a dysplastic scapula and loss of phalanges (Yoon et al., 2005; Yoon

et al., 2006). The compound conditional inactivation of *Smad1* and *Smad5* in the COL2-expressing chondrocytes phenocopies the *Bmp receptor type I* phenotypes. (Retting et al., 2009). These limb skeletal defects are a consequence of reduced proliferation and increased cell death in growth plate and impaired terminal differentiation of chondrocytes (Yoon et al., 2006). Surprisingly, conditional inactivation of *Smad4* using the *Col2-Cre* transgene results in dwarfism and delayed ossification, suggesting that the chondrogenic steps that follow the activation of COL2 in chondrocytes are mostly driven by *Smad4*-independent, *Smad1/*5-dependent mechanisms (Zhang et al., 2005).

Congenital limb malformations associated with aberrant BMP signaling

Limb phenotypes associated with impaired expression of BMP signaling-related molecules in the mouse often mirror the contribution of BMP signaling pathway during human limb development (for review see Zuniga et al., 2012). Congenital human limb malformations include several types of autosomal-dominant brachydactylies (OMIM Ref #112600, #611377 and #113100) associated with mutations affecting the coding sequence (CDS) or regulatory regions of BMP pathway genes such as *BmpR1b, Gdf5, Noggin* and *Bmp2* (Dathe et al., 2009; Lehmann et al., 2006; Lehmann et al., 2007; Ploger et al., 2008). Human cases of brachydactyly sometimes exhibit additional occurrence of proximal symphalangism (OMIM Ref #615298) and carpal synosthosis (OMIM Ref #186400; Degenkolbe et al., 2013; Lehmann et al., 2007). Homozygous disruption of the limb-specific *cis*-regulatory region of *Grem1* is associated with the rare autosomal recessive Cenani-Lenz syndactyly syndrome (OMIM Ref #212780; Dimitrov et al., 2010). In contrast mutations in the *Sclerostin* gene, which encodes another BMP antagonist, result in sclerostosis characterized by syndactyly and bone over-growth (OMIM Ref #269500; Collette et al., 2012). Mutations in *Bmp4* reading frame cause the Anophthalmia-microphthalmia multi-systemic disorder that includes polysyndactly (OMIM Ref #607932; Bakrania et al., 2008).

5. AIMS OF THE THESIS

I started my doctoral studies in developmental biology under the supervision of Prof. Dr. Rolf Zeller with the intent to widen my knowledge and technical skills with respect to the immunology background I acquired during my master's thesis. Indeed, the investigation of developmental processes has helped me to face the high complexity of gene behaviors, signal interactions and tissue dynamics.

The aim of this thesis is to dissect the genetic contribution of canonical signaling at different stages of limb development with the use of several limb-conditional inactivations of *Smad4*, alone or in the context of mutant backgrounds. In addition, I was expected to: 1) generate an *in vivo* sensor of the BMP activity, for a detailed temporal analysis of the signaling dynamics and perturbations upon pharmacological treatments or genetic defects; 2) implement new techniques in the laboratory, including the three-dimensional embryo/tissue optical projection tomography (OPT) scanning and the complementation assay for fast generation of *cis*-regulatory element reporter embryos/mice.

The genetic analysis of the *Smad4* mutation in the limb was accomplished at the beginning of my third year in this laboratory, contributing a co-first author paper (Benazet et al., 2012). On the other hand, the generation of the BMP activity sensor was delayed by several pitfalls, including problems in targeting and germ-line transmission. I have managed to successfully implement the OPT scanning technique in the lab with the help of Frédéric Laurent and Erkan Uenal, and the setting up of the aggregation chimera protocols is almost finalized.

6. MATERIAL AND METHODS

Genetic crosses of mouse strains

All strains are kept in C57BL/6 genetic background unless otherwise stated. All mice and embryos were genotyped by PCR amplification of diagnostic biopsies (primers are listed in Table 1).

Genetic crosses of Smad4 alleles

The *Smad4^{flox}* conditional allele (Yang et al., 2002) was inactivated either using the *Prx1-Cre^{Tg}* in the mouse limb bud mesenchyme from about 9.5 days post coitum (E9.5; Logan et al.), or using the *Hoxa13-Cre^{Tg}* knock-in allele during autopod development from about E10.75 onwards (Lopez-Rios et al., 2012; Scotti and Kmita, 2012). The *Smad4^{flox}* was crossed to the *Hoxb6-Cre^{Tg}* to inactivate *Smad4* in the hindlimb field and the posterior forelimb mesoderm (Lowe et al., 2000). The *Msx2-Cre* allele (Sun et al., 2000) was used to inactivate the *Smad4^{flox}* allele in the limb bud ectoderm from about E9.5 onward in the presence of two *Grem1* null alleles (*Grem1$^{\Delta}$*; see Michos et al., 2004). The *Smad4* null allele (Smad4$^{\Delta}$) was obtained by crossing *Smad4^{flox}* allele with a *CMV-Cre* deleter mouse strain (Schwenk et al., 1995). *Smad4$^{\Delta/\Delta}$* embryos are lethal between E6.5 and E8.5 due to defective epiblast proliferation and impaired mesoderm induction, whereas heterozygous animals are phenotypically normal (Yang et al., 1998a).

Inactivation of Smad4 in the mesenchyme

Prx1-Cre^{Tg}-positive mice were crossed with mice carrying the *Smad4$^{\Delta}$* allele to generate the *Prx1-Cre$^{Tg/+}$; Smad4$^{\Delta/+}$* compound heterozygous males. These males were crossed with *Smad4$^{flox/flox}$* females to obtain experimental embryos that carried a constitutive deleted and a conditionally inactivated allele (*Smad4$^{\Delta/\Delta M}$*). A similar procedure was used to generate *Hoxb6-Cre$^{Tg/+}$; Smad4$^{\Delta/+}$* males and *Smad4$^{\Delta/\Delta Hb6}$* experimental embryos. Moreover, mice carrying the conditional *β-Actin*-GFP locus in a Balb/c background were mated to *Hoxb6-Cre* transgene to generate reporter embryos to monitor the *Cre*-mediated recombination (Jagle et al., 2007). *Smad4$^{+/+}$*, *Smad4$^{flox/+}$*, *Smad4$^{flox/flox}$*, *Smad4$^{\Delta M/+}$*, *Smad4$^{\Delta Hb6/+}$* or *Prx1-Cre$^{Tg/+}$* embryos were used as controls and are collectively referred to as 'Wt'.

Inactivation of Smad4 in the autopod

Hoxa13-Cre^{Tg} knock-in transgene was crossed either with *Smad4*$^{\Delta/+}$ or *Smad4*$^{flox/flox}$ mice to get *Hoxa13-Cre*$^{Tg/+}$*; Smad4*$^{\Delta/+}$ and *Hoxa13-Cre*$^{Tg/+}$*; Smad4*$^{flox/+}$ males. These males were crossed with *Smad4*$^{flox/flox}$ females to obtain a total of 180 embryos. In *Hoxa13-Cre*$^{Tg/+}$*; Smad4*$^{flox/+}$ males, the *Hoxa13-Cre*^{Tg} transgene failed to ectopically recombine the *Smad4*^{flox} allele in the germ-line approximately 25% of all cases, thus providing the progeny with two conditional alleles to be inactivated. Thus, either *Smad4*$^{\Delta/\Delta A13}$ or *Smad4*$^{\Delta A13/\Delta A13}$ embryos were used as experimental samples. *Smad4*$^{+/+}$, *Smad4*$^{flox/+}$, *Smad4*$^{flox/flox}$, *Smad4*$^{\Delta M/+}$, *Smad4*$^{\Delta Hb6/+}$ or *Hoxa13-Cre*$^{Tg/+}$ embryos were used as controls and collectively referred to as 'Wt'.

Inactivation of Smad4 in the AER in a Grem1-deficient genetic background

In order inactivate *Smad4* in the AER of mouse embryos deficient for *Grem1* (*Grem1*$^{\Delta/\Delta}$*; Smad4*$^{\Delta/\Delta AER}$), the following genetic crosses were done: *Msx2-Cre*$^{Tg/+}$ males were mated with *Grem1*$^{\Delta/+}$ females to generate *Msx2-Cre*$^{Tg/+}$*; Grem1*$^{\Delta/+}$ mice, and to *Smad4*$^{\Delta/+}$ females to generate *Msx2-Cre*$^{Tg/+}$*; Smad4*$^{\Delta/+}$ mice. The compound mutant mice were inter-crossed to get *Msx2-Cre*$^{Tg/(Tg/+)}$*; Grem1*$^{\Delta/+}$*; Smad4*$^{\Delta/+}$ males. Compound *Grem1*$^{\Delta/+}$*; Smad4*$^{flox/flox}$ females were obtained by crossing *Grem1*$^{\Delta/+}$ males with *Smad4*$^{flox/flox}$ females and inter-crossing the progeny that exhibited a *Grem1*$^{\Delta/+}$*; Smad4*$^{flox/+}$ genotype. *Grem1*$^{\Delta/\Delta}$*; Smad4*$^{\Delta/\Delta AER}$ embryos were compared with *Grem1*$^{+/+}$*; Smad4*$^{L/+}$, *Grem1*$^{\Delta/+}$*; Smad4*$^{L/+}$, *Grem1*$^{+/+}$*; Smad4*$^{\Delta/L}$ (overall referred to as Wild-type controls 'Wt').

Inactivation of Smad4 in the limb bud mesenchyme of Shh deficient embryos

Shh$^{\Delta/\Delta}$*; Smad4*$^{\Delta/\Delta M}$ compound mutant embryos were obtained with the same kind of crosses as for *Grem1*$^{\Delta/\Delta}$*; Smad4*$^{\Delta/\Delta AER}$ embryos (*Shh*$^{\Delta}$ allele comes from St-Jacques et al., 1998).

Genetic crosses of Bmp2 and Bmp4 alleles

Prx1-Cre^{Tg} allele was used to inactivate both *Bmp2*^{flox} (Ma and Martin, 2005) and *Bmp4*^{flox} (Liu et al., 2004) conditional alleles to generate compound mutant embryos.

Briefly, *Prx1-Cre*$^{Tg/Tg}$ mice were crossed with *Bmp2*$^{flox/flox}$ and *Bmp4*$^{flox/flox}$ conditional alleles to get *Prx1-Cre*$^{Tg/+}$*; Bmp2*$^{flox/+}$ and *Prx1-Cre*$^{Tg/+}$*; Bmp4*$^{flox/+}$ compound transgenic mice, respectively. These mice were further mated to generate *Prx1-Cre*$^{Tg/(Tg/+)}$*; Bmp2*$^{flox/+}$*;*

Bmp4$^{flox/+}$ males. Females were generated by mating *Bmp2*$^{flox/flox}$ to *Bmp4*$^{flox/flox}$ mice and the progeny was inter-crossed to get the *Bmp2*$^{flox/flox}$; *Bmp4*$^{flox/flox}$ genotype. *Prx1-Cre*$^{Tg/+}$; *Bmp2*$^{\Delta M/\Delta M}$; *Bmp4*$^{\Delta M/\Delta M}$ embryos were compared to control embryos (*Bmp2*$^{flox/+}$; *Bmp4*$^{flox/+}$, *Bmp2*$^{flox/flox}$; *Bmp4*$^{flox/+}$ or *Bmp2*$^{flox/+}$; *Bmp4*$^{flox/flox}$).

Table 1. Genotyping primers

Gene	Forward primer	Reverse primer	Allele
Cre	5'-GCCTGCATTACCGGTCGATGCAACGA-3'	5'-GTGGCAGATGGCGCGGCAACACCATT-3'	Tg
Prx1-Cre	5'-GGGCTCTCTCCTTAGCTTCCC-3'	5'-CCTGGCGATCCCTGAACATGTCC-3'	Tg
Msx2-Cre	5'-AACAACTCTGCTGACTGCTCCTG-3'	5'-CCTGGCGATCCCTGAACATGTCC-3'	Tg
Hoxa13-Cre	5'-CGTAATCTGGCATTTCTGGGGATTG-3'	5'-CCAGAGTCATCCTTAGCGCCGTAAA-3'	Tg (knock-in)
Hoxb6-Cre	5'-GCTAAAACCCAATCTCGGCTAT-3'	5'-AGCATTTTCCAGGTATGCTCAG-3'	Tg
Smad4	5'-GGGCAGCGTAGCATATAAGAC-3'	5'-CCTGACCCAAACGTCACCTTC-3'	Wt/Flox allele
		5'-AAGAGCCACAGGTCAAGCAG-3'	Null allele
Grem1	5'-ATGAATCGCACCGCATACACTG-3'	5'-TCCAAGTCGATGGATATGCAACG-3'	Wt allele (Michos et al.,2004)
	5'-GGCACATGGCTGAATATCGACGG-3'	5'-AAGCGCCTCCCCTACCCGGTA-3'	Null allele (Michos et al.,2004)
Bmp2	5'-GCTTGGTCTGGTAATCTTCCT-3'	5'-AGGGATGCTGCTGTTTCTGGA-3'	Wt/flox allele
		5'-AAGCGCCTCCCCTACCCGGTA-3'	Null allele
Bmp4	5'-GCTAAGTTTTGCTGGTTTGC-3'	5'-GCCCATGAGCTTTTCTGAGA-3'	Wt/flox (Liu et al., 2004)
Shh	5'-GAAGAGATCAAGGCAAGCTCTGGC-3'	5'-ATGCTGGCTCGCCTGGCTGTGGAA-3'	Wt allele
		5'-GGACACCATTCTATGCAGGG-3'	Null allele

Whole Mount In Situ Hybridization (WISH)

The protocol for WISH was previously described (Probst et al., 2013) and is an adaptation of the original protocol from Wilkinson (1992) .

Embryos were dissected, phenotyped and number of somites recorded (counted up to E12.0) and fixed overnight (ON) at 4°C in 4% paraformaldehyde (PFA) in phosphate buffer saline (PBS). The day after they were dehydrated in progressively higher methanol concentration in PBS and 0.1% Tween-20 (PBT), and stored at -20°C for further use. Unless stated, all steps were performed with gentle rocking for mixing.

The first day of WISH, experimental and control embryos were age-matched by somite number and limb shape, re-hydrated through progressively lower methanol concentration into PBT and cleared in 6% hydrogen peroxide (AppliChem) in PBT for 15 min. Embryos were washed with PBT (3 times) and digested with 10 µg/ml Proteinase K (PK, Merck) for a time period ranging from 15 min and 1 h according to embryos size and sample thickness. For ectodermal probes, a 4-min digestion with 5 µg/ml PK was used. From PK treatment until re-fixation, samples are kept still – i.e. not rocking -. The PK digestion was stopped using freshly prepared 2 mg/ml glycine in PBT and embryos were

washed twice in PBT. Embryos were re-fixed with 0.2% glutaraldehyde, 4% PFA in PBT for 20 min at Room-Temperature (RT) and washed twice with PBT. Embryos were then equilibrated into pre-warmed pre-hybridization mix at 70°C for 1 hr or longer and pre-hybridization mix was then replaced by probe solution (10 µl of probe in 1 ml of pre-hybridization mix) ON at 70°C. Digoxigenin-labelled antisense riboprobes were prepared from linearized and transcribed plasmid containing the cloned cDNA of interest. The riboprobes were purified using two steps of ethanol precipitation, the first with and the second without adding linearized polyacrylamide. Probes were heated 5 min at 85°C in pre-hybridization mix and equilibrated at 70°C before use. Probes were re-used several times and stored at -20°C.

The second day of WISH, embryos were brought through several steps (100%, 75%, 50%, 25%) of pre-hybridization solution/ 2x SSC (pH 4.5) at 70°C. Embryos were then washed twice in 2x SSC, 0.1% CHAPS (Sigma) for 30 min at 70°C and treated with 20 µg/ml RNase A (Sigma) in 2x SSC, 0.1% CHAPS for 25 min at 37°C. Embryos were then washed twice with maleic acid buffer (10 min at RT) and twice for 30 min at 70°C. Embryos were washed further in TBST (3 times for 5 min RT) and blocked in 10% goat serum in TBST (blocking buffer) for at least 1 h. Blocking buffer was replaced with anti-digoxigenin fragment antigen-binding conjugated with alkaline phosphatase (Roche) diluted 1:5000 in 1% goat serum in TBST. Samples were incubated ON at 4°C.

The third day of WISH, embryos were washed RT several times with TBST over the day and left in TBST ON at 4°C.

The fourth day of WISH, embryos were equilibrated in NTMT for 3 times, 10 min each at RT and then moved into 1 ml of BM Purple (Roche cat. No 11442074001). Samples were developed in the dark, then washed with PBT at least 3 times and moved into PBS. Results were documented using a Leica stereomicroscope with digital camera.

Alternatively, WISH was performed for OPT imaging. To this end, the following modifications were used in order to ensure a better penetrance of the chromogenic substrate into the embryos:

First day WISH: hydrogen peroxide treatment was kept for 1 hr instead of 15 min; glycine step was not used; re-fixation was performed at 4°C for 1 hr; incubation with pre-hybridization solution was performed 1 x 20 min RT and 1 x 3 hr at 70°C.

Second day WISH: embryos were moved in post-hybridization solution and, from here, to progressively higher concentration of 2x SSC. After SSC equilibration, embryos were washed twice in 2x SSC + 0.1% CHAPS at 70°C for 30 min, then once with 0.2x SSC + 0.1% CHAPS at 70°C for 30 min and finally once with 0.2x SSC + 0.1% CHAPS while cooling down to RT for 30 min; samples were then washed with TNT once for 10 min and

blocked in blocking solution at 4°C for 4 hr. Antibody was diluted 1:2000 in blocking solution and incubation was performed ON at 4°C.

Third day WISH: washes were performed with TNT + 0.1% bovine serum albumin (BSA).

Fourth day WISH: embryos were equilibrated in NMT + 0.1% Triton x-100 twice for 30 min, then washed 3 times 10 min in NMT and stained with a mix of nitro-blue tetrazolium and 5-bromo-4-chloro-3-indolyphosphate: BCIP (3.5 µg/ml) + NBT (0.3 µg/ml) in NMT.

Embryo trunk culture and limb bud grafting

Embryos were isolated either at E10.5 – E10.75 (34-39 somites) or E11.5 (45 – 50 somites) in tissue culture-grade PBS in plastic Petri dishes, then moved into 6-well plates containing pre-equilibrated culture medium (see below) and kept inside the incubator (37°C, 5% CO_2). Embryos were then processed individually: the head and the hindlimb together with the posterior-most part were removed and the remaining trunk was further cleaned of the heart and the ventral tissue. Then, a small hole was made into the right forelimb with a sharpened tungsten needle and the customized heparin-coated beads (see below) were placed into the hole. The trunks were positioned on a V-shaped metal grid in a 24-well plate at the interface between culture medium and air, with the help of thin pins. Trunks were cultured for the indicated time at 37°C, 6.5% CO_2. After the incubation period, pins were removed and the trunks were washed 3 x 5 min in PBS before imaging. An ON fixation with 4% PFA in PBS at 4°C followed if the samples were to be processed for WISH.

Culture Medium for embryo trunk culture

(prepared freshly on the day of use):

- 500 ml Dulbecco's Modified Eagle Medium (1x), liquid (high glucose) (Cat. 41966-029, Gibco)
- 5 ml L-glutamine (Cat. 25030-024, Gibco)
- 2.5 ml penicillin-streptomycin (Cat. 15140-122, Gibco)
- 5 ml non-essential amino acids (Cat. 11140-035, Gibco)
- 5 ml sodium pyruvate (Cat. 11360-039, Gibco)
- 5 ml D-glucose (45% solution) (Cat. G8769, Sigma)
- 0.5 ml L-ascorbic acid (Cat. A4034, Sigma)

- 5 ml lactic acid (Cat. L4388, Sigma)
- 0.5 ml d-biotin/vitam B12 (Cat. B4639 and V6629 respectively, Sigma)
- 0.5 ml PABA (Cat. A9878, Sigma)

L-ascorbic acid and lactic acid were dissolved in PBS and DMEM, respectively, and filtered through a 0.22 µm sieve on the day of use.

Stocks:

- d-biotin: 0.2 mg per ml DMEM. Filter through 0.22 µm filter, 0.5 ml aliquots stored at -20°C;
- Vitamin B12: 40 µg per ml DMEM. Filter through 0.22 µm filter, 0.5 ml aliquots stored at -20°C;
- PABA: 2 mg per ml PBS. Filter through 0.22 µm filter, make 0.5 ml aliquots stored at -20°C.

Loading of beads with proteins

Heparin-Acrylic beads (Cat. H5263, Sigma) were washed in a drop of PBS before moving them in a drop of hrBMP4 (R&D, 0.1 mg/ml) and incubated on ice in a humidified environment for 30 min. After incubation, beads were left on ice in a drop of culture medium before implantation.

Skeletal preparations

Embryos older than E14 were isolated and placed in ice-cold PBS for anesthesia. Then they were euthanized by exsanguination. Subsequently the carcass was eviscerated and macerated ON in tap water, and dehydrated in 95% ethanol from one to several days. Liver biopsies were taken for genotyping. Alcian blue staining (30 mg Alcian Blue 8GX – Sigma -, 85% (v/v) ethanol, 20% (v/v) glacial acetic acid) was performed ON and was followed by one-day washing with 95% ethanol. Embryos were then cleared in 1% (w/v) potassium hydroxide (KOH) in distilled water for about 10 min, counterstained with Alizarin Red (50 mg Alizarin Red – Sigma -, in 1% (w/v) KOH) for 1 hr and cleared in 1% KOH for an additional hour. Embryos were then moved through progressively higher ratio of glycerol/1% KOH solutions according to the speed of the clearing process till a final stocking solution (80% glycerol in water). Embryos were pictured on a Leica stereomicroscope.

Whole mount immunofluorescence (WIF)

Embryos were dissected and processed for fixation and dehydration the same way as for WISH. The first day of WIF, embryos were rehydrated through decreasing methanol/PBT ratio solutions, washed once in PBT for 5 min and once in H_2O for 5 min. Embryos were further permeabilized in pre-chilled acetone at -20°C for 15-20 min, washed in PBT and moved in Immunoblock solution (5% goat serum in Immunowash solution) for at least 2 hr. Embryos were incubated for 4 days at 4°C in Immunoblock solution containing rabbit-monoclonal SMAD4 antibody (Abcam, ab40759) diluted 1:100 and 0.1% Na Azide. After primary antibody incubation, embryos were washed 7 x 15 min followed by 1 x 2 hrs in Immunowash solution and blocked in Immunoblock solution for about 2 hrs. Embryos were moved into Immunoblock solution containing Alexa Fluor 594 Goat-anti-Rabbit (Life Technologies) diluted 1:250 and 0.1% Na Azide, and were incubated ON at 4°C in the dark for additional 4 days. After incubation, embryos were washed 8 x 15 min in Immunowash solution and 2 x 5 min in PBT. After this step, samples were processed for OPT imaging.

OPT imaging

The OPT scanner (Bioptonics, MRC, Edinburgh) allows three dimensional (3D) imaging of tissue up to 15 mm in depth by picturing several projection of fluorescent or colored biological specimen and reconstructing the 3D signal (Sharpe et al., 2002). Processed biological specimen are embedded in a low-melting point agarose (Sigma) and glued on a magnet suited for OPT scanning (Bioptonics). Specimens were dehydrated in methanol ON and cleared in one part *Benzyl* Alcohol and two parts *Benzyl* Benzoate (BABB, Sigma) ON. Specimens were scanned at either high (1024x1024 pixels) or intermediate resolution (512x512 pixels) using Skyscan software (Bioptonics, MRC Technology). Auto-fluorescence in the GFP1 filter (425/40 nm, 475 nm LP) was used to detect sample anatomy. Bright field or the TXR filter (560/40 nm, 610 nm LP) was used to image NBT/BCIP stainings or fluorescent signals, respectively. Projection reconstruction was performed using NRecon software (SkyScan) and analyzed using Bioptonics Viewer (Bioptonics, MRC Technology). Rendering images were either taken using the maximum intensity projection function or creating iso-surfaces with Bioptonics Viewer (parameters: 25% iso-surface quality and 50% gaussian smoothing). Iso-surfaces were always compared to the strength and distribution of the original signal to exclude overt manipulation of the result.

Cell death detection using lysotracker

Lysotracker Red DND-99 (Invitrogen) is a fluorescent probe (max absorption 577 nm, max emission 590 nm) conjugated to a weak base. It is highly permeable to membranes and is trapped and accumulates in acidic organelles (mostly lysosomes), providing a specific and sensitive tool for cell death detection. Embryos were dissected in Hank's balanced salt solution (HBSS) and incubated in a pre-warmed solution of HBSS. Lysotracker probe was diluted 1:200, at 37°C in the dark for 45 min. Embryos were incubated in the Lysotracker solution and then washed 5 x 10 min with RT HBSS and fixed ON with 4% PFA in PBS at 4°C in the dark. The day after, samples were dehydrated in methanol through solutions of increasing methanol/PBT ratio, cleared in BABB and imaged at a Leica stereomicroscope. Auto-fluorescence was also captured and used to outline the limb profile with a white dotted line (image processing was performed in Adobe Photoshop®).

Quantitative Real-time PCR (RT-qPCR) analysis

Forelimb pairs were collected and stored in RNAlater (Ambion). Alternatively, embryoid bodies (EBs) were trypsinized and stored in RNAlater. RNA isolation was performed using the RNeasy Micro kit (Qiagen) or by phenol/chloroform extraction with addition of LPA carrier. cDNA was synthetized using Superscript III (Invitrogen). For quantification of transcript levels, the ABI Prism 7000 real time PCR machine and Power SYBR Green PCR Master Mix (Applied Biosystems) were used. Primers are listed in Table 2. The relative quantification cycle values (Cq) were normalized over Cq values of the ribosomal protein L19 (RPL19), which was used as internal standard. The values obtained for samples of mutant limb bud were calculated relative to the mean value obtained from controls set for 100%. Statistical significance was assigned using Mann-Whitney tests and results are reported as mean ± Standard Variation (SD). At least eight samples were used per experiment and each one is represented by a dot.

Table 2. Primers for RT-qPCR

cDNA	Forward primer	Reverse primer
Bmp2	5'-ATGTGGAGACTCTCTCAATG-3'	5'-ACGCTAGAAGACAGCGGTC-3'
Bmp4	5'-AGCCGAGCCAACACTGTGA-3'	5'-GTTCTCCAGATGTTCTTCGTGATG-3'
Bmp7	5'-TGTGGCAGAAAACAGCAGCA-3'	5'-TCAGGTGCAATGATCCAGTCC-3'
Dcn	5'-GCACAGCATAAGTATATCCAGGTCG-3'	5'-GCTCGGCAGAAGTCATTTTGC-3'
Fgf8	5'-GCTAAAACCCAATCTCGGCTAT-3'	5'-AGCATTTTCCAGGTATGCTCAG-3'
Lgals8	5'-TACAAAAGCCAGGCAAGCTCCA-3'	5'-TCGGGCATTGGTGTTCACTTCC-3'
Ncam1	5'-GATATTGTTCCCAGCCAAGGA-3'	5'-TTGGGGGAGAACCAGGAGATGT-3'
RhoC	5'-TGCGATCCGAAAGAAGCTGGTG-3'	5'-CCATCCACTTCGATGTCGGCTA-3'
Rpl19	5'-ACCCTGGCCCGACGG-3'	5'-TACCCTTTCCTCTTCCCTATGCC-3'
Scx	5'-AACACCCAGCCCAAACAGAT-3'	5'-TTCTGTCACGGTCTTTGCTCA-3'
Smad4	5'-TTTCCAATCATCCTGCTCCTGA-3'	5'-AACGTCTCTCCTACCTGAACGTCC-3'
Sox9	5'-TCGACGTCAATGAGTTTGACCA-3'	5'-ATGCCGTAACTGCCAGTGTAGG-3'

Limb bud mesenchymal cell culture

Forelimbs were dissected in ice-cold PBS and digested with 2% trypsin-EDTA for 30 min at 4°C mildly shaking. Single-cell suspension was obtained by pipetting up-and-down in DMEM/F12 medium supplemented with 100 Units/ml penicillin, 100 µg/ml streptomycin and 10% FBS (Gibco-BRL). Cells were centrifuged at 1200 rpm for 5 min, re-suspended at 7.5 x 10^5 cells/ 300µl and seeded into eight-well chamber slides (Ibidi, 300µl per well). Cells were cultured for 48 hr, washed in PBS and fixed in 4% PFA in PBS for 30 min RT. After fixation, cells were washed 3 x 5 min in PBS RT and permeabilized with 0.3% Triton x-100 in PBT, 15 min RT. Blocking was performed in 10% goat serum, 0.3% triton x-100 in PBT, 1 hr RT. Cells were incubated with rabbit polyclonal anti-SOX9 (Millipore) 1:500 and mouse monoclonal anti-collagen type II (Thermo Scientific) 1:200 in 1% goat serum in PBS, ON at 4°C. The day after, cells were washed 3 x 5 min in PBT at RT and incubated with secondary antibody goat anti-mouse Alexa Fluor 488 diluted 1:500 or goat anti-rabbit Alexa Fluor 594 diluted 1:500 in 1% goat serum in PBS, 1 hr at RT in the dark. Cells were washed 3 x 5 min in PBT, counterstained with Hoechst (1 µg/ml) 5 min and washed again, then stored at 4°C in PBS in the dark. Samples were analysed using a SP5 Leica confocal microscope.

General cloning protocols

Restriction digestions of vectors and inserts were performed with restriction enzymes either from Roche or New England Biolabs (NEB). Digestion products were gel-extracted and purified with the QIAquick Gel Extraction Kit (QIAGEN). For vector de-phosphorylation, the rAPID alkaline phosphatase kit (Roche) was used. The T4 ligase (NEB) was used for ligation reaction at RT for 10-15 min or ON at 4°C. Dialysis was accomplished using nitrocellulose MF™-Membrane Filters (Millipore) for 30 min at RT. Electroporation was performed in chemical or electrical competent bacteria (XL1 blue or HB101) using a MicroPulser™ (BioRad). Purification of plasmid DNA from bacteria was performed using the QIAGEN Plasmid Midi Kit or the NucleoBond® Xtra Midi Kit (Macherey Nagel).

Embryonic stem cells (ES cells) and embryonic fibroblasts (EMFI) cultures

ES cell lines were cultured at 37°C in 7.5% CO_2 and checked daily under the microscope for morphological assessment. Medium was replaced every day and cells were split every second day at 1:4, 1:5 or 1:6 according to necessity and type of cell line. ES cells were grown on a layer of EMFIs prepared in the laboratory. An EMFI vial was thawed at 37°C in 10 ml of EMFI medium, spun at 1200 rpm for 5 min and re-suspended in 3 ml of EMFI medium. Cells were then diluted and seeded onto 5 x 10 cm cell culture dishes (BD). They were kept in culture for 2-3 days till they reached confluence and either passaged or mitomycin-treated. For passaging, cells were washed with 4 ml pre-warmed trypsin, 0.05% EDTA (Millipore) and incubated for 5 min at 37°C, collected with 7 ml of EMFI medium, spun and seeded between 1:2 to 1:8 according to necessity. EMFI were passaged maximum twice. EMFIs were growth-arrested by Mitomycin treatment using 10 µg/ml Mitomycin C (Sigma) in EMFI medium for 2 hr. Mitomycin C-treated dishes of confluent EMFIs were used no longer than one week. ES cells were split using pre-warmed trypsin-EDTA (0.05%; Sigma): a first wash was followed by a 15 min incubation at 37°C (3 ml for 10 cm dishes and 2 ml for 6 cm dishes). ES cells were then pipetted up-and-down (7-10 times) to prepare a single-cell suspension, ES cell medium added (7 ml for 10 cm dishes and 4 ml for 6 cm dishes) and cells pipetted up-and-down 4-5 times for blocking the trypsin digestion. Pre-plating for 15 min allowed most EMFIs to attach to the dish. Cells in suspension were collected and spun 1200 rpm for 5 min. Cells were re-suspended in fresh media and plated.

Alternatively gelatin-coated plates were used. To this end, a 0.1% solution of gelatin in water (Sigma) was autoclaved and stored sterile for up to 4-5 months at RT. Cell culture

dishes were treated with gelatin for 5-10 min at RT and left to dry for an additional 5-10 min before use. ES cells were frozen in freshly-prepared pre-cooled ES cell freezing media; about 5-6 1.5 ml pre-cooled NUNC Cryovials were filled with 1.5 ml of ES cell suspension collected from a 10 cm culture dish, stored ON at -80°C and moved to liquid nitrogen the day after. ES cells were thawed at 37°C in a water bath; cells were then resuspended in 10 ml ES cell medium, spun and resuspended in fresh ES cell medium for seeding onto culture dishes.

Media for ES cell and EFMI:

- ES cell medium

DMEM + 4.5g/l Glucose (Gibco 41966029)	500 ml	
Hyclone Fetal Calf Serum (FCS)	94 ml	(15%)
Penicillin-Streptomycin (100u-0.1mg/ml) (Gibco 15140-122)	6.25 ml	
L-Glutamin (200mM) (Gibco 25030-024)	6.25 ml	
β Mercapto-Ethanol (Gibco 31350-010)	1.25 ml	
Leukemia Inhibitory Factor (LIF) (10^7U/ml) (EsGRO LIF ^{TM} Gibco 13275-029)	62.5 µl	
Non Essential Amino Acids (100X) (Gibco 11140-035)	10 ml	
Sodium Pyruvate (100mM) (Gibco 11360-039)	10 ml	

FCS (tested for germ-line transmission) was 0.22 µm filtered (NOT heat-inactivated).

- EMFI medium

DMEM + 4.5g/l Glucose (Gibco 41966029)	500 ml	
FCS (same as for ECS medium)	58 ml	(10%)
Penicillin-Streptomycin (100U-0.1mg/ml) (Sigma P-0781)	5.8 ml	
L-Glutamin (200mM) (Sigma G-7513)	5.8 ml	

- ES cell freezing medium

40% FCS (cold)

10% DMSO (Sigma D-8418)

Cold 50% ES medium (- LIF; cold)

Filtered with syringe and kept cold until use.

Embryoid body (EB) culture

$2x10^4$ ES cells were incubated in a loosened-cap conical polypropylene 1.5ml screw cap micro tube (Sarstedt) in 1ml of differentiation medium (ES cell medium – see above - without LIF) for 5 days at 37°C, 5% CO_2 to obtain EBs according to the established protocol (Kurosawa et al., 2003). The EBs were then transferred to a gelatin-coated IBIDI chamber (suited to confocal imaging) and cultured in differentiation medium for up to 12 days at 37°C, 5% CO_2.

Statistics

The statistics used to quantitatively assess the experimental results are specified in the relative sections or in the Figure legends. Prism (GraphPad) and/or Excel (Microsoft) were used for statistical analysis and graphic design.

Note: the reproducibility of all results was assessed in at least (i.e. minimally) three independent experiments.

Additional and general solutions

- Pre-hybridization mix

50% formamide (deionized, extra pure)

5x SSC pH 4.5

2% Blocking Powder (Roche Cat. No. 1096176)

0.1% Tween-20

0.5% CHAPS (Sigma)

50 µg/ml yeast RNA (Sigma R-8759)

5 mM EDTA

50 µg/ml heparin (Sigma H5515)

- Post-hybridization mix

50% formamide (deionized, extra pure)

5x SSC pH 4.5

0.1% Triton x-100

0.5% CHAPS (Sigma)

- 20x SSC, pH 4.5

3M NaCl

0.3 M Na_3citrate:$2H_2O$

Adjust pH to 4.5 with 1M HCl

- Maleic Acid Buffer

100 mM maleic acid

150 mM NaCl

Adjust pH to 7.5

- TBST

140 mM NaCl

2.7 mM KCl

25 mM Tris HCl, pH 7.5

1% Tween-20

- NTMT (prepared fresh)

100 mM NaCl

100mM Tris 9.5

50 mM $MgCl_2$

1% Tween-20

- TNT

50 mM Tris HCl pH 7.5

150 mM NaCl

0.1% Triton x-100

- NMT

100 mM Tris HCl pH 9.5

100 mM NaCl

50 mM $MgCl_2$

- Blocking solution for OPT-oriented protocol

6.5 % goat serum

2% (w/v) BSA

50 mM Tris HCl pH 7.5

150 mM NaCl

0.1% Triton x-100

- Immunowash solution

1% (w/v) BSA

1% dimethyl sulfoxide (DMSO)

1% Triton x-100

0.1% Tween-20

Bring to volume with PBS

7. RESULTS

Some of the results contained in this section have been published in:

Benazet, J.D.*, E. Pignatti*, A. Nugent, E. Unal, F. Laurent, and R. Zeller. 2012. **Smad4 is required to induce digit ray primordia and to initiate the aggregation and differentiation of chondrogenic progenitors in mouse limb buds.** *Development*. 139:4250-4260. * First co-authors.

Conditional inactivation of *Smad4* in the limb bud mesenchyme

Space- and time-restricted inactivation of *Smad4* allowed us to study BMP signaling requirements in a focused manner and, at the same time, to target the canonical BMP pathway in a global fashion, avoiding complex genetic experiments based on inactivating multiple ligands or receptors.

Prx1-Cre-mediated inactivation of *Smad4* in the limb mesenchyme (*Smad4*$^{\Delta/\Delta M}$) led to the formation of stunted paddle-like limb structures (Fig. 1A). In addition, gross morphological analysis of *Smad4*$^{\Delta/\Delta M}$ mutant embryos revealed reduced liver size and the formation of a sub-epithelial edema dorsally to the neural tube at E14.5 (Fig.1A). Skeletal preparations showed that both forelimbs and hindlimbs were devoid of skeletal elements, with the exception of a remnant of the pelvis at E14.5 (Fig. 1B), whereas the axial skeleton was unaffected. The residual pelvis skeletal element was likely a consequence of the delayed activation of the *Prx1-Cre* transgene in the hindlimb mesenchyme (between E9.5 and E10.5) in comparison to the forelimb mesenchyme (E9.25; Logan et al., 2002). Since this initial analysis suggested a late-onset phenotype, we looked at the clearance of *Smad4* transcripts and products. We noted that recombination of *Smad4* occurs around E9.5 in the forelimb mesenchyme, whereas levels of *Smad4* in the paraxial mesoderm are also reduced due to the presence of a constitutive null allele (Fig. 1C). Whole-mount immunofluorescence revealed that SMAD4 protein was cleared from the forelimb mesenchyme at about E9.75 (Fig. 1D). As expected, recombination of *Smad4* did not occur in the ventral ectoderm and SMAD4 proteins maintained in the ectoderm (Fig. 1D, arrowheads in central and right-most panels). In addition, the expression of *Msx2*, which is a well-established BMP signaling readout (see Introduction), was down-regulated in the mesenchyme by E10.0 (Fig. 1E); the residual *Msx2* expression is likely due to long-lived transcripts.

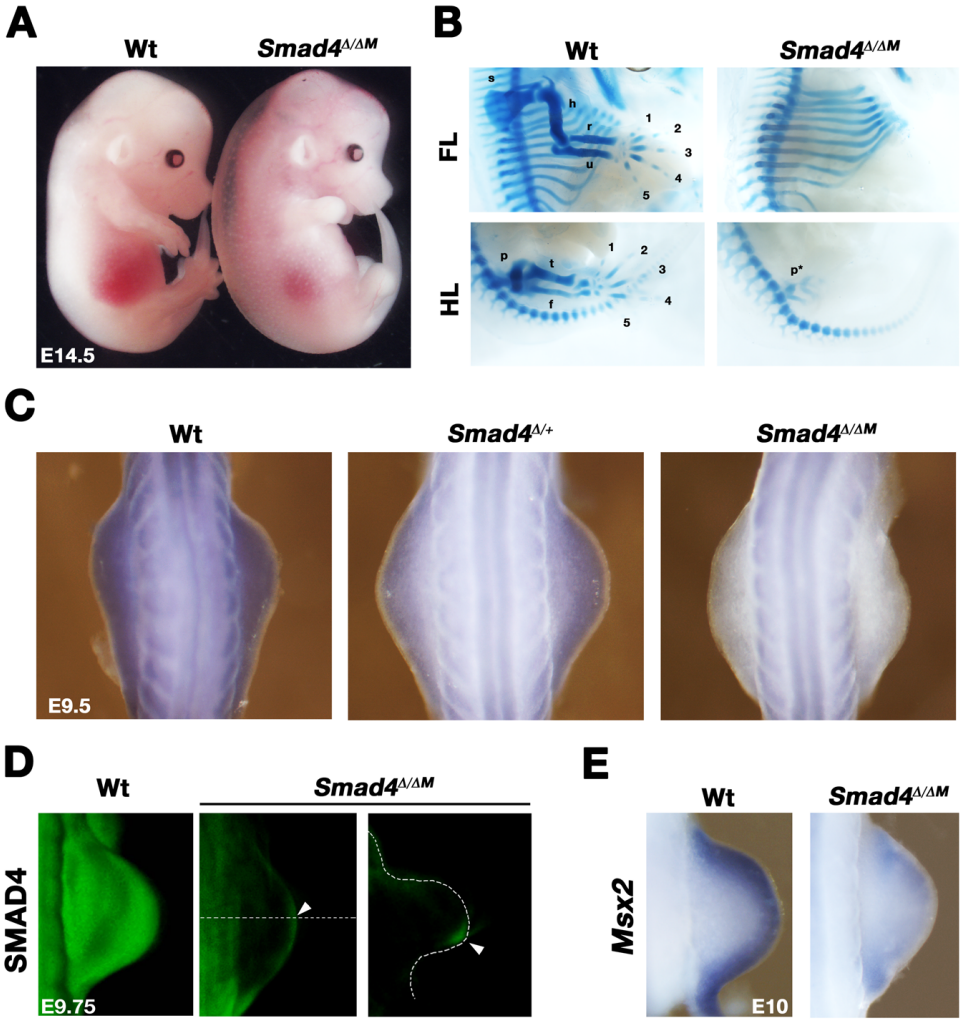

Fig.1. *Smad4* inactivation in the limb mesenchyme driven by *Prx1-Cre* transgene. (A) Dark-field picture of whole embryo at day E14.5 allows gross morphological analysis of *Smad4*$^{\Delta/\Delta M}$ phenotype; stunted paddle-like structures replace the elongated wild-type limb and no finger primordia appear in the mutant (experiment by J.D.B.). **(B)** Alcian blue-stained skeletal preparations at E14.5 reveal the absence of any forelimb and hindlimb skeletal structure in the *Smad4*$^{\Delta/\Delta M}$ mutant embryos, apart from a remnant of pelvis skeleton (experiment by J.D.B.). **(C)** WISH with a *Smad4* probe covering exon 8, which is deleted in the adopted *Smad4*$^{\Delta}$ allele. At 23-24 somites, amounts of *Smad4* transcripts in the forelimbs correlate with the number of wild-type alleles (experiment by J.D.B.). **(D)** OPT rendering of a whole-mount immunofluorescence experiment on forelimbs at 29 somites (wild-type) and 27 somites (*Smad4*$^{\Delta/\Delta M}$), showing deletion of SMAD4 proteins in the mutant mesenchyme and persistence of proteins in the ventral ectoderm (white arrowheads) with respect to the wild-type limb. The dotted line in the central panel indicates the approximate position of the OPT virtual section shown in the right-most panel. **(E)** *Msx2* gene transcripts are detected as readout of BMP signaling activity in the *Smad4*$^{\Delta/\Delta M}$ mutant in

comparison to the wild-type forelimb at 30 somites. 1-5: digit identities; r: radius; u: ulna; h: humerus; s: scapula; t: tibia; f: fibula; p: pelvis. FL: forelimb; HL: hindlimb.

Smad4 functions as part of the SHH/GREM1/FGF feedback loop

Previous studies revealed that the expression of *Grem1* depends on both *Bmp4* and *Shh* (see Introduction and Benazet et al., 2009). In light of this, we sought to understand whether BMP4-driven signaling was mediated by canonical SMAD4-transduced pathway during patterning of the forelimb. Conditional inactivation of *Smad4* in the limb mesenchyme led to down-regulation of *Grem1* transcripts, and particularly impaired the anterior expansion of its expression (Fig. 2A, panels on the left). *Grem1* expression levels were also down-regulated upon constitutive inactivation of *Shh* (see Chiang et al., 2001). In addition, $Shh^{\Delta/\Delta}$ forelimbs exhibited ectopic expression of *Grem1* in the proximal posterior-most forelimb domain, partially overlapping the *Shh* and *Tbx2* expression domains (see e.g. Farin et al., 2013 for Tbx2 expression domain). We found that compound inactivation of *Shh* and *Smad4* results in loss of *Grem1* expression, revealing that *Smad4* is required for the *Shh/Grem1/Fgf4* feedback loop (Fig. 2A, left-most panel).

The AER-*Fgf4/8* domains in the $Smad4^{\Delta/\Delta M}$ limb buds are enlarged along the D-V axis in comparison to wild-type controls (Fig. 2A, right panels), which points to a defect in AER compaction. Quantitative transcript analysis revealed the up-regulation of *Fgf8* expression in $Smad4^{\Delta/\Delta M}$ limbs at E10.5 (Fig. 2E). *Shh* inactivation results in down-regulation of *Fgf8* expression levels and clearance of *Fgf4* transcripts (Chiang et al., 2001). The additional inactivation of *Smad4* in the mesenchyme did not further alter AER-*Fgf8* and *Fgf4* expression in the $Shh^{\Delta/\Delta}$ genetic background.

We also noticed that the *Shh* transcription domain was expanded proximally in the $Smad4^{\Delta/\Delta M}$ limb bud mesenchyme (Fig. 2B, black arrowhead), likely as a consequence of the proximal expansion of AER-FGF domain (Fig. 2A, dorsal view of *Fgf8* expression in the $Smad4^{\Delta/\Delta M}$ mutant background).

Analysis of later stages (E11.75 and E12.5) showed that *Shh*, *Fgf4* and *Fgf8* transcripts were maintained in the $Smad4^{\Delta/\Delta M}$ limb for longer than in the wild-type controls (Fig. 2C,D; see arrowheads). This is indicative of delayed termination of the SHH/GREM1/AER-FGF feedback loop. Indeed, *Shh* expression was stronger in the $Smad4^{\Delta/\Delta M}$ mutant forelimb buds with respect to wild-type controls at E11.75 (Fig. 2C, upper panels); at E12.5, $Smad4^{\Delta/\Delta M}$ limb buds showed a residual posterior-proximal domain of *Shh* expression (Fig. 2C, lower panels, see black arrowhead). Similarly, expression of *Fgf4* transcripts, which was terminated around E11.75 in the wild-type,

persisted in an anterior domain in mutant forelimb buds (Fig. 2D, upper panels). Furthermore, *Fgf8* expression was also prolonged in comparison to matched wild-type forelimb buds (Fig. 2D, lower panels).

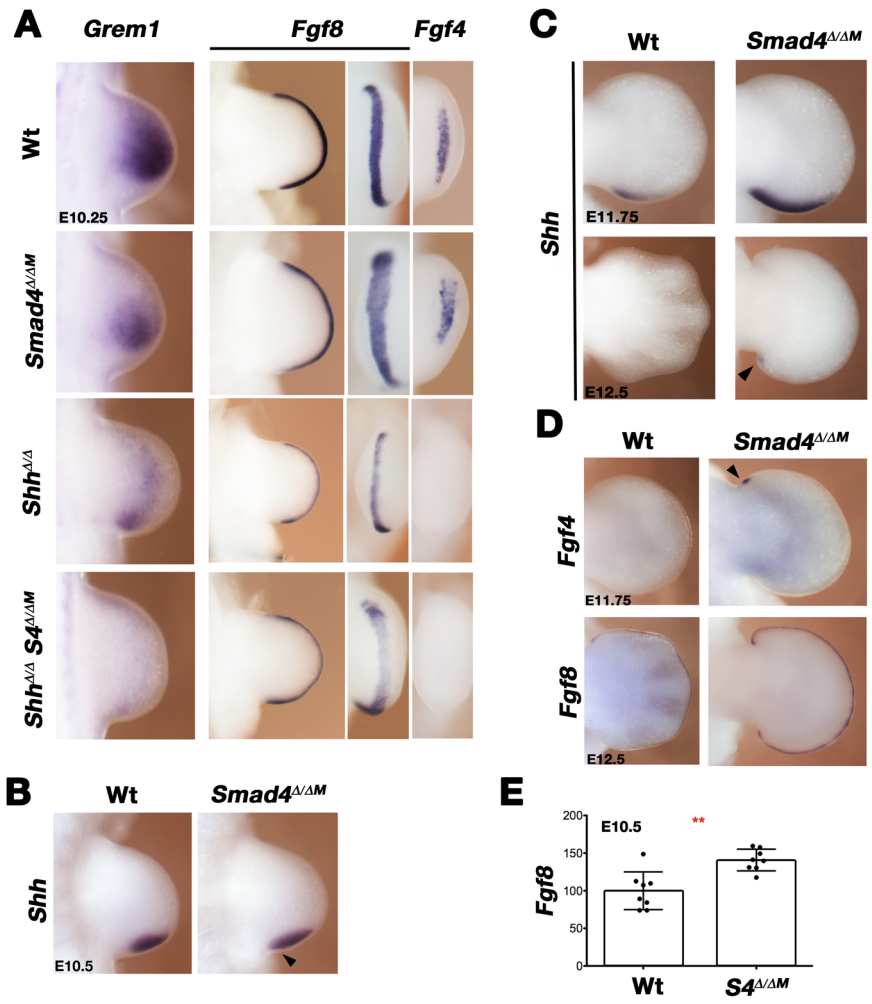

Fig. 2. Genetic involvement of mesenchymal *Smad4* in the SHH/GREM1/AER-FGF feedback loop. (A) (From left to right) *Grem1*, *Fgf8*, *Fgf4* transcripts expression in wild-type, *Smad4*$^{\Delta/\Delta M}$, *Shh*$^{\Delta/\Delta}$ and *Smad4*$^{\Delta/\Delta M}$*; Shh*$^{\Delta/\Delta}$ forelimbs at E10.25 (31-35 somites). For *Fgf8* probe, a dorsal and AER-oriented view are reported. *Fgf4* signal is only depicted from the AER. **(B)** *Shh* expression in wild-type and *Smad4*$^{\Delta/\Delta M}$ forelimbs at 35 somites. The arrowhead points at proximal expansion of *Shh* domain in the mutant limb. **(C)** *Shh* expression at E11.75 (50 somites, upper panel) and E12.5 (60 somites, lower panel) in wild-type and *Smad4*$^{\Delta/\Delta M}$ mutant forelimbs. The black arrowhead points at the delayed termination of *Shh* transcripts in the mutant limb. **(D)** Delayed termination of *Fgf4* and *Fgf8* transcripts (upper panel – 50 somites - and lower panel – 60 somites -, respectively) in wild-type and *Smad4*$^{\Delta/\Delta M}$ forelimbs. Black arrowhead points at residual *Fgf4*

transcripts in the anterior-proximal region of mutant forelimb. **(E)** *Fgf8* transcript levels quantified by RT-qPCR in E10.5 (~35 somites) forelimbs from wild-type and *Smad4*$^{\Delta/\Delta M}$ mutant embryos. Expression is significantly higher in the mutant samples (P≤0.01). Data are shown as mean ± SD. All the experiments of this figure were performed by J.D.B. apart from *Fgf4* and *Fgf8* panels shown in (A).

Expression of BMP ligands depends on Smad4 in the mesenchyme

We wondered whether *Smad4* is required in the mesenchyme to modulate the expression of BMP ligands. We then used WISH and RT-qPCR quantification on E10.5 forelimbs to analyze the expression of BMP ligands. We observed that *Bmp2* transcripts were up-regulated in the posterior domain and down-regulated in the AER of *Smad4*$^{\Delta/\Delta M}$ limb buds (Fig. 3A). Both *Bmp4* and *Bmp7* were slightly up-regulated in mutant limb buds, although their spatial distribution was unchanged. RT-qPCR quantification revealed significant up-regulation of *Bmp7* transcripts, while *Bmp4* levels were not significantly altered (Fig. 3B,C). Altogether, these results point to the possible presence of a *Smad4*-dependent feedback loop regulating the expression of BMP ligands.

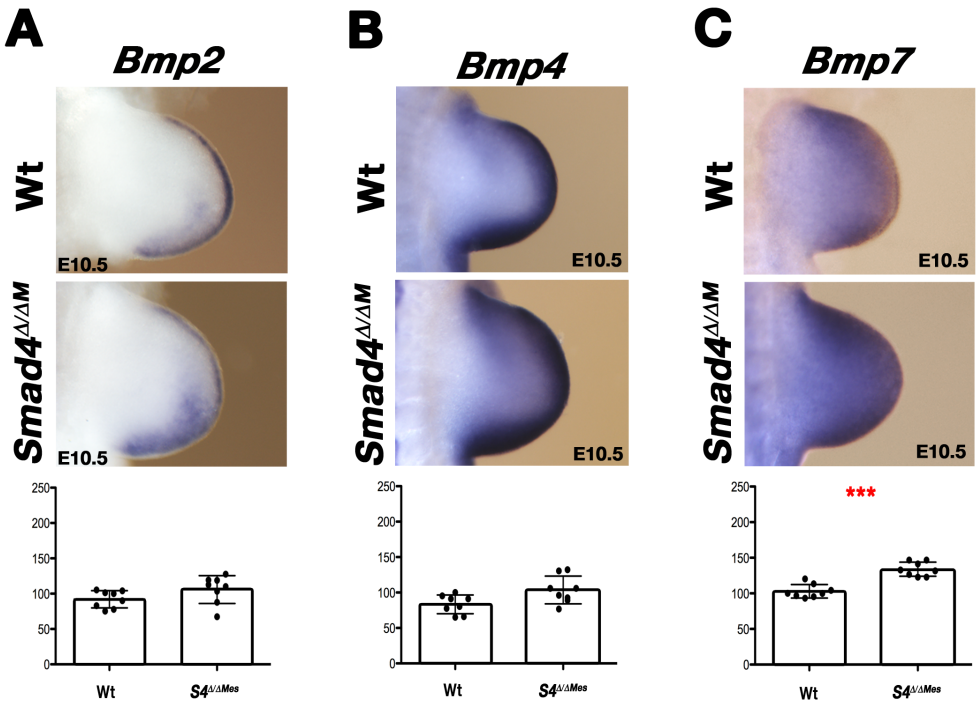

Fig. 3. Effects of mesenchymal inactivation of *Smad4* on BMP ligands. (A,B,C) BMP ligands were quantified in wild-type versus *Smad4*$^{\Delta/\Delta M}$ mutant forelimbs by WISH (upper panels) and by RT-qPCR (lower panels) at E10.5 (~35 somites). RT-qPCR results are reported as mean ± SD. Three-stars indicate significance at P≤0.001. *S4*$^{\Delta/\Delta M}$: *Smad4*$^{\Delta/\Delta M}$.

Analysis of A-P axis development in mouse limb buds lacking mesenchymal *Smad4* expression

Mesenchymal inactivation of *Bmp4* by *Prx1-Cre*^{Tg} results in anterior expansion of posterior genes and down-regulation of anterior genes in mutant limb buds (Selever et al., 2004). Thus, we wondered to which extent the mesenchymal *Smad4* deficiency would phenocopy the *Bmp4* inactivation. We looked at the SHH-dependent *Gli1* and *Ptch1* transcripts in the posterior-most limb region and at *Alx4* transcripts in the anterior-most region in *Smad4* mutant limb buds at E10.5 (Fig. 4A,B). We noted that the *Gli1* expression pattern was unchanged, while *Ptch1* and *Alx4* transcripts were slightly down-regulated. *Ptch1* transcripts were also more distally restricted (Fig. 4A). In the hindlimb, both posterior markers were more distally restricted, whereas *Alx4* transcripts were extended slightly more posterior (Fig. 4B). Altogether, molecular analysis revealed minor alterations, but failed to show major alterations in A-P axis development.

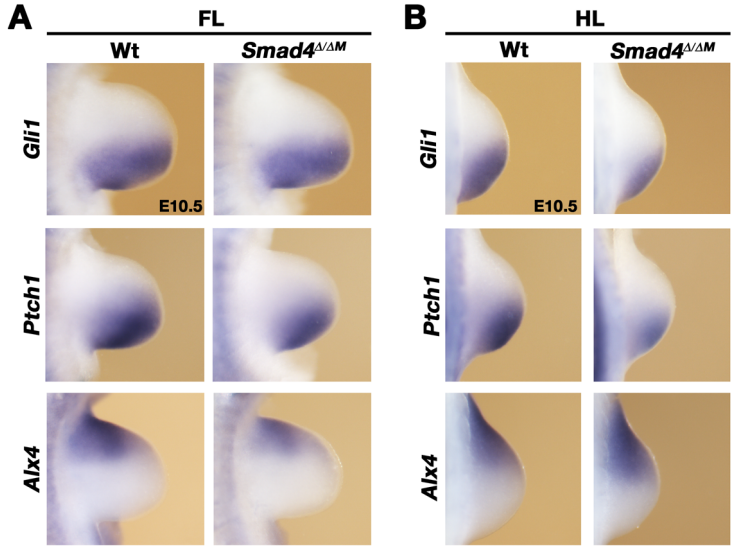

Fig. 4. Analysis of A-P axis upon mesenchymal inactivation of *Smad4*. SHH-dependent *Gli1* and *Ptch1* genes associated with posterior limb compartment and *Alx4* in the anterior compartment were analyzed in wild-type and *Smad4*$^{\Delta/\Delta M}$ mutant limb buds (at 37, 36 and 35 somites, respectively). **(A)** In the forelimbs, *Gli1* expression pattern (upper panel) is unchanged. Conversely, *Ptch1* transcript levels in the posterior and *Alx4* transcripts in the anterior limb are slightly down-regulated (middle and lower panels). **(B)** In hindlimb buds both *Gli1* and *Ptch1* transcript levels are slightly reduced while *Alx4* expression is slightly expanded. FL: forelimb; HL: hindlimb.

Smad4 inactivation in the autopod primordia

The *Hoxa13-Cre* knock-in transgene (*Hoxa13-Cre^{Tg}*) drives Cre recombinase expression in the prospective forelimb autopod starting at about 36 somites (see Material and Methods). The activity of the *Hoxa13-Cre^{Tg}* is restricted to the autopod in forelimb buds, whereas it is also active in the lateral mesoderm at the level of the hindlimb bud (see Material and Methods; see Scotti and Kmita, 2012). Therefore, only forelimb buds were analyzed. *Hoxa13-Cre^{Tg}*-mediated inactivation of *Smad4* was used to temporally uncouple the patterning phase of low BMP signaling (between ~28 to ~38 somites) from a later phase in which BMP signaling rises to induce mesenchymal condensations and modulate (see Introduction). We generated two mutant embryo models that either carry one or two conditionally inactivated alleles (*Smad4$^{\Delta/\Delta A13}$*; *Smad4$^{\Delta A13/\Delta A13}$*, respectively). Apart from a glove-like handplate, no additional abnormalities were detected in *Smad4$^{\Delta/\Delta A13}$* embryos at E14.5 (Fig. 5A). *Smad4$^{\Delta/\Delta A13}$* and *Smad4$^{\Delta A13/\Delta A13}$* embryos at E14.5 showed no carpal, metacarpal and phalangeal bones (Fig. 5B) and no additional differences were detected between the two mutant genotypes.

We found that *Smad4* expression was cleared slightly before 38-somite stage in the distal and posterior mesenchyme (Fig. 5C, left-most panel). This clearance of *Smad4* transcripts expanded anteriorly in the distal mesenchyme, eventually encompassing the entire autopod primordia by 50 somites (Fig. 5C, central and right-most panels). As expected, *Smad4* transcripts remained expressed in the proximal limb bud mesenchyme, where the *Hoxa13-Cre^{Tg}* allele is not expressed (Fig. 5D). Because two conditional alleles have to be inactivated in *Smad4$^{\Delta A13/\Delta A13}$* autopod primordia, we expected the SMAD4 clearance to be slower than in the *Smad4$^{\Delta/\Delta A13}$* handplates. This should allow us to study the potential differential requirements of *Smad4* over a narrow time window during limb bud development.

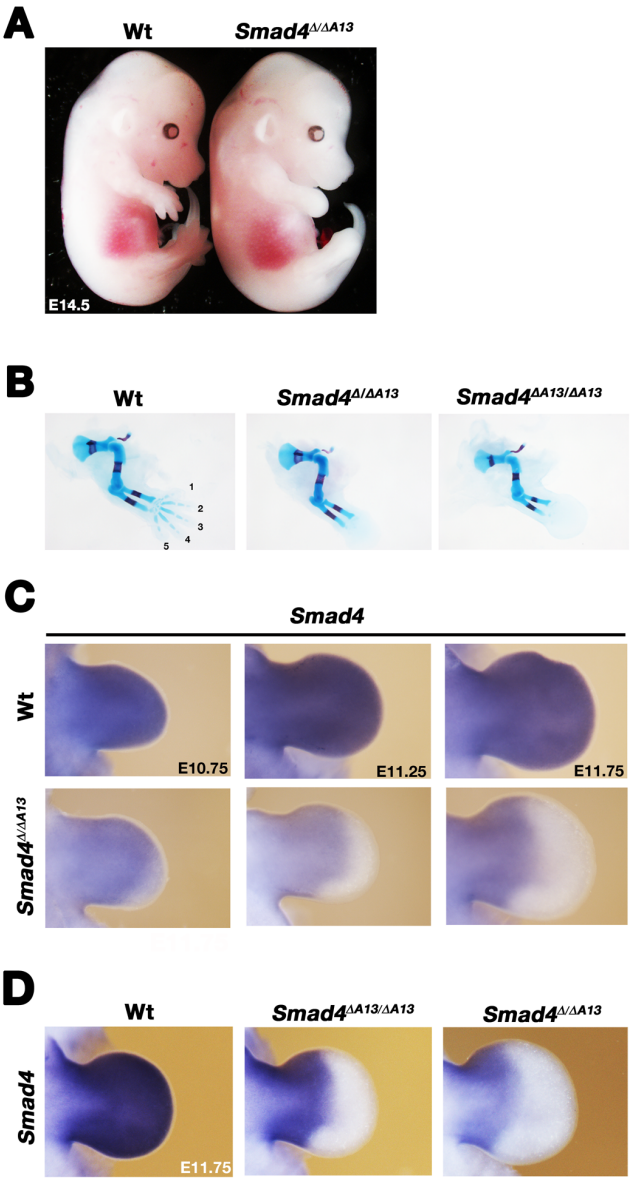

Fig. 5. *Smad4* inactivation in the limb autopod at late stages driven by *Hoxa13-Cre* knock-in transgene. (A) Bright-field picture of whole embryo at E14.5 reveals the absence of finger-like appendages in the *Smad4*$^{\Delta/\Delta A13}$ mutant handplates (experiment by J.D.B.). **(B)** Alcian-blue and Alizarin-red stained skeletal preparations at E14.5 show that carpal, metacarpal and phalangeal bones are missing in the *Smad4*$^{\Delta/\Delta A13}$ and *Smad4*$^{\Delta A13/\Delta A13}$ mutant forelimbs (lower panels). **(C)** WISH with *Smad4* probe outlines the kinetics of *Hoxa13-Cre*-driven recombination in the forelimb at the stage of 39 somites (left-most panel), 41 somites (central panel) or 50 somites (right-most panel) in the *Smad4*$^{\Delta/\Delta A13}$ genetic background. **(D)** *Smad4* transcripts in the prospective autopod (distal-most part of the limb) are cleared in both *Smad4*$^{\Delta/\Delta A13}$ and *Smad4*$^{\Delta A13/\Delta A13}$ mutant forelimbs at the stage of 50 somites (central and right-most panels). *Smad4* transcript levels in the proximal part of the limb, where *Hoxa13-Cre*^{Tg} is not active, are dependent on the absence or presence of a constitutive null *Smad4* allele. 1-5: digit identities.

Smad4 is necessary for initiating chondrogenic differentiation and formation of digit rays

Since *Smad4*$^{\Delta/\Delta M}$ mutant forelimbs did not develop any skeleton, we determined if *Sox9*-expressing chondrogenic progenitors were affected at early stages of limb bud development. In *Smad4*$^{\Delta/\Delta M}$ mutant forelimbs, the *Sox9* expression pattern was mostly unchanged in comparison to the wild-type controls until E11.0 (Fig. 6A, two left-most panels). At E11.5 the donut-like expression of *Sox9* in wild-type limb buds was broken into a proximal element and a distal half-moon shape in *Smad4*$^{\Delta/\Delta M}$ mutant forelimb buds.

This altered pattern remained at E12.25, while the *Sox9* transcripts outlined the digit primordia in wild-type controls (Fig. 6A, two right-most panels). Moreover, the *Sox9* expression pattern was overall proximalized in the absence of mesenchymal *Smad4*, likely due to increased FGF signaling by the AER (Fig. 6A, second-last images from the right, white brackets). OPT image analysis showed the increase of *Sox9*-positive chondrogenic precursors in the prospective stylopod element and the concurrent thinning of the distal-most *Sox9* domain in the mutant forelimbs (Fig. 6B, white arrowheads and brackets). In the absence of mesenchymal *Smad4*, *Sox9* transcripts never extended to the distal limb bud where the digit primordia appear by E12.0 (Fig. 6B, right-most panels).

To gain further insight, we used the *Hoxa13-Cre^{Tg}* knock-in transgene to study the *Smad4* requirement directly during handplate development and specification of digit primordia between around 36- to 40-somites (E10.75 – E11.0). We first established that the knock-in *Hoxa13-Cre^{Tg}* transgene did not result in a phenotype on its own or in combination with one conditional *Smad4* allele (Fig. 6C, two left-most panels). In *Smad4$^{\Delta A13/\Delta A13}$* mutant limb buds, four *Sox9*-positive digit primordia formed, while only the two posterior-most digit primordia formed in the *Smad4$^{\Delta/\Delta A13}$* limb buds (Fig. 6C, two right-most panels). We inferred that the two posterior digit primordia are either specified earlier than the anterior primordia, or require *Smad4* for a shorter time. This analysis reveals the tight time frame in which digit primordia depend on *Smad4* for specification of their chondrogenic fate.

In *Bmp2$^{\Delta M/\Delta M}$*; *Bmp4$^{\Delta M/\Delta M}$* double mutant limb bud, the *Sox9*-positive primordia for the two posterior-most digits fail to form (see Bandyopadhyay et al., 2006). We reproduced this result, looking at 50-somite forelimbs. Consistently with previous results, *Sox9* was not expressed in the posterior forelimb domain and only anterior *Sox9*-positive digit rays formed (Fig. 6D, panels on the left). Moreover, *Decorin* (*Dcn*) transcripts, which encode a small leucine-rich proteoglycan that regulates the assembly of non-chondrogenic collagen fibers (Danielson et al., 1997), label the region of the posterior digit primordia in the *Bmp2$^{\Delta M/\Delta M}$*; *Bmp4$^{\Delta M/\Delta M}$* mutant forelimb, whereas in the anterior digit rays *Dcn* is no longer expressed (Fig. 6D, two right-most panels).

To understand whether the autopod was specified in the absence of mesenchymal *Smad4* we analysed the expression of *Hoxa13.* The spatial distribution of the *Hoxa13* transcripts (labeling the prospective autopod) was not altered in *Smad4* mutant limb buds, but digit and interdigit domains (labeled by *Cyp26b1* and *Dlx5*, respectively) were lost (Fig. 6E), consistent with the failure to form digits in *Smad4$^{\Delta/\Delta M}$* mutant limb buds.

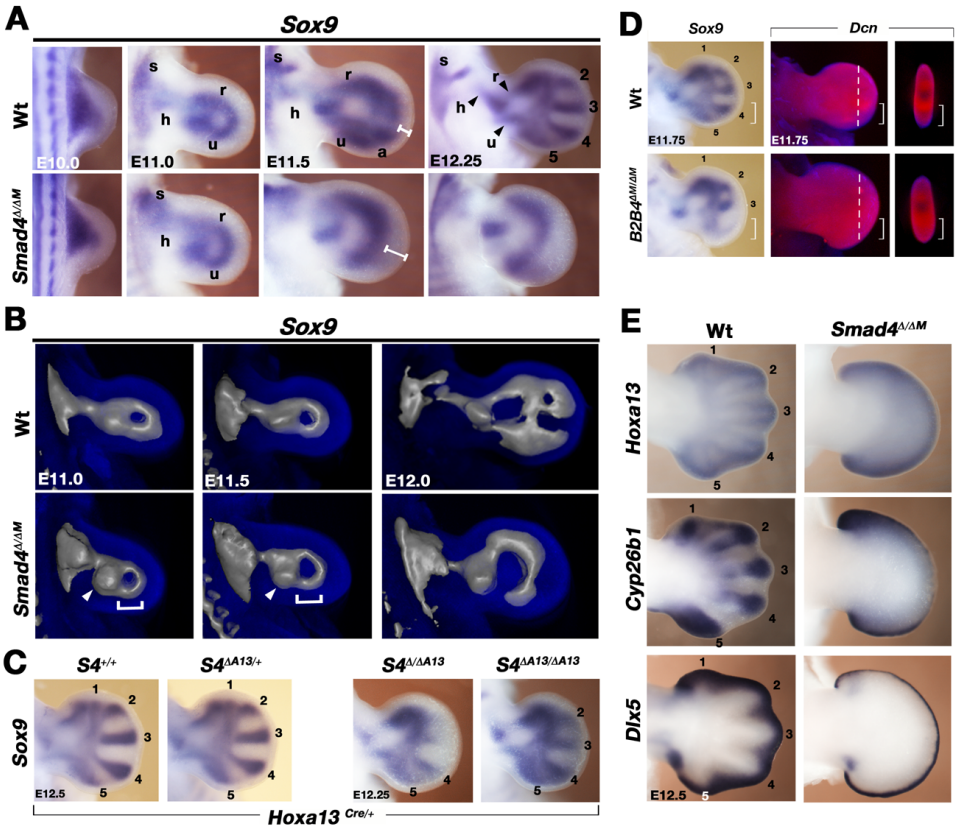

Fig. 6. *Smad4* regulates *Sox9*-mediated chondrogenic specification in digit primordia. (A) WISH time-course (from E10 to E12.25) for *Sox9* transcripts in wild-type and *Smad4*$^{\Delta/\Delta M}$ mutant forelimbs. White bars span the distance between the distal-most *Sox9* expression domain and the AER. Experiment performed by J.D.B. **(B)** Iso-surface OPT rendering of the *Sox9* expression domains in wild-type and *Smad4*$^{\Delta/\Delta M}$ mutant forelimbs at E11 (41 somites), E11.5 (44 somites) and E12 (52 somites). White brackets mark the length of the arch that *Sox9* expression pattern outlines in the limb core. White arrows point at a proximal element specified by *Sox9* expression, most likely corresponding to the prospective stylopod. **(C)** Spatial distribution of *Sox9* in the digit primordia of E12.5 forelimbs from *Hoxa13-Cre*^{Tg}-positive embryos carrying different combinations of conditional or constitutive *Smad4* alleles. The two left-most pictures were taken by J.D.B. **(D)** On the left panels, *Sox9* expression pattern in wild-type and *Bmp2*$^{\Delta M/\Delta M}$;*Bmp4*$^{\Delta M/\Delta M}$ forelimbs at E11.75 (50 somites); in the middle panels, OPT-captured expression pattern of *Dcn* on wild-type and *Bmp2*$^{\Delta M/\Delta M}$;*Bmp4*$^{\Delta M/\Delta M}$ mutant forelimbs at about 50 somites from a dorsal view. The white broken line represents the approximate levels at which the artificial sections from an AER-oriented view are taken in the panels on the right. Brackets indicate the posterior-most part of the limb, to highlight the differences in *Dcn* expression between wild-type and *Bmp2*$^{\Delta M/\Delta M}$;*Bmp4*$^{\Delta M/\Delta M}$ limbs. **(E)** Spatial distribution of *Hoxa13*, *Cyp26b1* and *Dlx5* transcripts in wild-type and *Smad4*$^{\Delta/\Delta M}$ mutant forelimbs at E12.5 (experiment performed by J.D.B). s: scapula; h: humerus; r:radius; u:ulna; 1,2,3,4,5: identities of the digit primordia.

Smad4 is required for cell aggregation and initiation of chondrogenic differentiation

We established a high-cell density *in vitro* culture system for an in-depth analysis of the dynamic properties and molecular features of limb bud mesenchymal cells lacking *Smad4*. Wild-type limb bud cells cultured for 48 hrs (obtained from E11.5 embryos), formed cellular aggregates that express the SOX9 protein and COL type II in the core (Fig. 7A). In contrast, *Smad4*-deficient cells did not form aggregates and did not produce COL type II protein. Furthermore, mutant cells did not maintain the expression of SOX9, which appeared down-regulated in comparison to wild-type controls (Fig. 7B). Next, we treated wild-type derived high-density cultures with two small molecule inhibitors, dorsomorphin and SB431542, that specifically block either BMP- or TGFβ-specific receptor activity, respectively (Yu et al., 2008; Inman et al., 2002). Both treatments resulted in phenotypes similar to the ones of limb bud mesenchymal cells lacking *Smad4* (compare results in Fig.7 and Fig.8). Taken together, this analysis shows that both BMP and TGFβ receptor-driven pathways are fundamental for cell aggregation, early chondrogenic differentiation (COL type II expression) and maintenance of SOX9 expression (Fig. 8A,B,C).

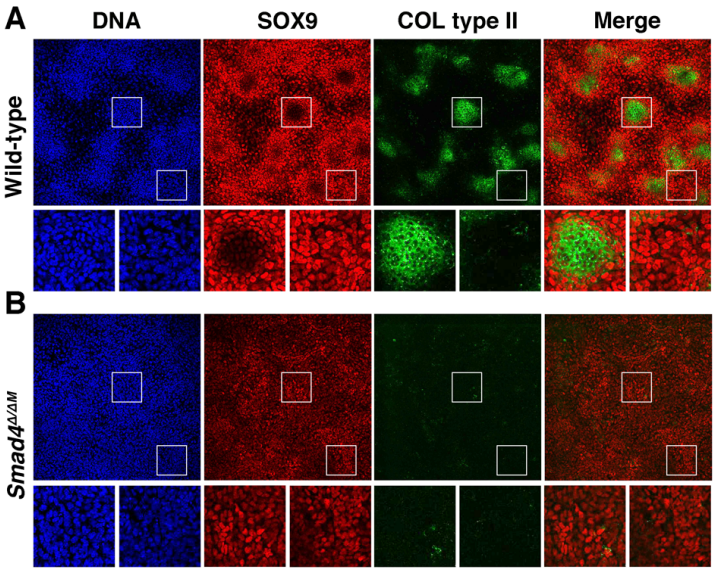

Fig. 7. Mesenchymal Smad4 is fundamental for formation of aggregates, chondrogenic differentiation and maintenance of SOX9 in a cell-based model. (A) Immunofluorescence using high-density cultures at 48 hrs (mesenchymal cells obtained from limbs at E11.5) reveals aggregates outlined by SOX9 (red) and marked by COL type II (green) expression in wild-type samples. **(B)** High-density culture performed using *Smad4*$^{\Delta/\Delta M}$ cells results in reduced SOX9 expression, impaired cell aggregation and differentiation. White rectangles indicate the positions of the enlargements shown below. (Experiment performed by Frédéric Laurent).

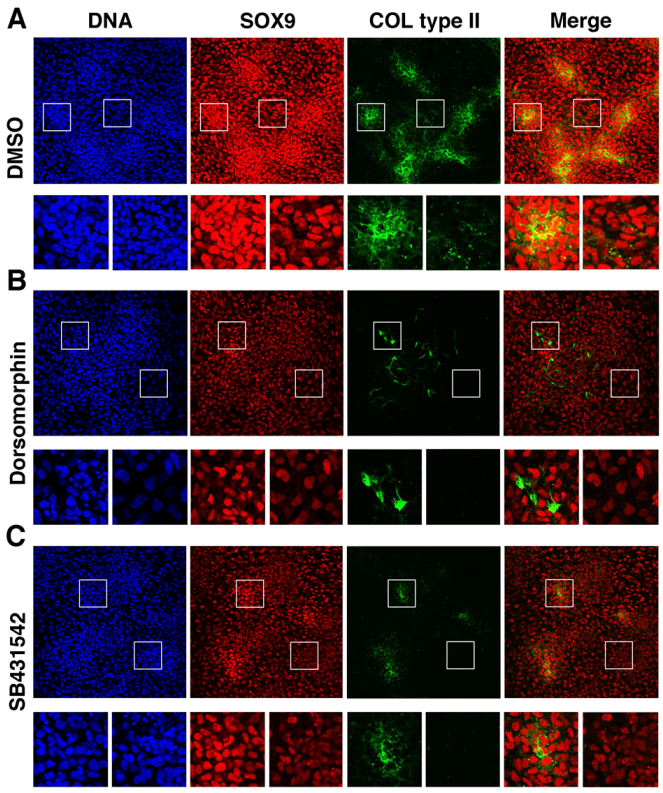

Fig. 8. Small-molecule treatment of a high-density culture system reveals the importance of both BMP and TGFβ receptors for initiation of chondrogenesis. (A) Immunofluorescence on 48-hours high-density culture (mesenchymal cells obtained from limbs at E11.5) reveals aggregates outlined by SOX9 (red) and marked by COL type II (green) expression in the wild-type samples in the presence of 0.1% DMSO (same solvent concentration used for experiments in panels B and C). **(B,C)** When high-density cultures are treated either with Dorsomorphin (10μM, inhibitor of BMP receptors) or SB431542 (10μM, inhibitor of TGFβ receptors), aggregation and chondrogenic differentiation are impaired, and SOX9 expression is not maintained. White rectangles indicate the positions of the enlargements shown below.

Smad4 controls chondrogenic differentiation and restricts non-chondrogenic cell fates

The potential role of *Smad4* in regulating limb cell fates was assessed by analyzing the distribution of specific markers for different cell lineages specification. *Col2a1* is activated downstream *Sox9* and marks cells that undergo chondrogenic differentiation (e.g. during formation of digit primordia), whereas *Col1a2* expression marks connective tissues such as skin, tendons, ligaments and muscle-associated connective tissues (Fig. 9A, upper panels; see Introduction). Upon mesenchymal inactivation of *Smad4, Col2a1* transcripts were down-regulated in the forelimbs. At E12.5 and E13.5, the *Col2a1* expression was very much reduced. Conversely, *Col1a2* expression was strongly up-regulated from E11.5 onwards in mutant limb buds in comparison to wild-type controls. In particular, the *Col1a2* expression domain extended into the limb distal mesenchyme of mutant limb buds by E13.5, pointing to the absence of restrictive cues. The same applies to the expression domains of *Dcn*, *Scx* and *Fjx1*, the latter being a marker for ligament

progenitors. *Dcn* expression in *Smad4*$^{\Delta/\Delta M}$ mutant limb buds was up-regulated and spread throughout the limb, including the distal region normally occupied by mesenchymal condensations (compare Fig. 9C with Fig. 6D). The *Scx* expression domain, which was localized in the sub-ectoderm at the level of the digit primordia in wild-type limb buds, expanded throughout the entire sub-ectodermal region in the *Smad4*$^{\Delta/\Delta M}$ mutant limb (Fig. 9D). The *Fjx1* domain, which localized to the prospective joints in the wild-type limb buds, was also spread throughout the mutant mesenchyme (Fig. 9E). Interestingly, for all three molecules expression levels were up-regulated already at E11.5 (between 47- and 50-somite stage), before the differentiation of mesenchymal cells took place in wild-type limb buds (Fig. 9C,D,E). *Dcn* and *Scx* transcripts were found up-regulated also by RT-qPCR, whereas *Sox9* transcripts were significantly reduced (Fig. 9G). We then looked at the progenitors of the skeletal muscles (marked by *MyoD1* transcription factor), which migrate from the somites into limb buds (reviewed in Buckingham et al., 2003). The spatial distribution of *MyoD1* transcripts was unchanged at E11.5 (Fig. 9F, left-most panel). We found that *MyoD1*-labeled migrating progenitors could not organize properly in the *Smad4*$^{\Delta/\Delta M}$ mutant limb at E12.5-E13.5 (Fig. 9F, right-most panels). This phenotype is likely caused by the lack of cartilaginous structures and tendon progenitors, which are responsible for organizing muscle precursors during tissue differentiation (Blitz et al., 2009).

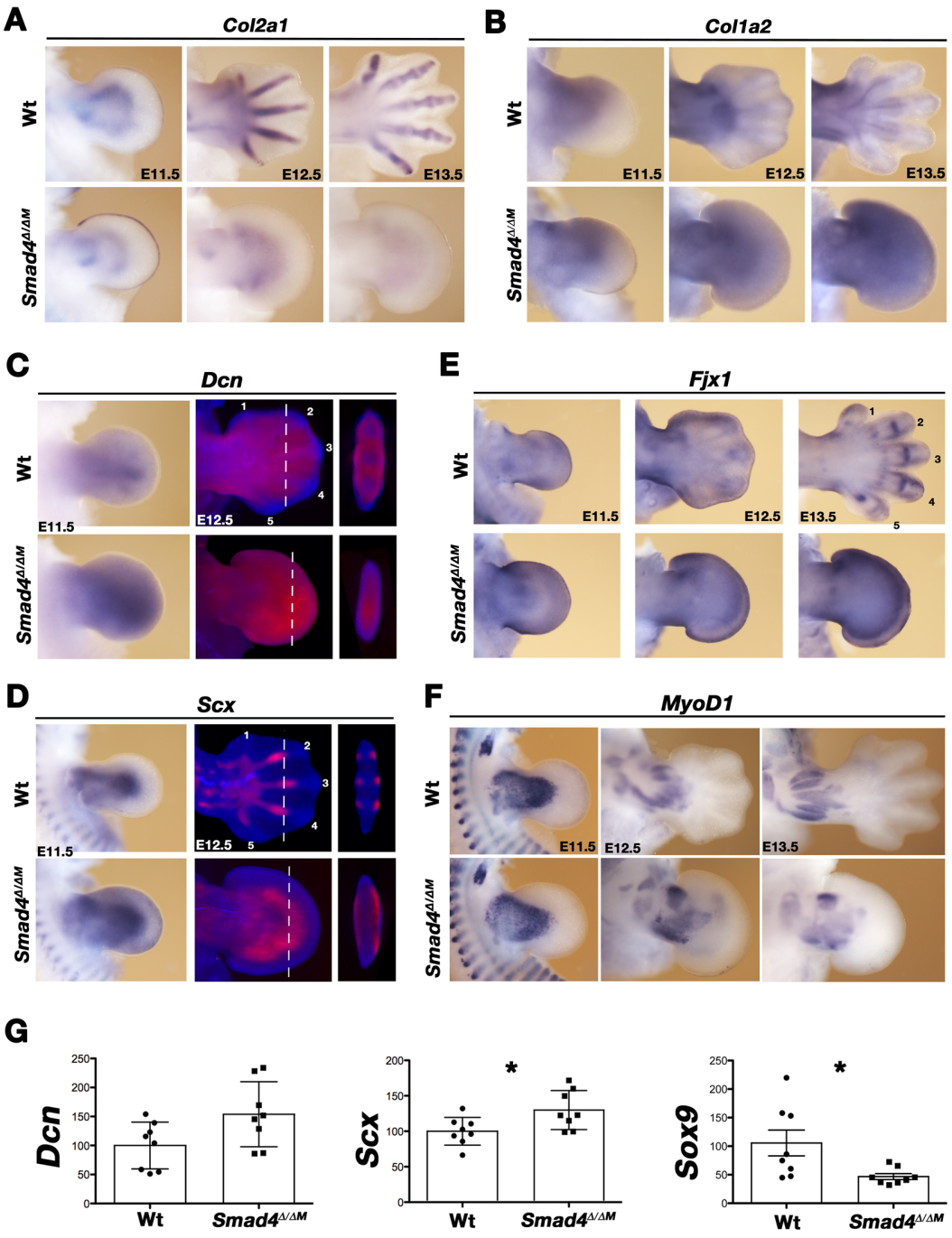

Fig. 9. *Smad4* controls a switch in chondrogenic cell fate while restricting alternative lineages. (A,B) Spatial distribution of Col2a1 **(A)** and Col1a2 **(B)** transcripts in wild-type and *Smad4*$^{\Delta/\Delta M}$ mutant forelimbs at E11.5 (~47-50 somites), E12.5 and E13.5. **(C,D)** Distribution of *Dcn* **(C)** and *Scx* **(D)** transcripts in wild-type and *Smad4*$^{\Delta/\Delta M}$ mutant forelimbs at E11.5 (left panel) or with OPT rendering at E12.5 (middle and right panels). Middle panels show a dorsal view. The white broken line represents the approximate levels at which the artificial sections from an AER-oriented view are taken in the right-most panels. OPT scans in these panels were performed by Erkan Uenal. **(E,F)** Distribution of *Fjx1* **(E)** and *MyoD1* **(F)** transcripts in wild-type and *Smad4*$^{\Delta/\Delta M}$ mutant forelimbs at E11.5 (~47 somites), E12.5 and E13.5 **(G)** RT-qPCR quantification. *Dcn* and

Scx transcripts are up-regulated in *Smad4*$^{\Delta/\Delta M}$ mutant limb buds (P≤0.06 and P≤0.05, respectively), whereas *Sox9* transcripts are down-regulated in comparison to wild-type controls. RNA was obtained from E11.75 (about 50 somites) forelimb buds; 8 *Smad4*$^{\Delta/\Delta M}$ limb buds were processed and compared to stage-matched controls. Results are reported as mean ± SD. Significance, one star: P≤0.05. See Material and Methods for additional information.

Minor alterations in cell death are observed following mesenchymal inactivation of *Smad4*

As part of our analysis we checked for possible alteration in cell death and proliferation. In the *Smad4*$^{\Delta/\Delta M}$ mutant limb we detected an ectopic/enhanced spot of cell death in the limb core around E10.5 and E11.5 (Fig. 10A,B; white and black arrowheads on left-most panels). As expected, interdigital cell death was suppressed in *Smad4*$^{\Delta/\Delta M}$ mutant limb buds at E13.5 (Fig. 10A,B; right-most panels). Cell death was assessed using the fluorescent probe Lysotracker® and by analysis of the *Cathepsin D (Cstd)* expression pattern (Zuzarte-Luis et al., 2007). No differences where apparent in comparing the two methods (Fig. 10, compare panels A and B).

Concomitantly, cell proliferation was addressed by Dr. Ashleigh Nugent with a Ki67 immunostaining on limb sections (see Benazet et al., 2012), but no alterations in proliferation were observed up to E12.5.

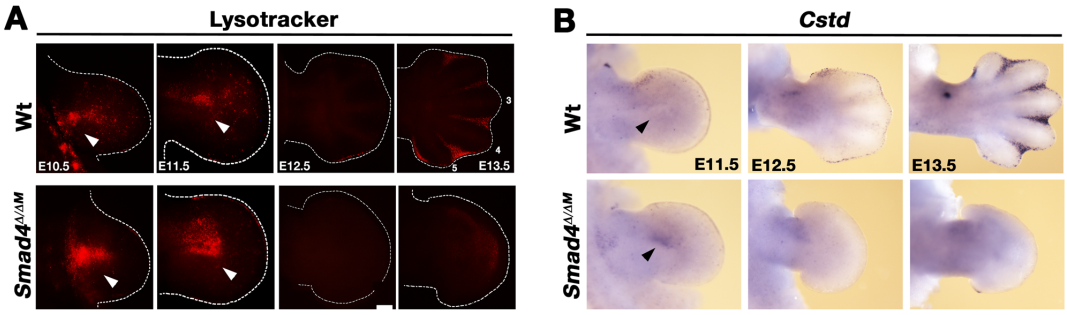

Fig. 10. Cell death is not significantly altered by inactivation of mesenchymal *Smad4*. (A) Detection of cell death in wild-type and *Smad4*$^{\Delta/\Delta M}$ mutant forelimbs with LysoTracker® tracer in a time-course experiment from E10.5 to E13.5. White arrowheads point at cell death domains in the limb core at E10.5 and E11.5. **(B)** *Cathepsin D* (*Cstd*) probe labels active lysosomes and describes cell death pattern in a less sensitive fashion with respect to LysoTracker® tracer. Black arrowheads point at the cell death domains in the limb core at E11.5. Stages of analysis are indicated in the panels.

Genetic analysis of *Smad4* requirements during limb bud initiation (unpublished results).

Smad4 was inactivated in the hindlimb field using the *Hoxb6-Cre* transgene to study potential roles of *Smad4* during limb bud initiation. While recombination in the hindlimb is complete, recombination in the forelimb occurs only in the posterior limb domain at about E10.0 (Fig. 11A). This early *Smad4* inactivation resulted in a high degree of developmental arrest by about E8.5 associated with heart hypertrophy (Fig. 11B). Mutant embryos that survived this early arrest developed to E10.25/E10.5. At this stage, dead embryos were recognized as they no longer expressed *Sox9* and *Grem1* in somites (Fig. 11C). In $Smad4^{\Delta/\Delta Hb6}$ mutant forelimbs *Smad4* remained expressed in the anterior limb bud mesenchyme, consistent with the posterior activity of the *Hoxb6-Cre* transgene (Fig. 11D, arrowhead). *Grem1* expression was either unaltered or appeared more diffuse in both fore- and hindlimb buds of $Smad4^{\Delta/\Delta Hb6}$ mutant embryos (Fig. 11E, left and central panels). Preliminary results indicated that mutant $Smad4^{\Delta/\Delta Hb6}$ embryos failed to activate *Sox9* expression in the core mesenchyme of early limb buds (Fig. 11E, right panel).

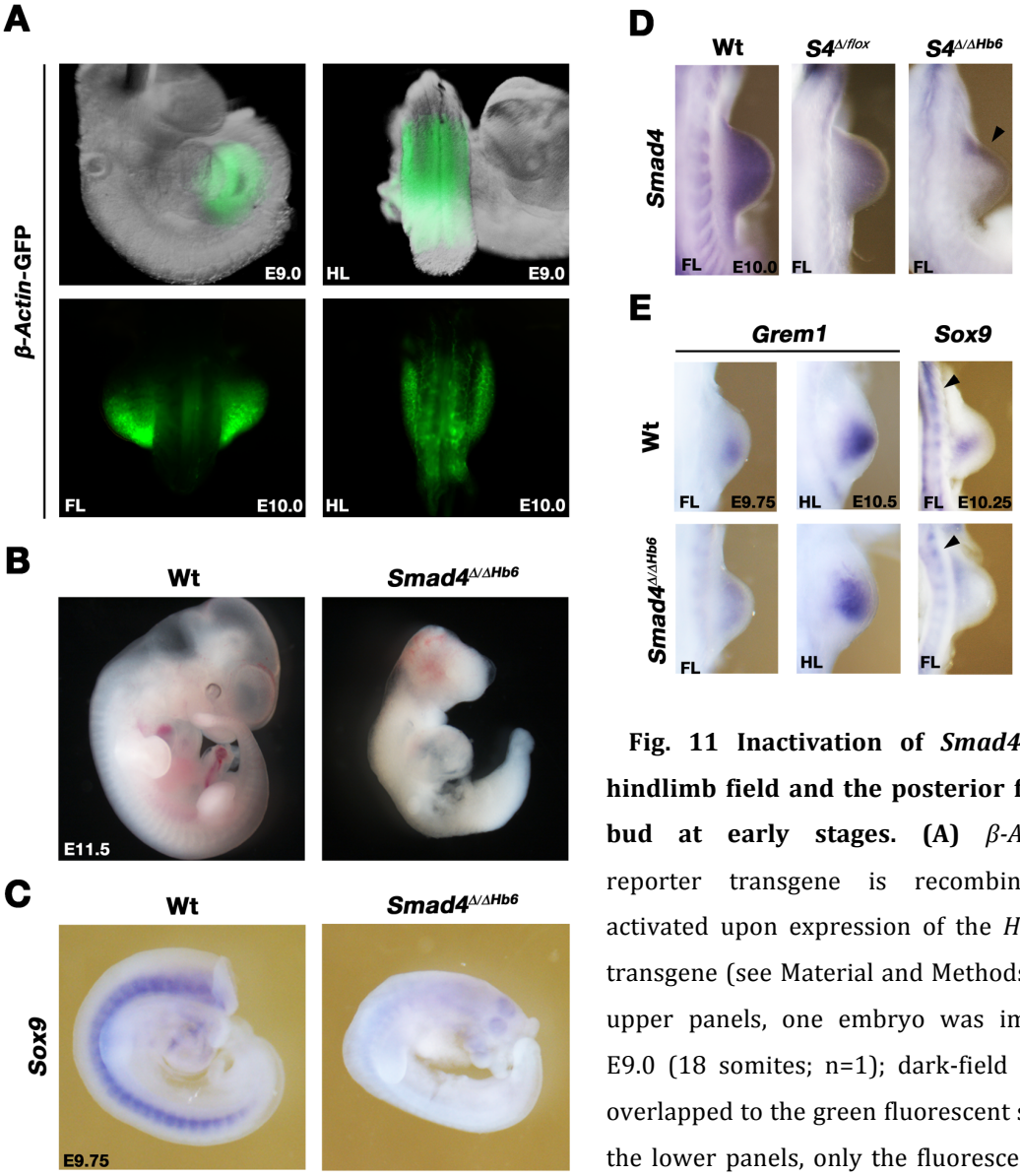

Fig. 11 Inactivation of *Smad4* in the hindlimb field and the posterior forelimb bud at early stages. (A) *β-Actin*-GFP reporter transgene is recombined and activated upon expression of the *Hoxb6-Cre* transgene (see Material and Methods). In the upper panels, one embryo was imaged at E9.0 (18 somites; n=1); dark-field image is overlapped to the green fluorescent signal. In the lower panels, only the fluorescent signal in the forelimbs (left) and hindlimbs (right) is reported at E10.0 (31 somites; n=3; contributed by Marco Osterwalder). Recombination only occurs in the hindlimb field and the correspondent axial mesodermal segment of the embryo at E9.0, whereas recombination extends to the posterior region of the forelimbs at E10.0. **(B)** Dark-field micrographs of representative wild-type and retarded *Smad4*$^{\Delta/\Delta Hb6}$ embryos collected at E11.5. *Smad4*$^{\Delta/\Delta Hb6}$ embryos were retrieved with mendelian ratios. However, more than half showed an arrest in development at around E8.5 and limb agenesis. Therefore, only embryos of the expected age were collected from each litter. **(C)** *Sox9* transcripts detected in wild-type and *Smad4*$^{\Delta/\Delta Hb6}$ embryos at E9.75 (26 somites; n=2). The absence of signal in all tissues of mutant embryos indicates that developmental arrest occurred before collection. **(D)** Detection of transcripts of *Smad4* exon 8 in forelimbs of wild-type, *Smad4*$^{\Delta/flox}$ and *Smad4*$^{\Delta/\Delta Hb6}$ at E10 (30 somites, n=2). The *Hoxb6-Cre* transgene is expressed in the posterior forelimb mesenchyme, which explains the residual anterior expression of *Smad4* transcripts (black arrowhead). **(E)** *Grem1* and

Sox9 transcripts (n=3 and n=1, respectively). On the left, forelimbs from wild-type and *Smad4*$^{\Delta/\Delta Hb6}$ mutant embryos are shown at E9.75 (28 somites). Mutant forelimb buds show more diffuse *Grem1* expression in comparison to wild-type controls. At E10.5, *Grem1* expression is similar in wild-type and mutant hindlimbs (36 somites). On the right, *Sox9* transcripts are expressed in somites (black arrowheads) but are absent from the posterior mutant forelimb mesenchyme at E10.25 (32 somites). FL, forelimb; HL, hindlimb; S4, Smad4.

8. DISCUSSION

In the present study, we used a genetic approach to investigate the roles of SMAD4-mediated canonical BMP signal transduction during limb development. We found that SMAD4 is involved in specification of digit primordia and initiation of chondrogenesis.

Inactivation of *Smad4* in the limb mesenchyme during AER formation and compaction (E9.5- E9.75) ultimately results in agenesis of the limb skeleton. Similarly, inactivation of *Smad4* in the prospective handplate at later stages (E10.75-E11.0) leads to loss of autopod skeletal structures. These results provide genetic evidence for a role of SMAD4, and likely canonical BMP signal transduction, in initiation of chondrogenesis. Moreover, using *Hoxa13-Cre*-mediated *Smad4* inactivation we obtain evidence for a narrow time window for the SMAD4 to induce digit primordia. Previous genetic analysis focused mainly on BMP functions in AER formation or in maintenance of chondrocyte proliferation and differentiation failed to uncover roles of BMP signalling in initiating chondrogenic differentiation. For instance, inactivation of *BmpR1a* in the ventral ectoderm results in limb agenesis due to impaired AER formation (Ahn et al., 2001; Pajni-Underwood et al., 2007); and compound inactivation of *BmpR1b* and *BmpR1a* in chondrocytes results in severe chondrodysplasia due to increased cell death and impaired chondrocyte differentiation (Yoon et al., 2005).

Experiments with mesenchymal progenitors in culture show that *Smad4*-deficient mesenchymal cells do not initiate aggregation, which is the first step during formation of the cartilage primordia. This *Smad4* requirement is the first obvious defect observed in limb buds lacking mesenchymal *Smad4*, as, in contrast to other BMP pathway-related molecules, AER establishment is not impaired and only minor defects in endochondral bone formation are observed (Benazet et al., 2012; Pajni-Underwood et al., 2007; Zhang et al., 2005). This points to SMAD4-independent BMP signal transduction during limb development. Besides non-canonical BMP signal transduction, evidence supporting SMAD4-independent, SMAD-dependent signaling transduction exists (Liu et al., 1997). Previous analysis of high-density limb bud mesenchymal cell cultures defined several steps of mesenchymal condensation: sorting, aggregation, cluster formation and compaction, the last of which was shown to require BMPs (Barna and Niswander, 2007).

We show that mesenchymal *Smad4* is required for *Sox9*-specification of digit primordia around the time when the autopod is shaped. In the early stages, *Sox9* expression is unaffected by loss of mesenchymal *Smad4* (E9.75 to E10.75), which is consistent with

BMP activity being low due to GREM1 antagonism during this phase of limb patterning and outgrowth (Benazet et al., 2009). However, when the increase of BMP activity is required for mesenchymal progenitors to undergo chondrogenesis (Lopez-Rios et al., 2012), *Smad4* is required to propagate the expression of *Sox9* in the prospective digit primordia in the forming autopod. In the absence of *Smad4, Sox9*-positive chondrogenic precursors accumulate proximally (likely at the level of the prospective stylopod) while the distal expression is disrupted. This could be attributed to a cell-autonomous mesenchymal defect or to high and prolonged AER-FGF signalling in distal *Smad4* mutant limb buds, which inhibits differentiation of the mesenchyme (Benazet and Zeller, 2013). These results indicate that SMAD4 could be part of the novel molecular circuitry that had to evolve during formation of the autopod and digits in tetrapods (Woltering and Duboule, 2010).

The impact of *Smad4*-medited signal transduction on *Sox9* expression was further addressed in high-density mesenchymal progenitor cell cultures, which provide evidence that *Smad4* is necessary to sustain SOX9 expression downstream BMP (and TGFβ) receptors. In addition, I have obtained genetic evidence in support of a role for BMP signalling in activation of *Sox9* in the limb bud mesenchyme at very early stages. My genetic evidence corroborates cell-based studies that show that *Sox9* is a direct transcriptional target of both canonical and non-canonical BMP signal transduction (Gao et al., 2013; Pan et al., 2008).

Furthermore, conditional inactivation of *Smad4* in the autopod unveiled its differential requirement for formation of anterior and posterior digit primordia. The mesenchymal progenitors giving rise to the posterior digits 4/5 requires canonical BMP signalling for a shorter time, or activate BMP signalling earlier than the anterior compartment as a possible consequence of the progressive anterior displacement of *Grem1* expression domain (Michos et al., 2004). In light of these results, the loss of the posterior primordia in the *Bmp2; Bmp4* mutant mesenchyme shows that BMP2 and BMP4 mediate up-regulation of BMP activity in the posterior limb mesenchyme prior to its increase in the anterior mesenchyme (Bandyopadhyay et al., 2006). In addition, this study shows that BMP7 is required to specify the digit primordia in the anterior limb bud mesenchyme. Genetic inactivation of *Smad4* in the autopod also revealed a posterior-to-anterior order of specification of digit primordia, which apparently contrast with the results obtained by temporal conditional inactivation of *Shh* (Zhu et al., 2008). Zhu and colleagues proposed that digit determination and formation follows a specific sequence: namely 4, 2, 5 and 3, and the Shh-independent digit 1 appearing last (Zhu et al., 2008). These results can be

reconciled with our results by proposing that the anterior digit 2/3 and the posterior digit 4/5 primordia arise from single *Sox9*-positive condensation that branches subsequently during limb bud development.

We demonstrate that mesenchymal *Smad4* is also required during limb bub outgrowth and patterning in the context of the positive feedback loop SHH/GREM1/AER-FGF. Despite not being essential for the establishment of the limb signalling centers, *Smad4* modulates AER-FGF and *Shh* expression. Indeed, upon mesenchymal removal of *Smad4*, *Fgf8* is up-regulated and its expression is prolonged, while *Shh* expression pattern is extended proximally. Notably, similar alterations were detected following inactivation of BMP ligands (Bandyopadhyay et al., 2006; Selever et al., 2004), indicating that SMAD4 transduces the low levels of BMP activity during limb bud outgrowth and patterning.

The roles of BMP signalling in initiation of chondrogenesis at a molecular level are not clear. I have obtained evidence for a role for *Smad4* in regulating the small GTPase RhoC (data not shown), which is known to be involved in cell rearrangements and motility by acting on the cytoskeleton (Kitzing et al., 2010). Indeed, RhoC is expressed by the cells of the perichondrium and is supposed to inhibit chondrogenesis and define the boundary between condensing and non-condensing tissues (Montero et al., 2007). Moreover, parallel experiments run in the lab indicate that expression of N-cadherin is dependent on mesenchymal *Smad4*. Altogether, these data point at a possible role of *Smad4* in rearranging the actin cytoskeleton during initiation of chondrogenesis. These rearrangements are known to involve β-catenin as a structural component and as transcriptional modulator (Modarresi et al., 2005; Ouyang et al., 2013). This is relevant as canonical Wnt signalling, which is mediated by β-catenin, inhibits chondrocyte differentiation (Rudnicki and Brown, 1997).

Smad4 inactivation in the limb mesenchyme results in soft, non-organized tissues that lack bone and any differentiated structures. Further molecular analysis revealed the up-regulation and wide-spread expression of markers for non-chondrogenic lineages. In particular, *Col type I*, its downstream target *Scx* (Cserjesi et al., 1995; Schweitzer et al., 2001), *Fjx1* (Rock et al., 2005) and *Dcn* (Danielson et al., 1997) were up-regulated and co-expressed in regions that would normally undergo chondrogenesis. This is consistent with the results obtained by Pizette and Niswander following misexpression of Noggin in the chicken wing buds. In such wing buds *Gdf5*, which marks tendon progenitors, was up-regulated in regions of chondrogenic condensations (Pizette and Niswander, 2000).

Altogether, these results point to a role of SMAD4 in restraining non-chondrogenic versus chondrogenic cell fates, and reveal that this is fundamental prerequisite to initiate chondrogenic differentiation. This conclusion is of particular interest since experimental evidence indicates that BMP activity in the limb bud mesenchyme down-regulates Wnt signalling in the ectoderm to prevent tendon and connective soft tissue differentiation of core mesenchymal cells (Collette et al., 2012; Collette et al., 2010; Kamiya et al., 2010; ten Berge et al., 2008). Together these results suggest that the modulation of BMP and WNT activities and signal transduction define chondrogenic and non-chondrogenic territories.

Inactivation of SMAD4 in the limb bud mesenchyme interferes with both canonical BMP and TGFβ signal transduction, but does not allow discrimination between single pathways. However, genetic analysis has not provided evidence for essential roles of TGFβ signaling in onset of chondrogenesis. Instead, TGFβ ligands and receptors have been associated with the organization of muscles and tendons, which in turn affects organization of skeletal elements (Pryce et al., 2009; Sanford et al., 1997). Inactivation of *TGFβR2*, which is a common type II receptor for all TGFβ ligands, results in dwarfism (Spagnoli et al., 2007), but the underlying alterations are unknown. Inhibition of TGFβ receptor activity in mesenchymal cell cultures causes a block in mesenchymal condensations and COL type II expression similar to inhibition of BMP receptors activity by small molecules and to genetic inactivation of *Smad4*. Therefore, shedding light on the spatio-temporal requirements of both pathways will be of vital importance for cartilage and bone engineering (see e.g. Jiang et al., 2010; Sanchez-Adams and Athanasiou, 2012). Experimental evidence suggests that TGFβ may prime mesenchymal cells for BMP-mediated induction of chondrogenesis (see e.g. Karamboulas et al., 2010; Leonard et al., 1991; Roark and Greer, 1994).

The high dynamic modulation of BMP activity can account for the various morpho-regulatory properties of BMP signalling pathway throughout limb development. BMP activity in the limb is high during establishment of the AER, low during limb patterning and outgrowth, and is increased again to function in initiation of chondrogenesis (see Introduction). Furthermore, the discrete and regular fashion by which skeletal primordia are laid down along the A-P limb axis (Newman and Bhat, 2007) and the tight regulation of digit identity by BMP activity (Suzuki et al., 2008) suggest that classical morphogen gradients alone cannot explain the dynamic modulation of BMP signalling activity. Therefore, a real-time analysis of the dynamics of BMP activity is required to reveal the for sure highly dynamic exposure of progenitors to BMP signalling.

9. CONCLUSIONS AND OUTLOOK

The present study on the multiple roles of BMP signalling and in particular SMAD4 requires much more in-depth analysis. Here I report only two considerations:

1. SMAD4-mediated BMP signalling is fundamental to initiate chondrogenesis, as it has been established in several cell-based studies, see e.g. Barna and Niswander (2007) and in the genetic studies during my PhD. However, the mechanisms that underlie the initiation of chondrogenesis by cell condensation events are still largely unknown. Evidence suggests that SOX9 acts downstream of BMP signalling to mediate its function in initiating chondrogenesis by the up-regulation of early chondrogenic markers such as *Col type II* (reviewed in Hall and Miyake, 2000). Indeed, *Sox9* inactivation results in skeletal agenesis similar to *Smad4* inactivation (Akiyama et al., 2002, and my studies). Some studies report that BMPs can also directly activate early chondrogenic factors (Haas and Tuan, 1999; Inai et al., 2013; Morgan et al., 2011). Therefore genetic analysis in combination with high-throughput RNA/protein profiling is necessary to gain insight into the complex cell and tissue rearrangements that occur during initiation of chondrogenesis. In addition, direct visualization of cell behavior during formation of aggregates has to be used to investigate the early steps of aggregation of chondrocytic progenitors in combination with molecular analysis (Barna and Niswander, 2007).

2. The present study also opens several questions on how and when digits are specified and determined during limb bud development. As discussed in the previous chapter, discrete temporal requirement of *Shh* for patterning unveils an order of digit specification (Zhu et al., 2008) that differs from the posterior-to-anterior progression of specification suggested by inactivation of *Smad4* (my studies). Independently of the order of digit specification, it is important to clarify the genetic interactions occurring between SHH and BMP morpho-regulatory signals, especially in the light of their dynamic activities with respect to the A-P limb axis formation and their requirement for final determination and shaping of digits (Dahn and Fallon, 2000; Suzuki et al., 2008; Suzuki et al., 2004).

10. ACKNOWLEDGMENTS

I first thank Rolf Zeller for being my enthusiastic mentor and having so much patience with me, and Aimée Zuniga for co-supervision.

I thank Prof. Markus Affolter and Prof. Verdon Taylor for being members of my thesis committee.

I thank Jean-Denis Bénazet, who taught me how to take a 'tough line' with research. A great part of this study would not have been possible without of him.

I thank Javier Lopez-Rios and Gretel Nusspaumer for their great support and advice, on how to 'tackle' pipettes and human beings as well.

I thank all my former colleagues, and especially Alexandre Gonçalves and Simone Probst, for all their teachings.

Frédéric Laurent, Dario Speziale and Ashleigh Nugent, Erkan Uenal, Sumit Jaiswal, Marco Osterwalder, I thank you all because you shaped me the way I am now (including, first of all, food; then scientific and moral support, then… each one of you knows).

I thank all the people I have met during these years, with whom I have shared words, feelings and thoughts; or whom I have just passed by: sometimes, the most negligible event is also the most important.

11. APPENDIX 1 _ INACTIVATION OF SMAD4 AND GREM1 IN THE AER

Background

Ablation of BMP activity in the established AER results in a variety of phenotypes that include interdigital webbing, polydactyly, phalanx bifurcation and ectrodactyly (Pajni-Underwood et al., 2007). On the other hand, inactivation of *Grem1* and reduction of *Bmp4* in the mesenchyme restores the limb skeleton for a large extent (Benazet et al., 2009), indicating that GREM1 is the main extracellular antagonist of BMPs in the limb bud mesenchyme. Therefore, we sought to understand if reduction of BMP activity through *Smad4* from the AER could compensate for the at least the sub-ridge mesenchymal cell death phenotype associated with inactivation of *Grem1*.

Results

To this aim, we inactivated *Smad4* (using a *Msx2-Cre* transgene) in a *Grem1* deficient genetic background to get $Grem1^{\Delta/\Delta}$; $Smad4^{\Delta/\Delta AER}$ embryos (n=3, see Material and Methods). We found that the compound mutants retain the interdigital soft tissue webbing to the extent of $Smad4^{\Delta/\Delta AER}$ embryos (Fig. 1A). *Grem1* deficient forelimbs have three rudimentary digits, while $Grem1^{\Delta/\Delta}$; $Smad4^{\Delta/\Delta AER}$ forelimbs exhibit between 3 and 4 digits which are however thickened and in some cases bifurcated (Fig. 1B, compare the forelimbs 'FL' in the lower panels). This phenotype is indicative of a minor distal rescue with respect to the *Grem1* loss-of-function. In addition, 2 of 3 hindlimbs of the compound mutant embryos showed a variable phenotype characterized by oligodactyly, ectrodactyly and ectopic sprouting of phalanges, which are associated with the $Smad4^{\Delta/\Delta AER}$ deficiency (Fig. 1B, hindlimb 'HL' in the lower-right panels). In all cases, fore- and hindlimb buds show variable degrees of bifurcations of the distal phalanges, which is likely due to excessive AER-FGF signalling (Pajni-Underwood et al., 2007).

The fusion of the zeugopodal elements in forelimbs of $Grem1^{\Delta/\Delta}$; $Smad4^{\Delta/\Delta AER}$ is strikingly similar to $Grem1^{\Delta/\Delta}$ forelimbs. In contrast, the double mutant zeugopod in hindlimbs is more affected and a unique ossification forms proximally (arrowed in Fig. 1C).

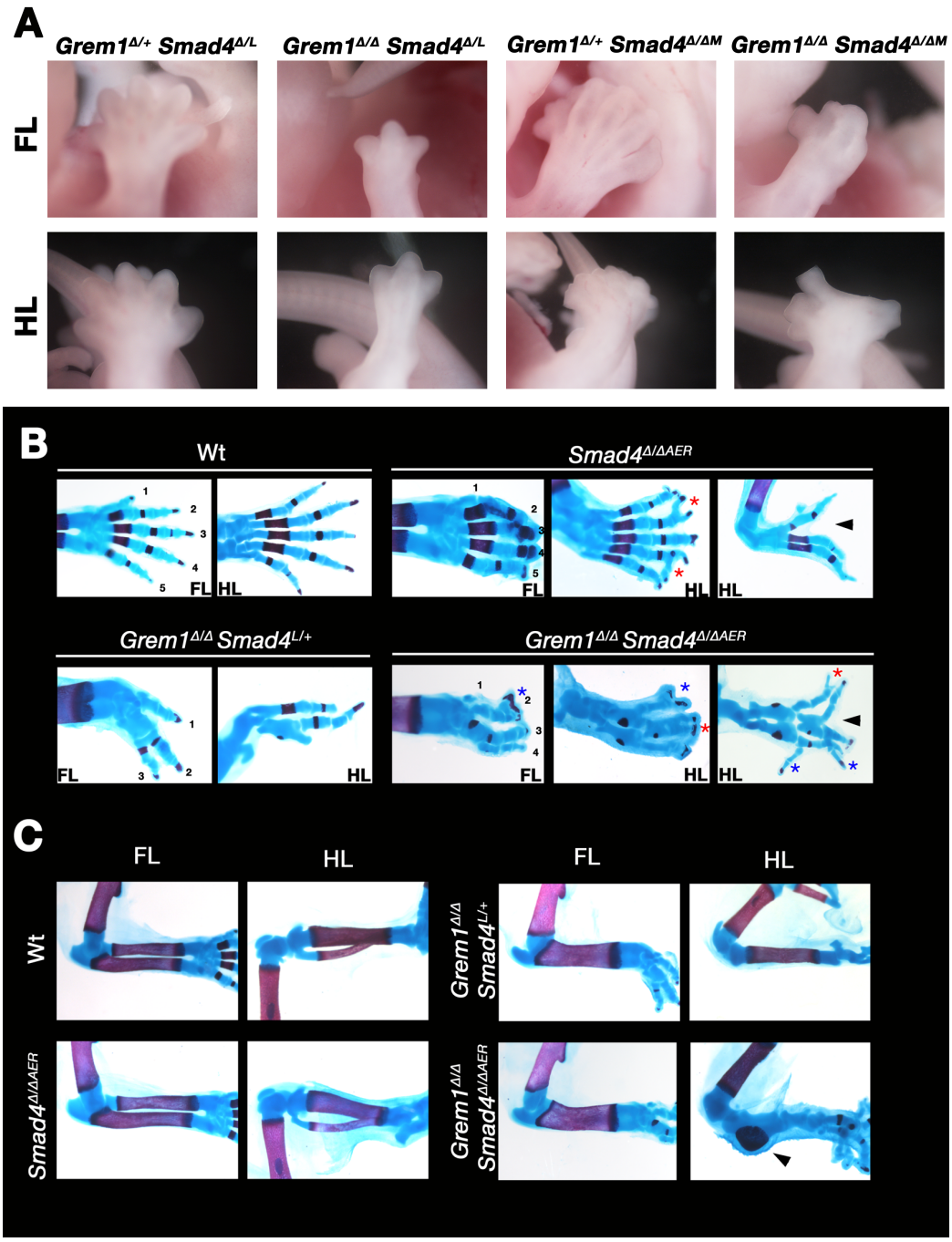

Fig. 1. (A) Allele series of compound mutants for constitutive *Grem1* inactivation and AER-*Smad4* inactivation (using *Msx2-Cre*^{Tg}). E14.5 forelimbs (FL, upper panels) and hindlimbs (HL, lower panels) are pictured on dark field. Note that the interdigital webbing is retained whenever *Smad4* is cleared from the AER. **(B)** Skeletal preparations at E18.5 are stained with Alcian Blue (cartilage) and Alizarin Red (bone matrix) to detect alterations in digit number and morphology in forelimbs (FL) and hindlimbs (HL). Red asterisks mark bifurcation of the last phalanges typical of the AER-*Smad4* removal; blue asterisks point at ectopic sprouting of phalanges; black arrows indicate a ectrodactylous phenotype. Double *Grem1*; AER-*Smad4* limbs are compared to stage-matched controls, either Wt or single mutants (*Grem1*$^{\Delta/\Delta}$*; Smad4*$^{L/+}$ phenotype is comparable with

a single *Grem1*$^{\Delta/\Delta}$ mutant). **(C)** Skeletal preparations at E18.5 of zeugopod are stained like in **(B)**. Both FL and HL are pictured. In total, 3 double mutant embryos were collected. 1-5: digit/ metacarpal identities.

12. APPENDIX 2 _ ATTEMPTS TO GENERATE A BMP SENSOR MOUSE

Aim of the project and background

The establishment of a BMP-sensor mouse model would be ideal to study the spatio-temporal dynamics of BMP signaling. For the analysis during limb development, a reporter that is rapidly induced and degraded would be important for detecting the postulated variations in BMP activity during initiation, outgrowth and differentiation during limb bud development (Benazet et al., 2009). The BMP sensor models generated so far have some drawbacks that impair either sensitivity or dynamic properties of the readout with respect to the original signal.

Mostly, the BMP-responsive element (BRE; Korchynskyi and ten Dijke, 2002) was used to trace BMP signalling activity. The BRE is a minimal enhancer activated by pSMAD1 and pSMAD5, and the element is constituted of two head-to-head copies of the regions -1105 bp to -1080 bp and -1052 bp to -1032 bp upstream the *Id1* gene transcriptional start site (TSS; Korchynskyi and ten Dijke, 2002). *Id1* is a well-characterized BMP target gene that is activated by both BMP and TGFβ signalling (Hollnagel et al., 1999; Lopez-Rovira et al., 2002; Ogata et al., 1993; Ying et al., 2003). The *CMVe-(BRE)$_3$-MLP-EGFP* mouse line generated in Christine Mummery's laboratory (Monteiro et al., 2008) consists of cytomegalovirus immediate early promoter (CMVe) placed upstream three copies of the BRE cassette that controls the expression. The cassette is followed by an enhanced version of the green fluorescent protein (GFP). We imported this mouse strain and tested it for sensing BMP signaling in limb bud, but expression that mirrored the expression pattern of the BMP signaling targets *Msx2* and *Id1* was not detected (Fig. 1A; compare with the expression pattern in Fig. 3A). This result, together with the analysis of additional transgenic mouse models based on the BRE cassette (Blank et al., 2008; Collery and Link, 2011) suggested that the *BRE* minimal enhancer does not sense BMP activity during mouse limb bud development.

Another approach is based on inserting a reporter into the endogenous regulatory sequences responding to BMP signal transduction (Bensoussan et al., 2008; Nam and Benezra, 2009; Perry et al., 2008). We imported a mouse line generated by Benoît Robert's laboratory (Bensoussan et al., 2008). In these mice an *IRES-GFP* transgene is placed downstream of the endogenous *Msx2* allele. The mouse strain faithfully recapitulated *Msx2* expression pattern in the limb bud from E10.5 onwards (Fig. 1B). Next, beads loaded with hrBMP4 were implanted into limb buds to assess the sensitivity and dynamic regulation of the GFP transgene. We found that the GFP reporter signal

could not be detected after 3-4 hours of limb culture, whereas *Msx2* transcripts were already activated. Beads were implanted in different location to assess the ectopic activation of the *Msx2* target gene in limb buds (Fig. 1B). The ectopic GFP induction was visible about 6 hrs after bead implantation, when *Msx2* transcripts already begun to be down-regulated again (Fig. 1C, left panel). After 22 hours of culture, *Msx2* transcripts and GFP protein were mostly cleared around the bead in most of the experimental limb bud analysed (n=7, not shown). However, when the hrBMP4-loaded beads were implanted into the anterior limb bud mesenchyme (i.e. into the region corresponding to the strongest *Msx2* expression), GFP was detected up to 22 hrs of limb culture (Fig. 1C, right panel, n=2). This result suggests that the GFP protein (about 20 hours, see Nagai et al., 2002) is too stable to allow detection of rapid dynamic alterations in BMP activity. This reveals the need to generate a novel type of BMP sensor transgene.

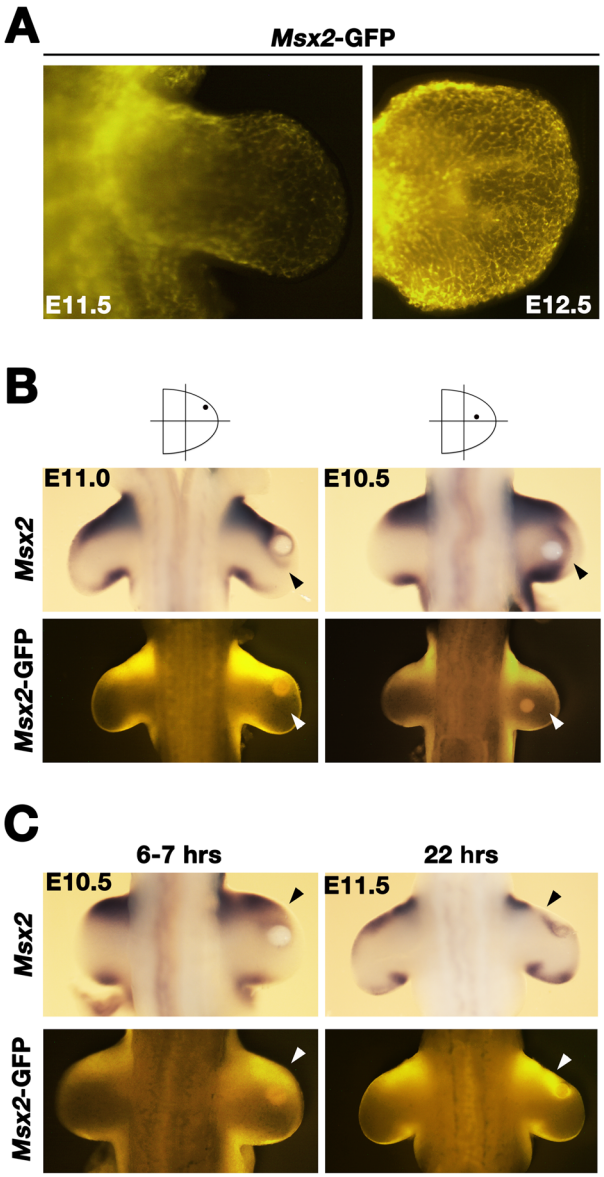

Fig. 1 Existing BMP-sensor mouse models are not specific or have insufficient dynamics to detect rapid changes in BMP activity (A) Epi-fluorescence images in the GFP channel of the mouse right forelimb at E11.5 (left panel) and E12.5 (right panel) of the BMP-sensing mouse strain generated by Monteiro et al. (2008). Note that GFP outlines the vasculature. GFP signal was transposed into golden color using the Photoshop Hue/Saturation tool, to achieve higher signal-to-noise ratio in printouts (parameter: Hue, -100). **(B,C)** Bright-field *in situ* images with the probes indicated (upper panels) and the corresponding epi-fluorescence images to detect GFP expression (lower panels) using the *Msx2*-GFP mouse strain generated by Bensoussan et al. (2008). **(B)** In the upper panels, heparin beads coated with 0.1 mg/ml hrBMP4 were implanted either into the anterior-distal *Msx2* expression domain (left panel) or the core mesenchyme (right panel) of the right forelimbs. Limb bud trunks were cultured for 3-4 hrs. Note that ectopic *Msx2* expression was triggered upon bead implantation either in the anterior *Msx2* expression domain (left-upper panel) or in the core mesenchyme in a domain located distally to the bead (right-upper panel; see arrowheads). Left limb buds serve as controls. Lower panels show that GFP corresponding to *Msx2* induction was not detectable after 3-4 hrs. Arrowheads point to the same region in both panels. **(C)** Heparin beads loaded with 0.1 mg/ml hrBMP4 were implanted in the anterior-distal *Msx2* expression domain into right forelimb buds, and cultured for either 6-7 hr (left panels) or 22 hrs (right panels) to assess changes in *Msx2* expression (upper panel, bright-field WISH images) and GFP fluorescence (lower panels). Left limbs served as controls. Black arrowheads point to the *Msx2* expression, which was reduced around the bead by 6-7 hr and cleared around 22 hr (upper panels). White arrowheads point to

GFP triggered by a hrBMP4-loaded bead at both 6-7 hr and 22 hr in the anterior *Msx2* domain (lower panels).

Toward BMP sensor: design of a standard vector to analyze *cis*-regulatory sequences in ES cells and mice

In order to generate a standard vector to test sequences for their potential enhancer activity, the pIGNA vector was generated at GeneArt® (Life Technologies, Fig. 2A, sequence available upon request). pIGNA vector contains a sequence encoding an enhanced version of the yellow fluorescent protein named Venus. Venus has reduced sensitivity for chloride ions and for low pH and is induced faster than the standard YFP (Aulehla et al., 2008; Nagai et al., 2002). To allow a better quantification of fluorescence signal in a tissue context, a Nuclear Localization Signal (NLS; sequence: PKKKRKV) was added downstream *Venus* Coding Sequence (CDS). Also, a protein degradation domain (PEST sequence) was added downstream the NLS to reduce the half-life of Venus from ~20 hr (Nagai et al., 2002) to less than 2 hr (Aulehla et al., 2008). The PEST sequence used was HGFPPAVAAQDDGTLPMSCAQESGMDRH, and the three underlined alanine residues replace three glutamic acid residues that characterize the original PEST sequence derived from mouse ornithine decarboxylase (Li et al., 1998). A polyadenylation signal (polyA) derived from the pCI-neo mammalian expression vector (Promega) was synthetized downstream the PEST sequence. Just upstream the *Venus* CDS, a chimeric intron cut-and-copied from the pCI-neo vector (Promega) was synthetized in order to facilitate the expression of the downstream reporter gene and prevent utilization of possible cryptic 5'-donor splice sites within the reporter (see Promega website; Gross et al., 1987; Huang and Gorman, 1990). The sequence block spanning from the chimeric intron to the polyA was flanked by two Cre recombination sites for lox511 (upstream *Venus)* and loxP (downstream the polyA) to allow targeting the conditional *Gt(Rosa)26Sor* locus (Tchorz et al., 2012) by Recombinase-Mediated Cassette Exchange (RMCE; Schlake and Bode, 1994). An FRT site was placed just upstream the loxP site to allow for eventual flippase-driven RMCE. Unique restriction sites (5'-3' order ClaI, KpnI, ApaI, HindIII, NheI, SalI, PacI, AatI) were placed in a Multiple Cloning Site (MCS) downstream the lox511 site and upstream the *Venus* CDS to insert the regulatory sequences of interest. Other unique restriction sites (FseI, BclI upstream lox511 and PmeI downstream loxP site) were placed outside the construct to allow excision of the entire sequence (Fig. 2A). The whole construct (1494bp) was cloned into

the pMA-RQ (ampR) backbone (GeneArt®) and propagated in *E. coli* K12 (dam+ dcm+ tonA rec-) bacteria.

Neomycin resistance coding gene (*NeoR*) was subcloned with XbaI from the pLoxpNeo-2 vector into a pBlueScript II KS(+) vector to generate the pBSNeoR vector. In order to maintain the NheI restriction site unique in the pIGNA MCS, the NheI site upstream the pGK promoter driving the expression of the *Neo* resistance was eliminated by blunting the protruding sequences of the cut restriction site with a T4 polymerase (NEB). A full-length chicken β-globin insulator sequence (Chung et al., 1997) was subcloned from the pXCHG3fwd vector (Dr. Alexander Aulehla) into a blunted EcoRI restriction site in the pIGNA vector, just upstream the FRT recombination site. The insulator was used to shield the transcriptional activity of the sensor from any unwanted activity of *cis*-acting regulatory element and from the promoter of the *Gt(Rosa)26Sor* locus. A second insulator was cloned from the pXCHG3fwd vector into a ClaI-Asp718 restriction locus downstream the lox511 site into the pIGNA vector. Then, the NeoR cassette was removed from the pBSNeoR vector with a single XbaI restriction digestion and cloned into the pIGNA vector taking advantage of the single-cutting XbaI site present in the sequence of the FRT recombination site. The obtained vector was named pIGNA(2xins)NeoR (Fig. 2B). This vector was supposed to be an easy-to-customize shuttle vector for analyzing the activity of *cis*-regulatory elements by inserting them into the *Gt(Rosa)26Sor* locus (Tchorz et al., 2012).

However, three targeting attempts were performed and consistently failed to contribute antibiotic-resistant ES cell colonies. Therefore, another ES cell line carrying a replaceable *Gt(Rosa)26Sor* locus was adopted from Andrew McMahon laboratory (Tsanov et al., 2012), and the targeting vector was modified accordingly (see the following sections).

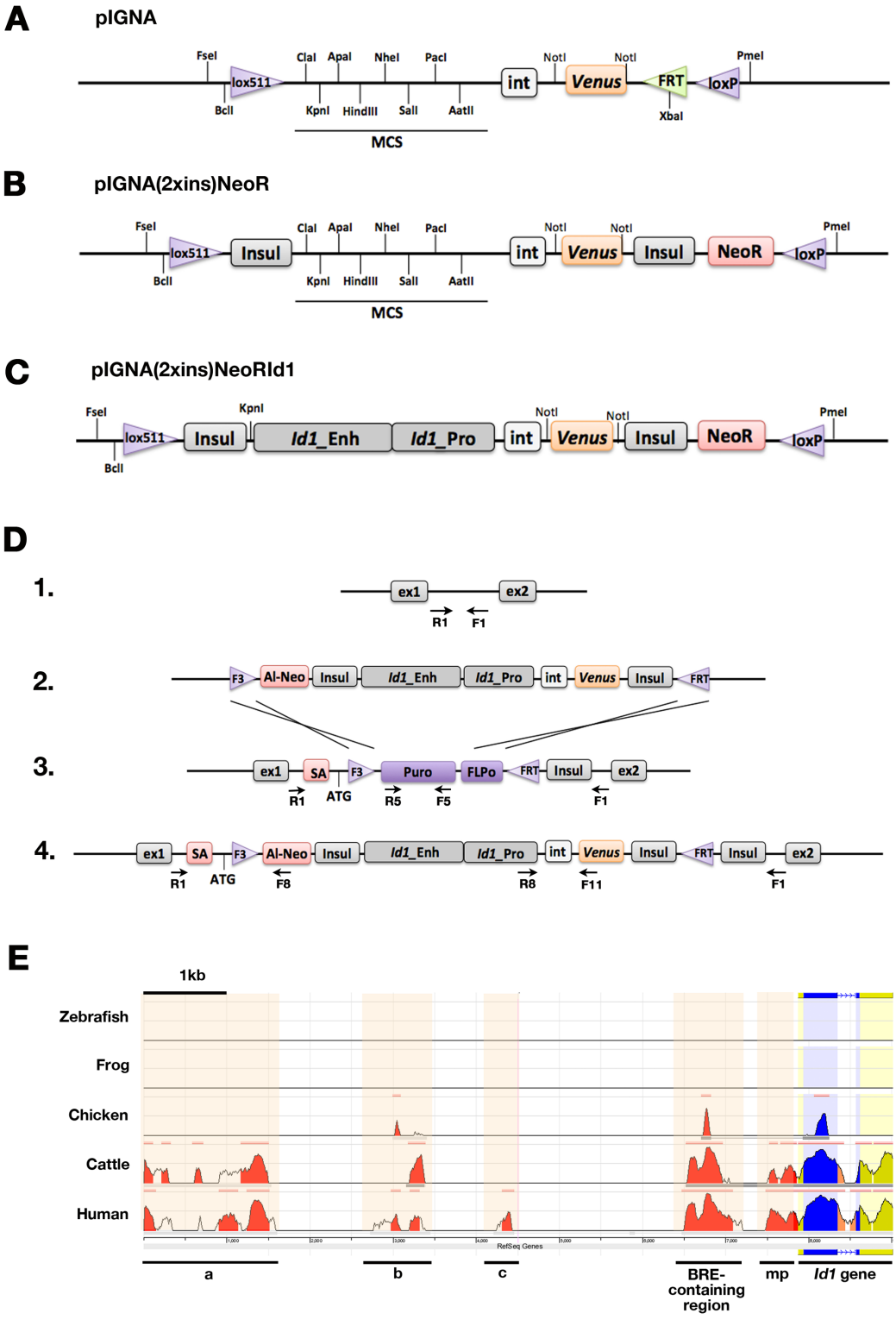

Fig. 2 Schematics of intermediate, targeting vectors and RMCE-mediated recombination process during ES cell targeting. (A) pIGNA vector as synthetized at GeneArt®. Two lox sites (lox511 and loxP, in a head-to-head orientation) enclose a multiple cloning site (MCS), a chimeric intron from the pCI-neo vector (Promega), a Venus reporter gene endowed with a nuclear localization signal, a degron element and a polyadenylation signal obtained from the pCI-Neo

vector (Promega). Two NotI restriction sites flank the Venus reporter, so that the cassette including *Venus-NLS-PEST* can be easily customized. An FRT site including a unique XbaI restriction site allows easy insertion of neomycin resistance cassette (NeoR) from an in-house vector. Unique sites are placed outside the lox sites to allow the excision of the whole sequence. **(B)** pIGNA(2xins)NeoR as an easy-fitting platform for the study of *cis*-regulatory elements. Two insulators from the chicken β-globin gene (~1.2 kb) and a NeoR cassette (~1.8 kb) were cloned into the pIGNA vector, destroying the original FRT recombination site. **(C)** pIGNA(2xins)NeoR vector was customized with a genomic sequence spanning 7874 bp upstream the *Id1* TSS and cloned within two separate blocks upstream the chimeric intron sequence, resulting in the pIGNA(2xins)NeoRId1 vector (see Results of this Appendix). **(D)** The panel shows a schematics of the wild-type *Gt(Rosa)26Sor* locus **(D,1.)**. Below, the RMCE-mediated recombination of the pXCHG3Id1 vector **(D,2.)** into the conditional locus **(D,3.)**, and the obtained recombined locus **(D,4.)**. Black arrows indicate relative position and orientation of the primers used for PCR screening. **(E)** Schematics of the Evolutionary Conserved Regions (ECR) obtained at the ECRBrowser (http://ecrbrowser.dcode.org) on the *cis*-regulatory region upstream *Id1* TSS (~7.8 kb), chosen for driving the reporter expression. Conserved regions are displayed on the vertical axis from the genomes of Zebrafish, Frog, Chicken, Cow and Human (from the top to the bottom). Conserved regions above the 70% of similarity were colored in red. Blue bars at exonic regions, Salmon at intronic regions, Green at untranslated region on the *Id1* gene. Five blocks of conserved regions were identified (named a, b, c, BRE-containing region, mp = minimal promoter). MCS, multiple cloning site; Insul, chicken β globin insulator; NeoR, Neomycin resistance cassette; *Id1*_Enh, *Id1* enhancer (from -7874 bp to -720 bp upstream *Id1* TSS); *Id1*_Pro, *Id1* minimal promoter (from -720 bp to -1 bp upstream *Id1* TSS); int, chimeric intron from pCI-neo mammalian expression vector (Promega); SA, splice acceptor.

Choice of *cis*-regulatory region to construct a BMP activity sensor

The best characterized BMP target genes in limb buds are *Id1*, *Msx2* and *Grem1* (see Introduction; Fig. 3A). *Id1* and *Msx2* are expressed from early stages onward in similar patterns. This includes a domain in the anterior limb bud mesenchyme and a smaller domain in the posterior mesenchyme connected by a sub-ectodermal mesenchymal domain (see Introduction and Fig. 3A). The *Id1* expression pattern appeared overall broader than the *Msx2* domain. *Id1* transcripts levels were higher than the ones of *Msx2* when BMP activity was high; this is seen best at early (22-28 somites) and late stages (38 somites onwards) (Fig. 3A; Benazet et al., 2009; Lopez-Rios et al., 2012). During low BMP activity (28 – 38 somites) *Id1* and *Msx2* transcript levels were rather similar. In order to evaluate the target gene that best recapitulates loss or gain of BMP activities, the mesenchymal *Smad4* and *Grem1* loss-of-function were used for analysis. Results showed

that *Id1* transcripts were lost more than *Msx2* in *Smad4* deficient limb buds both at E10.5 and E12.5, pointing to a more specific role of *Id1* in sensing the canonical BMP pathway (Fig. 3B,C). Up-regulation was similar for both *Id1* and *Msx2* in mouse limb buds lacking *Grem1* (Fig. 3B). These results indicated that *Id1* might be better suited as readout for BMP activity.

To choose the *cis*-regulatory region that might most faithfully mirror the dynamics of endogenous *Id1* expression in limb buds, we focused on the *cis*-regulatory regions surrounding the BRE. Since the BRE alone does not recapitulate the endogenous *Id1* expression in limb buds (Fig. 1A), we cloned a much larger fragment of the endogenous *Id1* promoter into the pIGNA(2xins)NeoR vector. The *Id1 cis*-regulatory region selected (Fig. 2E) encompasses 7874 bp upstream the *Id1* TTS and encodes two regions conserved in human, cattle and chicken genomes (–4895 bp to -4557 bp and -1397 bp to -785), one of which contains the well-characterized BRE (Korchynskyi and ten Dijke, 2002; Fig. 2E, regions b and BRE-containing element). The minimal promoter (mp) and a region spanning 1606 bp at the 5' limit of the element are conserved in the human and bovine genome (Fig. 2E, regions b and BRE-containing element). In addition, a short third region 'c' (-3560 bp to -3422 bp) is conserved between mouse and human genomes only (Fig 15E). These conserved regions were identified using the ECRBrowser server (http://ecrbrowser.dcode.org/) at a threshold of 70% of similarity.

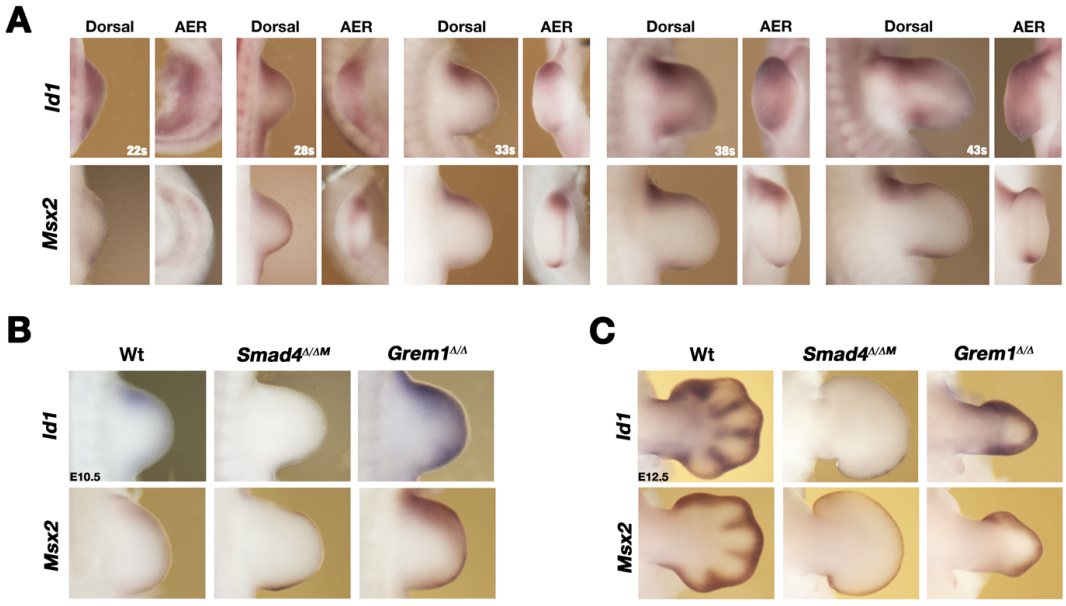

Fig. 3 Assessment of *Id1* and *Msx2* as target genes of BMP signaling through the canonical pathway. **(A)** Time-course WISH detection of *Id1* transcripts (upper panels) and *Msx2* transcripts (lower panels) at stages ranging from 22 to 43 somites; dorsal and frontal (AER) points of view of

the expression pattern are reported. **(B)** *Id1* (upper panels) and *Msx2* (lower panels) transcripts are detected by WISH in wild-type, *Smad4*$^{\Delta/\Delta M}$, and *Grem1*$^{\Delta/\Delta}$ limbs (from left to right), from dorsal and frontal (AER) points of view at E10.5 (33-35 somites; n=2). Results showed that both *Id1* and *Msx2* transcripts levels were responding to the amount of BMP signaling the limb was exposed to in the different genetic backgrounds. However, *Id1* transcripts are better cleared from the limb bud than *Msx2* transcripts when *Smad4* is removed from the mesenchyme in the *Smad4*$^{\Delta/\Delta M}$ background. **(C)** As in panel **(B)**, *Id1* and *Msx2* expression patterns are imaged in three genetic backgrounds. Limbs are staged E12.5; only dorsal view is displayed (n=2). As for limbs at E10.5, *Id1* transcripts clearance is more drastic in the *Smad4*$^{\Delta/\Delta M}$ background than for *Msx2* transcripts. s, somites.

Cloning steps for the targeting vector

The chosen mouse *Id1 cis*-regulatory region was assembled from a bacterial artificial chromosome (BAC), sequenced to exclude alterations and cloned into the pIGNA(2xins)NeoRmp vector to generate the pIGNA(2xins)NeoRId1 targeting vector (Fig. 2C). In order to target the *Gt(Rosa)26Sor* locus in V6.5 ES cells (Tsanov et al., 2012), the backbone and the recombination sites of the pIGNA(2xins)NeoRId1 vector were inserted into a shuttle vector provided by McMahon Lab, which was a prerequisite to obtain the targeting vector pXCHG3Id1 (~17.1 Kb).

RMCE-mediated insertion into the *Gt(Rosa)26Sor* locus

pXCHG3Id1 vector was electroporated in V6.5 ES cells (Eggan et al., 2001; Tsanov et al., 2012) carrying a customized *Gt(Rosa)26Sor* locus, which should provide a permissive environment for transcription (Turan et al., 2011; Zambrowicz et al., 1997). The intronic region between exons 1 and 2 was replaced with two sequences that encode a Puromycin resistance and a FLP recombinase, flanked by F3 and FRT recombination sites. Upstream the F3 site, a splice acceptor and an ATG translation starting codon were placed to allow for a selection cassette to be expressed by the endogenous *Gt(Rosa)26Sor* promoter; in addition, a full-length chicken β-globin insulator was cloned downstream the FRT site (Fig. 2D). The resulting customized and RMCE compatible ES cells were called FLPoC2 (Tsanov et al., 2012). These cells were used for targeting.

A vial of FLPoC2 cells at passage 15 was thawed 11 days before targeting on a monolayer of mitomycin-treated EMFI. Cells were kept in culture and passaged on a new mitomycin-treated EMFI monolayer every two days, whenever ES cell reached 75-80 % confluency. On the day of targeting 8 x 10 cm dishes of ES cell on EMFI were treated with trypsin as

for passaging and pre-plated for 12 min to let most of the EMFI cells to attach to the plate surface. Cells were pulled into two 50 ml falcon tubes; 10 µl were saved for counting cells and the rest was centrifuged at 2000 rpm for 5 min and the pellet was re-suspended in 2.6 ml of pre-warmed PBS without calcium and magnesium (GIBCO). The content of the two falcon tubes was pulled to get a total volume of 5.2 ml and a cell concentration of 18.75 x 10^6 cells/ml. pXCHG3Id1 targeting vector to a final concentration of 1 µg/µl in a total of 35 µl of water (GIBCO) was added to two cuvettes (Biorad Gene Pulser 165-2088). One cuvette carried 35 µl of water alone and was used as negative 'water' control. 800 µl of cell suspension in PBS was added to each cuvette and the content was gently mixed. Electroporation was achieved with 475 µF of capacitance and 0.24 KV of voltage on a BioRad Gene Pulser II. Cuvettes were incubated 20 min on ice and the content of each cuvette was resuspended in 9 ml of pre-warmed ES cell medium (see Material and Methods). The content of the two experimental cuvettes was pulled and plated 1:10 on 10 x 10 cm gelatin-coated dishes and 1:5 on 5 x 10 cm gelatin-coated dishes. 'Water' control was plated 1:10 on 2 x 10 cm dishes and 1:5 on 2 x 10 cm dishes. 800 µl of cells in PBS were not electroporated; they were re-suspended in 4.5 ml ES cell medium and plated the same way as the 'water' control.

The second day after targeting, ES cell were cultured in the presence of G418 (Life Technologies) at a concentration of 200 µg/ml (Tsanov et al., 2012). Medium was changed every day. On the fourth day from targeting, all plates showed massive cell death. On the sixth day from targeting, ES cell clones appeared. No ES cell clones were visible on the control dishes containing the 'water' control cells.

Nine days after electroporation, 14 clones on the experimental dishes were picked with a p200 Gilson pipette and single colonies were moved into a 48-well plate containing EMFI cells and ES cell medium without selection.

The medium was changed every day. ES cell clones were either tryplated or passaged 1:3 into a progressively larger plate (24-, 6-well plate, 6 cm plate, 10 cm plate). When cells were into a 24-well plates, were also passaged on a gelatin-coated plate for DNA retrieval for Southern Blot analysis (not shown). The rest of the pellet was used for PCR screening. ES cell clones were frozen in three vials when they displayed 75-80 % confluency either from a 6 cm or a 10 cm dish. 12 out of 14 clones were successfully expanded and frozen.

All 12 ES cell clones were screened by PCR and all of them showed correct integration at the F3 recombination site and the presence of an internal transgene sequence spanning the *Id1* minimal promoter and the *Venus* coding sequence. The frequency of recombinant colonies was about half the one reported by Tsanov et al. 2012 (~1 colony per 10^6 cells). This is likely due to the relatively large size of the targeting vector (~17

kb). Out of 12 ES cell clones, 7 were of mixed composition and were excluded from further analysis. The other 5 ES cell clones (whose screening by PCR is showed in Fig. 4A), were expanded and used for blastocyst injection. Screening conditions and primer sequences are reported in Table 1.

Target amplicon	Forward primer	Reverse primer	Annealing temp.	Cycle number
Rec. F3 site (F8-R1)	5'- CATGATGGATACTTTCTCGG -3'	5'- GTGATCTGCAACTCCAGTC -3'	56°C	31
Transgene (F11-R8)	5'- GGACACGCTGAACTTGTGG -3'	5'- GTCCTGAGTCACTGGCCAAC -3'	57°C	30
Cond. Locus (F5-R5)	5'- CTCAGAAAGCTGGTCATCAG -3'	5'- CATCACCGACATCGTGTC -3'	58°C	32
Wt allele (F1-R1)	5'- GGATATGAAGTACTGGGCTCT -3'	5'- GTGATCTGCAACTCCAGTC -3'	58°C	36

Table 1. PCR screening strategy. From the top to the bottom, efficient recombination of the conditional *Gt(Rosa)26Sor* locus in FLPoC2 cells was tested by amplification over the F3 recombination site, by checking the presence of the transgene, of the conditional locus (for incomplete recombination), and the wild-type allele. Primer sequences are reported and their position in the recombined locus is depicted in the schematics in Figure 15D. A standard PCR amplification protocol was used, with 1 minute of elongation at 72°C. Annealing temperature and cycle number are reported for each reaction.

Analysis of ES cell clones

Potential and dynamics of Venus expression in the different ES cell clones were tested initially in embryoid bodies (EB). In order to assess which EB differentiation stage exhibited the highest expression of *Id1*, R1 cells were differentiated into EBs and harvested at different time points (5, 8, 12, 16 days) for a PCR analysis. The levels of *Id1* and *Msx2* expression were quantified in comparison to *Hand2*, whose expression rises progressively during EB differentiation (PhD thesis by Marco Osterwalder). This analysis showed that the *Id1* transcriptional activity peaked between day 8 and 12 of differentiation, whereas *Msx2* transcripts remained constant (Fig. 4B). This analysis was used for further EB-based experiments, which were then conducted either at day 10 or day 12 of differentiation. Venus fluorescence and anti-GFP antibody staining were assessed in clone 1A1 (Fig. 4C,D; n=3) and on other clones (1A3, 1A6, 1C2; data not shown). Ubiquitous Venus expression driven by the histone H2B promoter in the context of the *Smad4* conditional locus served as a positive control (Osterwalder et al., 2010), whereas parental FLPoC2 cells as negative controls (Fig. 4C,D, right-most pictures). This analysis showed that the activity of *Id1-Venus* in clone 1A1 correlates well with the *Id1* transcript levels upon short-time (7 hr) stimulation with hrBMP4 protein (Fig. 4E, F).

Unexpectedly, *Id1* was not permanently induced by hrBMP4 treatment, but rather varied overtime (Fig 16F; n=1). This experiment was repeated with similar results using clone 1A3 (n=1; data not shown). These results indicate that the *Id1-Venus* reporter construct is able to sense changes in BMP activity with good temporal resolution (below 1 hr).

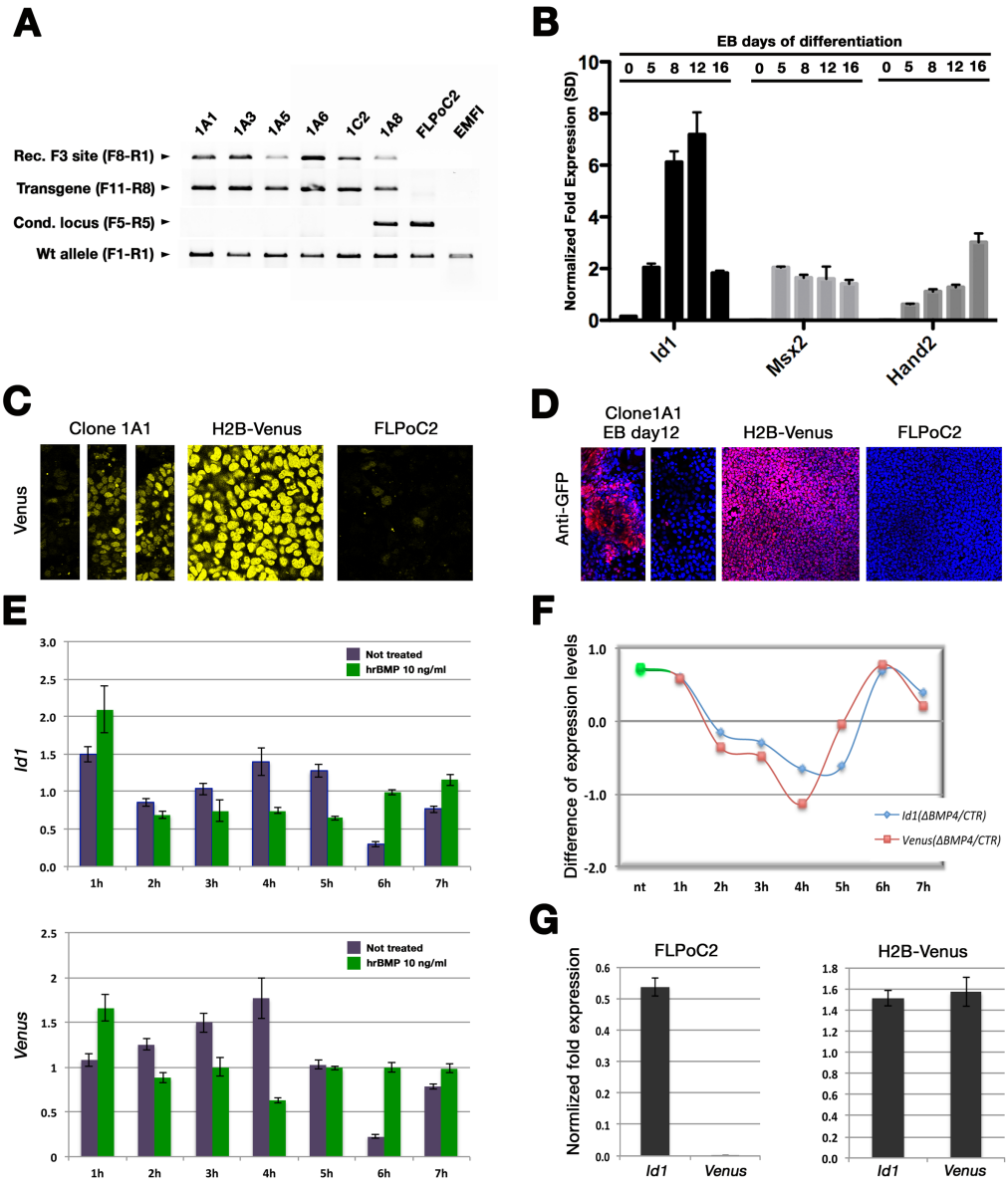

Fig. 4 (A) PCR screening of selected non-mixed ES cell clones. DNA samples from 1A8 mixed clone, FLPoC2 parental ES cells and EMFI cells were used as controls. From the top to the bottom, the PCR reactions were used to test: effective recombination over the F3 recombination site; presence of the transgene; presence of the conditional *Gt(Rosa)26Sor* locus (from FLPoC2 cells); presence of the wild-type *Gt(Rosa)26Sor* locus. The PCR screening reveals 5 successfully and

completely targeted clones, heterozygous for the *Id1-Venus* transgene in the *Gt(Rosa)26Sor* locus. **(B)** *Id1*, *Msx2*, *Hand2* transcripts were quantified by RT-qPCR on embryonic bodies (EBs) generated from R1 ES cells at day 5, 8, 12, 16 of differentiation. Time point 0 (days) is equivalent to non-differentiated ES cell. Values are reported as normalized fold expression ± SD (bars) calculated on the experiment replicates. The experiment was performed one time. Samples, either as EB pellets or purified RNA samples were provided by Dr. Marco Osterwalder. **(C)** Confocal fluorescence images (63x, oil immersion objective) of EB at day 10 of differentiation. EBs were obtained from clone 1A1 ES cell; H2B-Venus ES cell (Osterwalder et al., 2010) were used as positive control and FLPoC2 parental ES cell were used as negative control (from left to right, respectively). For the left-most panel, three sections from different fields-of-view were juxtaposed to indicate the variation in fluorescence intensity encountered in the samples. EBs from clone 1A1 were treated with 10 ng/ml hrBMP4 for 4 hours before cell harvesting to trigger *Venus* expression. **(D)** Confocal fluorescence images (20x) detecting Venus protein by use of the cross-reacting anti-GFP antibody in EBs. From left to right: EBs at day 12 of differentiation obtained from 1A1 ES cell; H2B-Venus cells (2 days in culture on gelatin-coated dish); parental FLPoC2 cells (also 2 days in culture on gelatin-coated dish). Two segments from different fields-of-view were juxtaposed in the left-most image to display the variety in fluorescent intensity among differently committed groups of cells. **(E)** RT-qPCR quantification of *Id1* (upper panel) and *Venus* (lower panel) transcripts from differentiated EBs at day 10 from clone 1A1, either treated with hrBMP4 (10ng/ml) at different time-points before harvesting (1 to 7 hr – on the horizontal axis -) – green color - or non-treated related controls – violet color-. **(F)** Plot of the differences between the *Id1* and *Venus* transcript levels (blue and red line/dots, respectively) of hrBMP4-treated versus non-treated samples reported in panel **(E)**. The green dots labeled as 'nt'= 'non-treated' samples do not represent a difference, but the absolute expression value of the transcripts at t=0. **(G)** RT-qPCR quantification of *Id1* and *Venus* transcripts from EBs at day 10 of differentiation, derived from FLPoC2 ES cell (left plot) and H2B-Venus ES cell (right plot) (used as negative and positive controls, respectively, for the experiment in panels **(E)** and **(F)**).

Blastocyst injection

Blastocyst injection procedure was outsourced at the Transgenic mouse facility at the Biozentrum (Basel), directed by Daniela Klewe-Nebenius. 1A1, 1A3, 1A5, 1A6 ES cell clones were injected in Balb/cxBalb/c, or C57Bl/6 J -Tyr<c-2j>/j x C57Bl/6 J -Tyr<c-2j>/j, or C57Bl/6 J x C57Bl/6 J blastocysts. Out of 43 injection attempts, 4 chimeras between 20% and 50% chimerism (based on coat color assessment) were obtained. No germ-line transmission was however obtained.

13. APPENDIX 3 _ ESTABLISHMENT OF THE AGGREGATION CHIMERA TECHNIQUE

Introduction and aim of the project

The necessity of dissecting *cis*-regulatory landscapes to understand developmental processes at a molecular level has become important (see for instance Andrey et al., 2013; Attanasio et al., 2013). To respond to this need, we sought to establish a fast and robust technique to get time- and cost-effective readouts of the activity of *cis*-regulatory regions of interest. Homologous recombination is the standard way to obtain site-specific integration of single-copy transgenes (Capecchi, 1989). Once suitable recombinase target sites are inserted into the genome by homologous recombination, specific targeting into the same locus can be repeatedly achieved by Recombinase-Mediated Cassette Exchange (RMCE) or dual RMCE (dRMCE) (see Osterwalder et al., 2010; Turan et al., 2013). The correctly engineered ES cells are either transferred into blastocoel cavity or aggregated with 8-cell stage embryos (Wood et al., 1993a) and then injected into pseudopregnant mothers (reviewed in Tanaka et al., 2009). On these bases, we sought to implement the ES cell aggregation chimera technique previously established (Wood et al., 1993b), with the technical support of Alexander Auhlela (EBML, Heidelberg) and Jean-Francois Spetz (FMI, Basel).

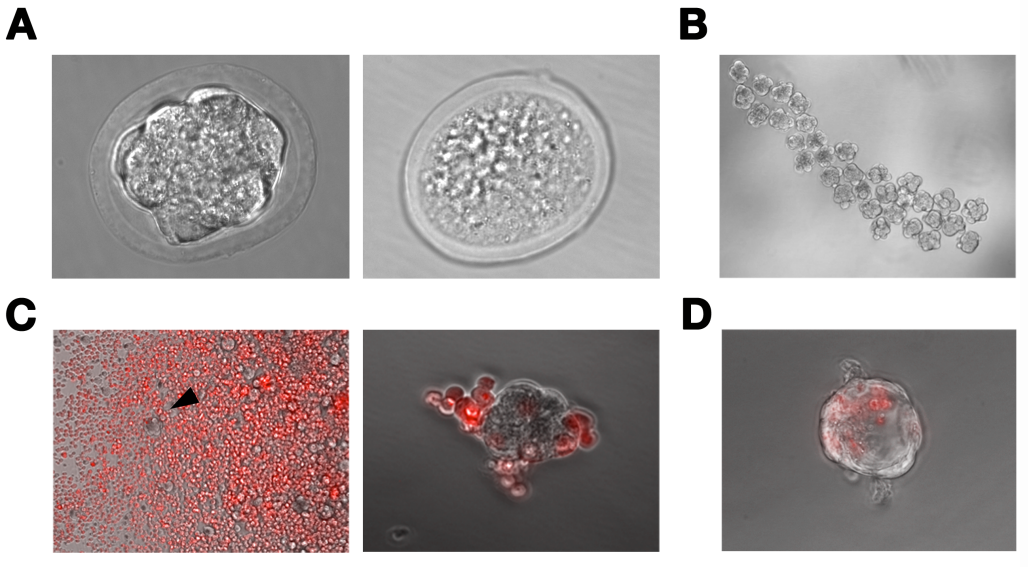

Fig. 1 Generation of aggregation chimeras. (A) Morula-stage embryos are flushed out of the uterus of donor mothers at E2.5. In the left panel, a good embryo with its cells surrounded by the *zona pellucida* (a glycoprotein membrane). In the right panel, a bad embryo appears translucent cell debris can be seen. These embryos were discarded. **(B)** The *Zona pellucida* was removed by digestion with Tyrode's acid. *Zona pellucida*-free embryos appear at morula stage **(C)** Left panel:

part of an aggregation drop is depicted. Phase contrast is overlapped with red-florescence to show the dsRed of the G4dsRed ES cells. The black arrowhead points at a morula stage embryos in the aggregation drop. After aggregation, morulas are cleaned from excess ES cells. Right panel: G4dsRed ES cells are aggregated with a morula. **(D)** After aggregation, ON incubation allows the morulas to develop into blastocysts and ES cells are incorporated into the inner cell mass (red fluorescence) giving rise to the embryos proper.

The aggregation procedure

ES cell handling

ES cells are treated according to the general protocol (see Material and Methods). On the day of aggregation, at least one 6 cm dish of ES cell cultured on a monolayer of mitomycin-treated EMFI cells must be ready for passage. The ES cells on this dish will be partly passaged 1:3 and partly used for aggregation. ES cells destined for aggregation are resupended in freshly prepared aggregation medium (18 ml DMEM 4,5 g/L Glucose [the same one used for ES cell], 66 mg Ca-lactate [Sigma Cat. 21185]). Mix well to dissolve. Add 2 ml FCS [Gibco] and filter solution with a 0.22 µm filter) to achieve a final concentration between 1.1 and 1.3 x 10^6 cells/ml. To make the aggregation plate, cells are pipetted as drops of ~35 µl into a 10 cm Petri dish and drops are covered with mineral oil. The aggregation plate is pre-equilibrated at 37°C, 5% CO_2 for at least 20 min.

The ES cells we have used for aggregation are: R1 (Nagy et al., 1993), FLPoC2-targeted ES cells clone 1A3 (see Appendix 1), H2B-Venus ES cells (Osterwalder et al., 2010), G4dsRed (Vintersten et al., 2004). 'G4dsRed' is a 129S6/B6-F1 ES cell line carrying a transgene encoding the dsRed fluorescent protein, and was used to maintain aggregation with non-fluorescent host embryos (Fig. 1).

Superovulation of donor females

Female NMRI mice of 3 to 5 weeks of age are injected intraperitoneally (25G needle) on day 0 with 5 I.U. PMSG (Pregnant Mare Serum Gonadotropin - *Pregnyl* from Organon). The PMSG powder is reconstituted in sterile PBS w/o calcium and magnesium from Gibco in 1ml aliquots to a final concentration of 50 I.U./ml and stored at -20°C in the dark. Gonadotropin working aliquots are kept at the above conditions for at least 2 months, or until decrease in the efficiency is detected. On day 2 the mice are injected with 5 I.U. hCG (Folligon from Intervet). hCG powder is reconstituted in sterile PBS to a final

concentration of 500 I.U./ml, and stored at -20°C in 100µl aliquots in the dark. Just before use, add 900 µl sterile PBS to dilute hCG to 50 I.U./ml. Both injections are performed at 1:30 pm on day 0 and day 2. After injection of hCG, the primed female mice are set to mate with proven stud males.

Material for collecting and processing embryos

- Dissecting microscope
- Forceps: one bent, one straight
- Warming plate set at 37°C close to the microscope
- M2 medium (prepared following the recipe _ see below)
- KSOM medium (MR-106-D from Millipore)
- Mouth pipette (A5177-5EA from Sigma)
- Pulled capillaries (7087 45 from BlauBrand); the aspiring hole diameter should be between 110 and 140 µm
- Needle (304000 from BD Microlance, 30G) blunted by scratching the tip over sand paper
- 1 ml syringes for flushing and 2 ml for making drops
- Cell Petri dishes (10 cm and 3.5 cm);
- Mineral oil (M5310 from Sigma – test every bottle before use – keep at RT in the dark)
- Tyrode's solution (T1788 from Sigma – aliquot in 2ml tubes and store at -20°). Alternatively, prepare the solution as follows (for 500ml):

NaCl	4 g
KCl	0.1 g
$CaCl_2.2H_2O$	0.13 g
$MgCl_2.6H_2O$	0.05 g
Glucose	0.5 g
(PVP)-40	2 g

Dissolve powders in about 450 ml of water. Adjust to pH 2.5 with 1M HCl. Top up to 500 ml. Sterilize by filtration with 0.22 µm stericup from Millipore, aliquot and store at -20°C. Thawed aliquots can be frozen once.

Notes about embryos handling

1. Mouth pipetting is advised;

2. To better visualize embryos, use light from below and play with the dark field to get the best observation point. When moving the embryos from one drop to the other, use a low magnification, such as you just see dots in place of cells. When observing the embryos, use a high magnification (like for digestion of the *zona pellucida*);

Embryo collection

On E2.5 (experimental day 5) embryos at morula stage (8-16 blastomeres) are collected (Fig. 1A).

M2 medium (for handling embryos outside the incubator) must be prepared in advance (about 20 ml per experiment); it must pre-equilibrated at 37°C and 5% CO_2.

Procedure:

1. Pre-warm the loaded flushing and drop-making syringes together with some 10 cm and 3.5 cm Petri dishes on the warming plate;
2. Kill superovulated and plugged females at E2.5 and collect the oviduct with about 5 mm of uterus piece attached (the oviduct must be dissociated from the ovary, use thin scissor to this aim). Remove as much fat as you can. Oviduct/uteri fragments are collected in a 3.5 cm Petri dish filled with pre-warmed M2 medium;
3. Embryo flushing: place a oviduct/uterus fragment in a small drop of M2 medium in a 10 cm Petri dish, so that the piece does not float but is hydrated. At this stage of development, embryos are morulas settled in between the ovary and the distal part of the uterus. Two alternative techniques can be used to collect embryos:
4. Use a M2-loaded 1-ml syringe with a blunted 30G needle to flush the medium through the ampulla (the distal-most part of the oviduct) while holding the ampulla and the needle inside it with forceps, in order to prevent medium reflux. Embryos are flushed out at the end of the uterus.
5. Separate the oviduct from the uterus and unravel the distal part of the uterus with forceps, to increase the opening. Flush the embryos out of the uterus with a M2-loaded 1-ml syringe, while clumping the uterus extremity and the needle inside it with blunt forceps, in order to avoid fluid reflux.
6. Collect the embryos and transfer them to a clean drop, preferably on a 3.5cm Petri dish that is kept on the warming plate.

7. Process all the pieces.

8. Select good embryos: good embryos appear opaque in dark field. Blastomeres fill the space and are surrounded by the *zona pellucida*.

9. Keep embryos and tissue pieces in M2 medium on the 37°C plate whenever are not handling them and while preparing the ES cell for aggregation. Make sure medium does not evaporate.

Removal of the zona pellucida

Note: remember to use a previously coated glass needle for these and all next steps, otherwise embryos will stick to the glass. For this reason, use only bacterial Petri dishes and NOT cell culture dishes.

1. Take a 10 cm Petri dish and dispose 4 drops of M2 at four opposite points at the border of the plate. Place a drop of Tyrode's acid in the center of the dish, so that each drop is not touching the others. All solutions must be pre-equilibrated at 37°C, 5% CO_2;
2. Rinse the collected embryos in one M2 drop;
3. Move about 20 embryos per time into the drop of Tyrode's acid; closely look at the *zona pellucida* to disappear;
4. As soon as the *zona pellucida* is removed, rinse the embryos in the remaining three drops of medium.

See Fig. 1B

ES cells-embryos aggregation

1. Place from 5 to 15 embryos per drop on the aggregation plate, where ES cell must have formed a monolayer.
2. Incubate the aggregation plate (ES cells and embryos) at 37°C 5% CO_2 during aggregation (1-2 hrs).
3. In the meantime, prepare the dish for ON culture: place several 35 µl drops of KSOM medium on a 10cm petri dish and cover the drops with mineral oil. Equilibrate the plate for at least 15 min at 37°C 5% CO_2 before use.
4. After aggregation period, gently pipette the embryos up and down to detach them from underlying layer of ES cell.
5. Move the embryos to one drop of KSOM and clean them from excess of ES cells by gently pipetting up-and-down.

6. Transfer the embryos to fresh KSOM drop. Pay attention not to put more than 3-4 embryos per drop and place them distant from one another to avoid embryo-embryo aggregation.
7. Incubate the aggregation plate ON at 37°C 5% CO_2.
See Fig. 1C,D.

Solutions for culturing embryos

M2 medium:

11 stock solutions are prepared and stored at -20°C, ready-made for quick medium preparation:

Stock number	Solution	Grams per 100ml
0	10x NaCl (Merck 1064041000)	6.4g
1	100x $NaHCO_3$ (Merck 1063290500)	3.49g
2	100x Na-Pyruvate (Merck 1066190050)	0.36g
3	100x Streptomyc. Sulf. (Sigma 56501)	0.5g
4	100x KH2PO4 (Merck 1048731000)	1.62g
5	100x Ca-Lactate.3H2O (Sigma 44388)	4.65g
6	100x KCl (Merck 1049361000)	3.56g
7	100x MgSO4.7H2O (Merck 1058860500)	2.94g
8	100x Glucose (Sigma G8270)	10g
9	10x HEPES (Sigma 54457)	see below
10	100x K-PenG (Sigma P7794)	0.75g

Stocks number 3 and 10 have a shelf life of about 12 months.

Hepes solution: dissolve 24.85 g of HEPES in 400 ml of Aqua ad inject (Braun/Aichele Medico, Cat. 530108) in a sterile plastic bottle. Prepare 25 ml of 2 N NaOH in Aqua ad inject and adjust HEPES solution to pH 7.4 (with about 20 ml 2 N NaOH). Add 1 ml of Phenol Red (Sigma P0290), filter sterilize (with 0.22 µm stericup from Millipore, Cat. SGMPU02RE) and store 10.5 ml aliquots at -20°C. When preparing the working medium, add the appropriate amount of each stock solution and bring to volume with Aqua ad inject. Filter sterilize (with 0.22 µm stericup from Millipore Cat. SGMPU02RE), add 400 mg BSA (Sigma Cat. A3311) per 100 ml of medium in sterile conditions and let it dissolve.

Shelf life for this medium is 2 weeks at 4°C. Medium can be frozen before adding BSA for long-term storage. Aqua ad inject can also be frozen.

Preparation for transfer

Transfers are generally performed around 2 pm of the day after aggregation. At this point, embryos should be at morula or blastocyst stages. Contribution of ES cell to the inner cell mass should be partial, since too high percentage of ES cell may lead to not-viable mice or not-fertile chimeras. Before transfer, the embryos are rinsed by serial passage through 4 drops of M2 pre-equilibrated medium in a 10 cm petri dish, using 4 different glass needles; each needle has to be coated with medium for at least 10 min before starting.

Embryo transfer

(done by Javier Lopez-Rios)

MATERIAL FOR EMBRYO TRANSFER

- FST 14381-43 (also Moria 8143A): Moria Bonn Scissors
- FST 11151-10 (curved fine forceps, serrated)
- FST 11154-10 (curved tissue forceps 1x2)
- FST 18374-44 (Moria Seraphine Bulldog clamp MC44)
- FST 18025-10 (Suturing forceps; used to hold the upper part of the uterus before punching a hole with the 30G needle)

ANESTHESIA FOR EMBRYO TRANSFER

Ketamine/xylazine/acepromazine anesthesia cocktail to be administer by i.p injection (10 ml):

- Ketamine (100 mg/ml) 1.0 ml
- Xylazine (20 mg/ml) 1.0 ml
- Acepromazine (10 mg/ml) 0.3 ml
- Sterile water or saline 7.7 ml

Store the mix at 4°C for a maximum of two weeks (it can also be frozen).

Mouse body weight	Volume cocktail (for surgery)
20 g	0.13 ml
25 g	0.16 ml
30 g	0.20 ml
35 g	0.23 ml

EMBRYO TRANSFER PROCEDURE

1. Three days before the transfer, set 1-2 NMRI females (6-8 weeks of age; older females will be more difficult to use for embryo transfer as they accumulate fat) in plug-check with vasectomized males (proven to be sterile). Plug check the next morning and stop the mating. Non-plugged females can be reused, while pseudopregnant animals that are not transferred can be used again in two weeks of rest.
2. Keep surgical instruments sterile (clean them with Ethanol 70%; heat-sterilize for 10 seconds at >200°C).
3. Anesthetize the mouse.
4. Shave the mouse on both sides between the hindlimb and last rib. Put protective gel on both eyes.
5. Clean the skin with 70% EtOH and cellulose pads in the direction of the hair.
6. Use the curved tissue forceps 1x2 to clip the skin and the Moria Bonn Scissors to cut, make an incision of around 5 mm in the skin, in the region where the ovary is (small depression on the side).
7. Use the same tools as above to detach the skin from the peritoneum on both sides of the wound.
8. Clean the wound again with cellulose pads soaked in 70% EtOH in the direction of the hair.
9. Under the microscope, locate the ovary by moving the wound like a window. Fat is white, while the ovary is orange and can be found close to the kidney (dark red).
10. Using the same tools, pinch and cut the peritoneal wall. Make a small cut, introduce the tip of the closed scissors through it and open the scissors to widen the opening. This helps to prevent bleeding. If bleeding occurs, it can be stopped with absorption pads.
11. Using the serrated and 1x2 curved fine forceps search for the ovary and pull it out by the fat, taking care not to touch the ovary, oviduct or uterus. Use a seraphine clamp on the fat to keep the uterus out of the body wall and in the right orientation for injection, always trying to avoid excessive tension on the uterus.
12. Load 8 (max. 10) embryos into the glass transfer capillary in the minimum amount of

media and make sure that two air bubbles are placed after the embryos, allowing to monitor a successful transfer.

13. Turn the mouse so that the uterus can be accessed with the needle in parallel. Ideally, hold a 30G needle/syringe and the transfer capillary in the same hand, while holding the uterus with suturing forceps. Make a hole with the 30G needle and immediately insert the glass capillary and blow the embryos into the uterus by making sure the bubbles are gone from the capillary.

14. Place the uterus back into the body cavity by holding the wall of the peritoneum with the 1x2 forceps; release the seraphine clamp and use the serrated fine curved forceps. Hold the sides of the peritoneum.

15. Put back the sides of the skin wound so that the inner sides are touching and you see the borders of the wound. Close it using two suture clips.

16. Repeat the whole procedure on the other side. One female can be transferred on both sides in around 20 minutes.

17. Place the mouse in its cage, cover with tissue and put under a heating lamp (or onto heating plate) until it regains consciousness (around 30-40 minutes after the end of the procedure). Provide mouse with analgesics at free will.

18. 10 days after surgery, remove the clips. Weight increase is a reliable sign of pregnancy.

Results

All the transferred pregnant females were allowed to deliver; no embryos were collected during pregnancy. Trial experiments with flushed and re-implanted embryos (without aggregation step) provided 7 and 18 pups from embryos without and with tyrode's acid treatment, respectively, out of a total 60 embryos transferred. From G4dsRed ES cells we obtained 5 chimeras – 3 males and 2 females - (10%, 30%, 50%, 95%, 100% of chimerism based on the agouti coat color) out of 24 pups from 35 mice transferred.

Chimeras and F1 pups were both phenotyped by detection of fluorescence in the red channel and genotyped by PCR (Fig. 2). From the FLPoC2-targeted ES cells clone 1A3 2 male chimeras (both 10% of chimerism) were obtained in a litter of 4 pups out of 10 mice transferred. Germline transmission has been achieved with the highest chimeric grade.

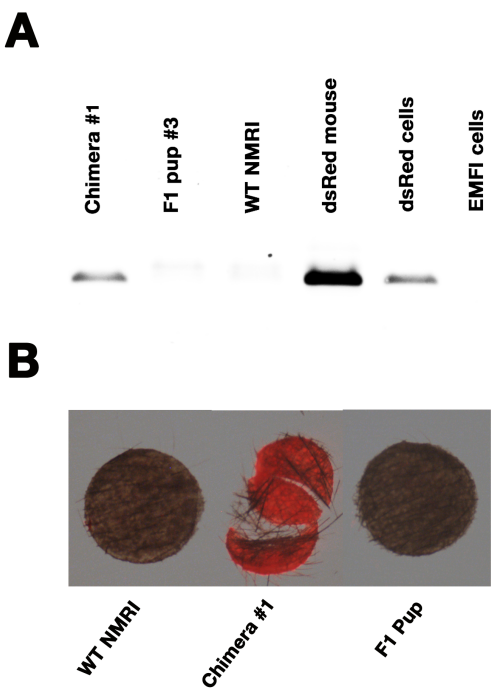

Fig. 2 Screening for the dsRed allele. Chimeras and F1 pups obtained from the transfer of embryos aggregated with G4dsRed cells were screened by PCR and by detection of the dsRed ubiquitous fluorescence directly in the ear biopsy. PCR screening was carried out using the protocol provided by Jackson Laboratory. (A) From left to right, PCR screening of chimera no. 1 (95% chimerism from coat color); F1 pup with black coat obtained from chimera no. 1 was found negative for the dsRed-expressing transgene; a wild-type NMRI biopsy was used as negative control; a biopsy taken from a mouse known to carry the dsRed transgene was used as a positive control; DNA extracted from G4dsRed ES cells ('dsRed' in the figure) was used as positive control; DNA extracted from EMFI cells was used as negative control. (B) Epi-fluorescent and bright-field overlapped images show the fluorescent ear biopsy taken from chimera no. 1 (in the center), in comparison with a negative control from a wild-type NMRI mouse (on the left) and the non-fluorescent ear piece taken from F1 pup no. 3 (on the right).

Acknowledgments

Dr. Aimee Zuniga, Dr. Javier Lopez-Rios, contributed to the work shown in Appendix 2. In addition, Dario Speziale, Nathalie Riesen and Julie Leclercq contributed to the work shown in this Appendix 3.

14. REFERENCES

Afrakhte, M., A. Moren, S. Jossan, S. Itoh, K. Sampath, B. Westermark, C.H. Heldin, N.E. Heldin, and P. ten Dijke. 1998. Induction of inhibitory Smad6 and Smad7 mRNA by TGF-beta family members. *Biochemical and biophysical research communications*. 249:505-511.

Ahn, K., Y. Mishina, M.C. Hanks, R.R. Behringer, and E.B. Crenshaw, 3rd. 2001. BMPR-IA signaling is required for the formation of the apical ectodermal ridge and dorsal-ventral patterning of the limb. *Development (Cambridge, England)*. 128:4449-4461.

Akiyama, H., M.C. Chaboissier, J.F. Martin, A. Schedl, and B. de Crombrugghe. 2002. The transcription factor Sox9 has essential roles in successive steps of the chondrocyte differentiation pathway and is required for expression of Sox5 and Sox6. *Genes Dev*. 16:2813-2828.

Andrey, G., T. Montavon, B. Mascrez, F. Gonzalez, D. Noordermeer, M. Leleu, D. Trono, F. Spitz, and D. Duboule. 2013. A switch between topological domains underlies HoxD genes collinearity in mouse limbs. *Science (New York, N.Y.)*. 340:1234167.

Attanasio, C., A.S. Nord, Y. Zhu, M.J. Blow, Z. Li, D.K. Liberton, H. Morrison, I. Plajzer-Frick, A. Holt, R. Hosseini, S. Phouanenavong, J.A. Akiyama, M. Shoukry, V. Afzal, E.M. Rubin, D.R. FitzPatrick, B. Ren, B. Hallgrimsson, L.A. Pennacchio, and A. Visel. 2013. Fine tuning of craniofacial morphology by distant-acting enhancers. *Science (New York, N.Y.)*. 342:1241006.

Aulehla, A., W. Wiegraebe, V. Baubet, M.B. Wahl, C. Deng, M. Taketo, M. Lewandoski, and O. Pourquie. 2008. A beta-catenin gradient links the clock and wavefront systems in mouse embryo segmentation. *Nature cell biology*. 10:186-193.

Bakrania, P., M. Efthymiou, J.C. Klein, A. Salt, D.J. Bunyan, A. Wyatt, C.P. Ponting, A. Martin, S. Williams, V. Lindley, J. Gilmore, M. Restori, A.G. Robson, M.M. Neveu, G.E. Holder, J.R. Collin, D.O. Robinson, P. Farndon, H. Johansen-Berg, D. Gerrelli, and N.K. Ragge. 2008. Mutations in BMP4 cause eye, brain, and digit developmental anomalies: overlap between the BMP4 and hedgehog signaling pathways. *American journal of human genetics*. 82:304-319.

Bandyopadhyay, A., K. Tsuji, K. Cox, B.D. Harfe, V. Rosen, and C.J. Tabin. 2006. Genetic analysis of the roles of BMP2, BMP4, and BMP7 in limb patterning and skeletogenesis. *PLoS genetics*. 2:e216.

Barna, M., and L. Niswander. 2007. Visualization of cartilage formation: insight into cellular properties of skeletal progenitors and chondrodysplasia syndromes. *Developmental cell*. 12:931-941.

Barna, M., P.P. Pandolfi, and L. Niswander. 2005. Gli3 and Plzf cooperate in proximal limb patterning at early stages of limb development. *Nature*. 436:277-281.

Barrow, J.R., K.R. Thomas, O. Boussadia-Zahui, R. Moore, R. Kemler, M.R. Capecchi, and A.P. McMahon. 2003. Ectodermal Wnt3/beta-catenin signaling is required for the establishment and maintenance of the apical ectodermal ridge. *Genes Dev*. 17:394-409.

Bastida, M.F., R. Sheth, and M.A. Ros. 2009. A BMP-Shh negative-feedback loop restricts Shh expression during limb development. *Development (Cambridge, England)*. 136:3779-3789.

Baur, S.T., J.J. Mai, and S.M. Dymecki. 2000. Combinatorial signaling through BMP receptor IB and GDF5: shaping of the distal mouse limb and the genetics of distal limb diversity. *Development*. 127:605-619.

Bell, D.M., K.K. Leung, S.C. Wheatley, L.J. Ng, S. Zhou, K.W. Ling, M.H. Sham, P. Koopman, P.P. Tam, and K.S. Cheah. 1997. SOX9 directly regulates the type-II collagen gene. *Nat Genet*. 16:174-178.

Benazet, J.D., M. Bischofberger, E. Tiecke, A. Goncalves, J.F. Martin, A. Zuniga, F. Naef, and R. Zeller. 2009. A self-regulatory system of interlinked signaling feedback loops controls mouse limb patterning. *Science (New York, N.Y.)*. 323:1050-1053.

Benazet, J.D., E. Pignatti, A. Nugent, E. Unal, F. Laurent, and R. Zeller. 2012. Smad4 is required to induce digit ray primordia and to initiate the aggregation and differentiation of chondrogenic progenitors in mouse limb buds. *Development*. 139:4250-4260.

Benazet, J.D., and R. Zeller. 2013. Dual requirement of ectodermal Smad4 during AER formation and termination of feedback signaling in mouse limb buds. *Genesis (New York, N.Y.: 2000)*. 51:660-666.

Bensoussan, V., Y. Lallemand, J. Moreau, C.S. Cloment, F. Langa, and B. Robert. 2008. Generation of an Msx2-GFP conditional null allele. *Genesis*. 46:276-282.

Bi, W., J.M. Deng, Z. Zhang, R.R. Behringer, and B. de Crombrugghe. 1999. Sox9 is required for cartilage formation. *Nat Genet*. 22:85-89.

Blank, U., M.L. Seto, D.C. Adams, D.M. Wojchowski, M.J. Karolak, and L. Oxburgh. 2008. An in vivo reporter of BMP signaling in organogenesis reveals targets in the developing kidney. *BMC developmental biology*. 8:86.

Blitz, E., A. Sharir, H. Akiyama, and E. Zelzer. 2013. Tendon-bone attachment unit is formed modularly by a distinct pool of Scx- and Sox9-positive progenitors. *Development*. 140:2680-2690.

Blitz, E., S. Viukov, A. Sharir, Y. Shwartz, J.L. Galloway, B.A. Pryce, R.L. Johnson, C.J. Tabin, R. Schweitzer, and E. Zelzer. 2009. Bone ridge patterning during musculoskeletal assembly is mediated through SCX regulation of Bmp4 at the tendon-skeleton junction. *Developmental cell*. 17:861-873.

Brugger, S.M., A.E. Merrill, J. Torres-Vazquez, N. Wu, M.C. Ting, J.Y. Cho, S.L. Dobias, S.E. Yi, K. Lyons, J.R. Bell, K. Arora, R. Warrior, and R. Maxson. 2004. A phylogenetically conserved cis-regulatory module in the Msx2 promoter is sufficient for BMP-dependent transcription in murine and Drosophila embryos. *Development*. 131:5153-5165.

Brunet, L.J., J.A. McMahon, A.P. McMahon, and R.M. Harland. 1998. Noggin, cartilage morphogenesis, and joint formation in the mammalian skeleton. *Science*. 280:1455-1457.

Buckingham, M., L. Bajard, T. Chang, P. Daubas, J. Hadchouel, S. Meilhac, D. Montarras, D. Rocancourt, and F. Relaix. 2003. The formation of skeletal muscle: from somite to limb. *Journal of anatomy*. 202:59-68.

Burke, A.C., C.E. Nelson, B.A. Morgan, and C. Tabin. 1995. Hox genes and the evolution of vertebrate axial morphology. *Development*. 121:333-346.

Butler, S.J., and J. Dodd. 2003. A role for BMP heterodimers in roof plate-mediated repulsion of commissural axons. *Neuron*. 38:389-401.

Capecchi, M.R. 1989. Altering the genome by homologous recombination. *Science (New York, N.Y.)*. 244:1288-1292.

Chang, H., D. Huylebroeck, K. Verschueren, Q. Guo, M.M. Matzuk, and A. Zwijsen. 1999. Smad5 knockout mice die at mid-gestation due to multiple embryonic and extraembryonic defects. *Development*. 126:1631-1642.

Charite, J., D.G. McFadden, and E.N. Olson. 2000. The bHLH transcription factor dHAND controls Sonic hedgehog expression and establishment of the zone of polarizing activity during limb development. *Development*. 127:2461-2470.

Chen, M.H., Y.J. Li, T. Kawakami, S.M. Xu, and P.T. Chuang. 2004. Palmitoylation is required for the production of a soluble multimeric Hedgehog protein complex and long-range signaling in vertebrates. *Genes Dev*. 18:641-659.

Chevallier, A., M. Kieny, and A. Mauger. 1977. Limb-somite relationship: origin of the limb musculature. *Journal of embryology and experimental morphology*. 41:245-258.

Chiang, C., Y. Litingtung, M.P. Harris, B.K. Simandl, Y. Li, P.A. Beachy, and J.F. Fallon. 2001. Manifestation of the limb prepattern: limb development in the absence of sonic hedgehog function. *Dev Biol*. 236:421-435.

Choi, K.S., C. Lee, D.M. Maatouk, and B.D. Harfe. 2012. Bmp2, Bmp4 and Bmp7 are co-required in the mouse AER for normal digit patterning but not limb outgrowth. *PloS one*. 7:e37826.

Chung, J.H., A.C. Bell, and G. Felsenfeld. 1997. Characterization of the chicken beta-globin insulator. *Proc Natl Acad Sci U S A*. 94:575-580.

Cohn, M.J., J.C. Izpisua-Belmonte, H. Abud, J.K. Heath, and C. Tickle. 1995. Fibroblast growth factors induce additional limb development from the flank of chick embryos. *Cell*. 80:739-746.

Collery, R.F., and B.A. Link. 2011. Dynamic smad-mediated BMP signaling revealed through transgenic zebrafish. *Dev Dyn*. 240:712-722.

Collette, N.M., D.C. Genetos, A.N. Economides, L. Xie, M. Shahnazari, W. Yao, N.E. Lane, R.M. Harland, and G.G. Loots. 2012. Targeted deletion of Sost distal enhancer increases bone formation and bone mass. *Proc Natl Acad Sci U S A*. 109:14092-14097.

Collette, N.M., D.C. Genetos, D. Murugesh, R.M. Harland, and G.G. Loots. 2010. Genetic evidence that SOST inhibits WNT signaling in the limb. *Developmental biology*. 342:169-179.

Crossley, P.H., G. Minowada, C.A. MacArthur, and G.R. Martin. 1996. Roles for FGF8 in the induction, initiation, and maintenance of chick limb development. *Cell*. 84:127-136.

Cserjesi, P., D. Brown, K.L. Ligon, G.E. Lyons, N.G. Copeland, D.J. Gilbert, N.A. Jenkins, and E.N. Olson. 1995. Scleraxis: a basic helix-loop-helix protein that prefigures skeletal formation during mouse embryogenesis. *Development*. 121:1099-1110.

Cunningham, T.J., X. Zhao, L.L. Sandell, S.M. Evans, P.A. Trainor, and G. Duester. 2013. Antagonism between retinoic acid and fibroblast growth factor signaling during limb development. *Cell reports*. 3:1503-1511.

Cygan, J.A., R.L. Johnson, and A.P. McMahon. 1997. Novel regulatory interactions revealed by studies of murine limb pattern in Wnt-7a and En-1 mutants. *Development*. 124:5021-5032.

Dahn, R.D., and J.F. Fallon. 2000. Interdigital regulation of digit identity and homeotic transformation by modulated BMP signaling. *Science*. 289:438-441.

Danesh, S.M., A. Villasenor, D. Chong, C. Soukup, and O. Cleaver. 2009. BMP and BMP receptor expression during murine organogenesis. *Gene expression patterns : GEP*. 9:255-265.

Danielson, K.G., H. Baribault, D.F. Holmes, H. Graham, K.E. Kadler, and R.V. Iozzo. 1997. Targeted disruption of decorin leads to abnormal collagen fibril morphology and skin fragility. *The Journal of cell biology*. 136:729-743.

Dathe, K., K.W. Kjaer, A. Brehm, P. Meinecke, P. Nurnberg, J.C. Neto, D. Brunoni, N. Tommerup, C.E. Ott, E. Klopocki, P. Seemann, and S. Mundlos. 2009. Duplications involving a conserved regulatory element downstream of BMP2 are associated with brachydactyly type A2. *American journal of human genetics*. 84:483-492.

Davidson, D., A. Blanc, D. Filion, H. Wang, P. Plut, G. Pfeffer, M.D. Buschmann, and J.E. Henderson. 2005. Fibroblast growth factor (FGF) 18 signals through FGF receptor 3 to promote chondrogenesis. *J Biol Chem*. 280:20509-20515.

de Jong, D.S., B.L. Vaes, K.J. Dechering, A. Feijen, J.M. Hendriks, R. Wehrens, C.L. Mummery, E.J. van Zoelen, W. Olijve, and W.T. Steegenga. 2004. Identification of novel regulators associated with early-phase osteoblast differentiation. *Journal of bone and mineral research : the official journal of the American Society for Bone and Mineral Research*. 19:947-958.

Degenkolbe, E., J. Konig, J. Zimmer, M. Walther, C. Reissner, J. Nickel, F. Ploger, J. Raspopovic, J. Sharpe, K. Dathe, J.T. Hecht, S. Mundlos, S.C. Doelken, and P.

Seemann. 2013. A GDF5 point mutation strikes twice--causing BDA1 and SYNS2. *PLoS Genet*. 9:e1003846.
Dimitrov, B.I., T. Voet, L. De Smet, J.R. Vermeesch, K. Devriendt, J.P. Fryns, and P. Debeer. 2010. Genomic rearrangements of the GREM1-FMN1 locus cause oligosyndactyly, radio-ulnar synostosis, hearing loss, renal defects syndrome and Cenani--Lenz-like non-syndromic oligosyndactyly. *Journal of medical genetics*. 47:569-574.
Dreyer, S.D., G. Zhou, A. Baldini, A. Winterpacht, B. Zabel, W. Cole, R.L. Johnson, and B. Lee. 1998. Mutations in LMX1B cause abnormal skeletal patterning and renal dysplasia in nail patella syndrome. *Nat Genet*. 19:47-50.
Dudley, A.T., M.A. Ros, and C.J. Tabin. 2002. A re-examination of proximodistal patterning during vertebrate limb development. *Nature*. 418:539-544.
Dunn, N.R., G.E. Winnier, L.K. Hargett, J.J. Schrick, A.B. Fogo, and B.L. Hogan. 1997. Haploinsufficient phenotypes in Bmp4 heterozygous null mice and modification by mutations in Gli3 and Alx4. *Dev Biol*. 188:235-247.
Dupe, V., N.B. Ghyselinck, V. Thomazy, L. Nagy, P.J. Davies, P. Chambon, and M. Mark. 1999. Essential roles of retinoic acid signaling in interdigital apoptosis and control of BMP-7 expression in mouse autopods. *Dev Biol*. 208:30-43.
Dupont, S., A. Mamidi, M. Cordenonsi, M. Montagner, L. Zacchigna, M. Adorno, G. Martello, M.J. Stinchfield, S. Soligo, L. Morsut, M. Inui, S. Moro, N. Modena, F. Argenton, S.J. Newfeld, and S. Piccolo. 2009. FAM/USP9x, a deubiquitinating enzyme essential for TGFbeta signaling, controls Smad4 monoubiquitination. *Cell*. 136:123-135.
Eggan, K., H. Akutsu, J. Loring, L. Jackson-Grusby, M. Klemm, W.M. Rideout, 3rd, R. Yanagimachi, and R. Jaenisch. 2001. Hybrid vigor, fetal overgrowth, and viability of mice derived by nuclear cloning and tetraploid embryo complementation. *Proc Natl Acad Sci U S A*. 98:6209-6214.
Estrada, K.D., K.N. Retting, A.M. Chin, and K.M. Lyons. 2011. Smad6 is essential to limit BMP signaling during cartilage development. *Journal of bone and mineral research : the official journal of the American Society for Bone and Mineral Research*. 26:2498-2510.
Estrada, K.D., W. Wang, K.N. Retting, C.T. Chien, F.F. Elkhoury, R. Heuchel, and K.M. Lyons. 2013. Smad7 regulates terminal maturation of chondrocytes in the growth plate. *Dev Biol*. 382:375-384.
Evans, S.M., and T.X. O'Brien. 1993. Expression of the helix-loop-helix factor Id during mouse embryonic development. *Dev Biol*. 159:485-499.
Fallon, J.F., A. Lopez, M.A. Ros, M.P. Savage, B.B. Olwin, and B.K. Simandl. 1994. FGF-2: apical ectodermal ridge growth signal for chick limb development. *Science*. 264:104-107.
Farin, H.F., T.H. Ludtke, M.K. Schmidt, S. Placzko, K. Schuster-Gossler, M. Petry, V.M. Christoffels, and A. Kispert. 2013. Tbx2 terminates shh/fgf signaling in the developing mouse limb bud by direct repression of gremlin1. *PLoS genetics*. 9:e1003467.
Fernandez-Teran, M., and M.A. Ros. 2008. The Apical Ectodermal Ridge: morphological aspects and signaling pathways. *The International journal of developmental biology*. 52:857-871.
Fischer, L., G. Boland, and R.S. Tuan. 2002. Wnt signaling during BMP-2 stimulation of mesenchymal chondrogenesis. *Journal of cellular biochemistry*. 84:816-831.
Francis-West, P.H., A. Abdelfattah, P. Chen, C. Allen, J. Parish, R. Ladher, S. Allen, S. MacPherson, F.P. Luyten, and C.W. Archer. 1999. Mechanisms of GDF-5 action during skeletal development. *Development*. 126:1305-1315.
Francis-West, P.H., L. Antoni, and K. Anakwe. 2003. Regulation of myogenic differentiation in the developing limb bud. *Journal of anatomy*. 202:69-81.
Galli, A., D. Robay, M. Osterwalder, X. Bao, J.D. Benazet, M. Tariq, R. Paro, S. Mackem, and R. Zeller. 2010. Distinct roles of Hand2 in initiating polarity and posterior Shh

expression during the onset of mouse limb bud development. *PLoS Genet*. 6:e1000901.
Gamer, L.W., K. Tsuji, K. Cox, L.P. Capelo, J. Lowery, H. Beppu, and V. Rosen. 2011. BMPR-II is dispensable for formation of the limb skeleton. *Genesis*. 49:719-724.
Gao, L., T.J. Sheu, Y. Dong, D.M. Hoak, M.J. Zuscik, E.M. Schwarz, M.J. Hilton, R.J. O'Keefe, and J.H. Jonason. 2013. TAK1 regulates SOX9 expression in chondrocytes and is essential for postnatal development of the growth plate and articular cartilages. *Journal of cell science*. 126:5704-5713.
Goff, D.J., and C.J. Tabin. 1997. Analysis of Hoxd-13 and Hoxd-11 misexpression in chick limb buds reveals that Hox genes affect both bone condensation and growth. *Development*. 124:627-636.
Gross, M.K., M.S. Kainz, and G.F. Merrill. 1987. Introns are inconsequential to efficient formation of cellular thymidine kinase mRNA in mouse L cells. *Molecular and cellular biology*. 7:4576-4581.
Gunnell, L.M., J.H. Jonason, A.E. Loiselle, A. Kohn, E.M. Schwarz, M.J. Hilton, and R.J. O'Keefe. 2010. TAK1 regulates cartilage and joint development via the MAPK and BMP signaling pathways. *Journal of bone and mineral research : the official journal of the American Society for Bone and Mineral Research*. 25:1784-1797.
Haas, A.R., and R.S. Tuan. 1999. Chondrogenic differentiation of murine C3H10T1/2 multipotential mesenchymal cells: II. Stimulation by bone morphogenetic protein-2 requires modulation of N-cadherin expression and function. *Differentiation; research in biological diversity*. 64:77-89.
Hall, B.K., and T. Miyake. 2000. All for one and one for all: condensations and the initiation of skeletal development. *BioEssays : news and reviews in molecular, cellular and developmental biology*. 22:138-147.
Harfe, B.D., P.J. Scherz, S. Nissim, H. Tian, A.P. McMahon, and C.J. Tabin. 2004. Evidence for an expansion-based temporal Shh gradient in specifying vertebrate digit identities. *Cell*. 118:517-528.
Hartmann, C., and C.J. Tabin. 2001. Wnt-14 plays a pivotal role in inducing synovial joint formation in the developing appendicular skeleton. *Cell*. 104:341-351.
Hisa, T., S.E. Spence, R.A. Rachel, M. Fujita, T. Nakamura, J.M. Ward, D.E. Devor-Henneman, Y. Saiki, H. Kutsuna, L. Tessarollo, N.A. Jenkins, and N.G. Copeland. 2004. Hematopoietic, angiogenic and eye defects in Meis1 mutant animals. *The EMBO journal*. 23:450-459.
Hollnagel, A., V. Oehlmann, J. Heymer, U. Ruther, and A. Nordheim. 1999. Id genes are direct targets of bone morphogenetic protein induction in embryonic stem cells. *J Biol Chem*. 274:19838-19845.
Horiki, M., T. Imamura, M. Okamoto, M. Hayashi, J. Murai, A. Myoui, T. Ochi, K. Miyazono, H. Yoshikawa, and N. Tsumaki. 2004. Smad6/Smurf1 overexpression in cartilage delays chondrocyte hypertrophy and causes dwarfism with osteopenia. *The Journal of cell biology*. 165:433-445.
Huang, M.T., and C.M. Gorman. 1990. The simian virus 40 small-t intron, present in many common expression vectors, leads to aberrant splicing. *Molecular and cellular biology*. 10:1805-1810.
Hui, C.C., and A.L. Joyner. 1993. A mouse model of greig cephalopolysyndactyly syndrome: the extra-toesJ mutation contains an intragenic deletion of the Gli3 gene. *Nat Genet*. 3:241-246.
Inai, K., J.L. Burnside, S. Hoffman, B.P. Toole, and Y. Sugi. 2013. BMP-2 Induces Versican and Hyaluronan That Contribute to Post-EMT AV Cushion Cell Migration. *PloS one*. 8:e77593.
Iwai, T., J. Murai, H. Yoshikawa, and N. Tsumaki. 2008. Smad7 Inhibits chondrocyte differentiation at multiple steps during endochondral bone formation and down-regulates p38 MAPK pathways. *J Biol Chem*. 283:27154-27164.

Jagle, U., J.A. Gasser, M. Muller, and B. Kinzel. 2007. Conditional transgene expression mediated by the mouse beta-actin locus. *Genesis (New York, N.Y.: 2000)*. 45:659-666.

Jiang, Y., L.K. Chen, D.C. Zhu, G.R. Zhang, C. Guo, Y.Y. Qi, and H.W. Ouyang. 2010. The inductive effect of bone morphogenetic protein-4 on chondral-lineage differentiation and in situ cartilage repair. *Tissue engineering. Part A*. 16:1621-1632.

Jones, J.B., and S.E. Kern. 2000. Functional mapping of the MH1 DNA-binding domain of DPC4/SMAD4. *Nucleic acids research*. 28:2363-2368.

Kamiya, N., T. Kobayashi, Y. Mochida, P.B. Yu, M. Yamauchi, H.M. Kronenberg, and Y. Mishina. 2010. Wnt inhibitors Dkk1 and Sost are downstream targets of BMP signaling through the type IA receptor (BMPRIA) in osteoblasts. *Journal of bone and mineral research : the official journal of the American Society for Bone and Mineral Research*. 25:200-210.

Karamboulas, K., H.J. Dranse, and T.M. Underhill. 2010. Regulation of BMP-dependent chondrogenesis in early limb mesenchyme by TGFbeta signals. *Journal of cell science*. 123:2068-2076.

Kawakami, Y., J. Capdevila, D. Buscher, T. Itoh, C. Rodriguez Esteban, and J.C. Izpisua Belmonte. 2001. WNT signals control FGF-dependent limb initiation and AER induction in the chick embryo. *Cell*. 104:891-900.

Khokha, M.K., D. Hsu, L.J. Brunet, M.S. Dionne, and R.M. Harland. 2003. Gremlin is the BMP antagonist required for maintenance of Shh and Fgf signals during limb patterning. *Nat Genet*. 34:303-307.

Kitzing, T.M., Y. Wang, O. Pertz, J.W. Copeland, and R. Grosse. 2010. Formin-like 2 drives amoeboid invasive cell motility downstream of RhoC. *Oncogene*. 29:2441-2448.

Kmita, M., N. Fraudeau, Y. Herault, and D. Duboule. 2002. Serial deletions and duplications suggest a mechanism for the collinearity of Hoxd genes in limbs. *Nature*. 420:145-150.

Kmita, M., B. Tarchini, J. Zakany, M. Logan, C.J. Tabin, and D. Duboule. 2005. Early developmental arrest of mammalian limbs lacking HoxA/HoxD gene function. *Nature*. 435:1113-1116.

Knezevic, V., R. De Santo, K. Schughart, U. Huffstadt, C. Chiang, K.A. Mahon, and S. Mackem. 1997. Hoxd-12 differentially affects preaxial and postaxial chondrogenic branches in the limb and regulates Sonic hedgehog in a positive feedback loop. *Development*. 124:4523-4536.

Korchynskyi, O., and P. ten Dijke. 2002. Identification and functional characterization of distinct critically important bone morphogenetic protein-specific response elements in the Id1 promoter. *J Biol Chem*. 277:4883-4891.

Kurosawa, H., T. Imamura, M. Koike, K. Sasaki, and Y. Amano. 2003. A simple method for forming embryoid body from mouse embryonic stem cells. *Journal of bioscience and bioengineering*. 96:409-411.

Lallemand, Y., M.A. Nicola, C. Ramos, A. Bach, C.S. Clement, and B. Robert. 2005. Analysis of Msx1; Msx2 double mutants reveals multiple roles for Msx genes in limb development. *Development*. 132:3003-3014.

Lamb, T.M., A.K. Knecht, W.C. Smith, S.E. Stachel, A.N. Economides, N. Stahl, G.D. Yancopolous, and R.M. Harland. 1993. Neural induction by the secreted polypeptide noggin. *Science*. 262:713-718.

Laufer, E., C.E. Nelson, R.L. Johnson, B.A. Morgan, and C. Tabin. 1994. Sonic hedgehog and Fgf-4 act through a signaling cascade and feedback loop to integrate growth and patterning of the developing limb bud. *Cell*. 79:993-1003.

Lechleider, R.J., J.L. Ryan, L. Garrett, C. Eng, C. Deng, A. Wynshaw-Boris, and A.B. Roberts. 2001. Targeted mutagenesis of Smad1 reveals an essential role in chorioallantoic fusion. *Dev Biol*. 240:157-167.

Lefebvre, V., R.R. Behringer, and B. de Crombrugghe. 2001. L-Sox5, Sox6 and Sox9 control essential steps of the chondrocyte differentiation pathway. *Osteoarthritis and cartilage / OARS, Osteoarthritis Research Society*. 9 Suppl A:S69-75.

Lehmann, K., P. Seemann, J. Boergermann, G. Morin, S. Reif, P. Knaus, and S. Mundlos. 2006. A novel R486Q mutation in BMPR1B resulting in either a brachydactyly type C/symphalangism-like phenotype or brachydactyly type A2. *European journal of human genetics : EJHG*. 14:1248-1254.

Lehmann, K., P. Seemann, F. Silan, T.O. Goecke, S. Irgang, K.W. Kjaer, S. Kjaergaard, M.J. Mahoney, S. Morlot, C. Reissner, B. Kerr, A.O. Wilkie, and S. Mundlos. 2007. A new subtype of brachydactyly type B caused by point mutations in the bone morphogenetic protein antagonist NOGGIN. *American journal of human genetics*. 81:388-396.

Leonard, C.M., H.M. Fuld, D.A. Frenz, S.A. Downie, J. Massague, and S.A. Newman. 1991. Role of transforming growth factor-beta in chondrogenic pattern formation in the embryonic limb: stimulation of mesenchymal condensation and fibronectin gene expression by exogenenous TGF-beta and evidence for endogenous TGF-beta-like activity. *Developmental biology*. 145:99-109.

Lettice, L.A., S.J. Heaney, L.A. Purdie, L. Li, P. de Beer, B.A. Oostra, D. Goode, G. Elgar, R.E. Hill, and E. de Graaff. 2003. A long-range Shh enhancer regulates expression in the developing limb and fin and is associated with preaxial polydactyly. *Human molecular genetics*. 12:1725-1735.

Lewandoski, M., X. Sun, and G.R. Martin. 2000. Fgf8 signalling from the AER is essential for normal limb development. *Nat Genet*. 26:460-463.

Li, Y., H. Zhang, Y. Litingtung, and C. Chiang. 2006. Cholesterol modification restricts the spread of Shh gradient in the limb bud. *Proc Natl Acad Sci U S A*. 103:6548-6553.

Lingbeck, J.M., J.S. Trausch-Azar, A. Ciechanover, and A.L. Schwartz. 2008. In vivo interactions of MyoD, Id1, and E2A proteins determined by acceptor photobleaching fluorescence resonance energy transfer. *FASEB journal : official publication of the Federation of American Societies for Experimental Biology*. 22:1694-1701.

Liu, F., C. Pouponnot, and J. Massague. 1997. Dual role of the Smad4/DPC4 tumor suppressor in TGFbeta-inducible transcriptional complexes. *Genes Dev*. 11:3157-3167.

Liu, W., J. Selever, D. Wang, M.F. Lu, K.A. Moses, R.J. Schwartz, and J.F. Martin. 2004. Bmp4 signaling is required for outflow-tract septation and branchial-arch artery remodeling. *Proceedings of the National Academy of Sciences of the United States of America*. 101:4489-4494.

Logan, M., J.F. Martin, A. Nagy, C. Lobe, E.N. Olson, and C.J. Tabin. 2002. Expression of Cre Recombinase in the developing mouse limb bud driven by a Prxl enhancer. *Genesis (New York, N.Y.: 2000)*. 33:77-80.

Long, F., and D.M. Ornitz. 2013. Development of the endochondral skeleton. *Cold Spring Harbor perspectives in biology*. 5:a008334.

Loomis, C.A., R.A. Kimmel, C.X. Tong, J. Michaud, and A.L. Joyner. 1998. Analysis of the genetic pathway leading to formation of ectopic apical ectodermal ridges in mouse Engrailed-1 mutant limbs. *Development*. 125:1137-1148.

Lopez-Rios, J., D. Speziale, D. Robay, M. Scotti, M. Osterwalder, G. Nusspaumer, A. Galli, G.A. Hollander, M. Kmita, and R. Zeller. 2012. GLI3 constrains digit number by controlling both progenitor proliferation and BMP-dependent exit to chondrogenesis. *Developmental cell*. 22:837-848.

Lopez-Rovira, T., E. Chalaux, J. Massague, J.L. Rosa, and F. Ventura. 2002. Direct binding of Smad1 and Smad4 to two distinct motifs mediates bone morphogenetic protein-specific transcriptional activation of Id1 gene. *J Biol Chem*. 277:3176-3185.

Lowe, L.A., S. Yamada, and M.R. Kuehn. 2000. HoxB6-Cre transgenic mice express Cre recombinase in extra-embryonic mesoderm, in lateral plate and limb mesoderm

and at the midbrain/hindbrain junction. *Genesis (New York, N.Y.: 2000)*. 26:118-120.
Luo, G., C. Hofmann, A.L. Bronckers, M. Sohocki, A. Bradley, and G. Karsenty. 1995. BMP-7 is an inducer of nephrogenesis, and is also required for eye development and skeletal patterning. *Genes Dev*. 9:2808-2820.
Lyden, D., A.Z. Young, D. Zagzag, W. Yan, W. Gerald, R. O'Reilly, B.L. Bader, R.O. Hynes, Y. Zhuang, K. Manova, and R. Benezra. 1999. Id1 and Id3 are required for neurogenesis, angiogenesis and vascularization of tumour xenografts. *Nature*. 401:670-677.
Ma, L., and J.F. Martin. 2005. Generation of a Bmp2 conditional null allele. *Genesis (New York, N.Y.: 2000)*. 42:203-206.
Maatouk, D.M., K.S. Choi, C.M. Bouldin, and B.D. Harfe. 2009. In the limb AER Bmp2 and Bmp4 are required for dorsal-ventral patterning and interdigital cell death but not limb outgrowth. *Dev Biol*. 327:516-523.
Mariani, F.V., C.P. Ahn, and G.R. Martin. 2008. Genetic evidence that FGFs have an instructive role in limb proximal-distal patterning. *Nature*. 453:401-405.
Marom, B., E. Heining, P. Knaus, and Y.I. Henis. 2011. Formation of stable homomeric and transient heteromeric bone morphogenetic protein (BMP) receptor complexes regulates Smad protein signaling. *The Journal of biological chemistry*. 286:19287-19296.
Massague, J., J. Seoane, and D. Wotton. 2005. Smad transcription factors. *Genes Dev*. 19:2783-2810.
Matzuk, M.M., T.R. Kumar, and A. Bradley. 1995. Different phenotypes for mice deficient in either activins or activin receptor type II. *Nature*. 374:356-360.
Medio, M., E. Yeh, A. Popelut, S. Babajko, A. Berdal, and J.A. Helms. 2012. Wnt/beta-catenin signaling and Msx1 promote outgrowth of the maxillary prominences. *Frontiers in physiology*. 3:375.
Menezes, M.E., A. Mitra, L.A. Shevde, and R.S. Samant. 2012. DNAJB6 governs a novel regulatory loop determining Wnt/beta-catenin signalling activity. *The Biochemical journal*. 444:573-580.
Mercader, N., E. Leonardo, M.E. Piedra, A.C. Martinez, M.A. Ros, and M. Torres. 2000. Opposing RA and FGF signals control proximodistal vertebrate limb development through regulation of Meis genes. *Development*. 127:3961-3970.
Michos, O., L. Panman, K. Vintersten, K. Beier, R. Zeller, and A. Zuniga. 2004. Gremlin-mediated BMP antagonism induces the epithelial-mesenchymal feedback signaling controlling metanephric kidney and limb organogenesis. *Development (Cambridge, England)*. 131:3401-3410.
Min, H., D.M. Danilenko, S.A. Scully, B. Bolon, B.D. Ring, J.E. Tarpley, M. DeRose, and W.S. Simonet. 1998. Fgf-10 is required for both limb and lung development and exhibits striking functional similarity to Drosophila branchless. *Genes Dev*. 12:3156-3161.
Miyazono, K., Y. Kamiya, and M. Morikawa. 2010. Bone morphogenetic protein receptors and signal transduction. *Journal of Biochemistry*. 147:35-51.
Modarresi, R., T. Lafond, J.A. Roman-Blas, K.G. Danielson, R.S. Tuan, and M.R. Seghatoleslami. 2005. N-cadherin mediated distribution of beta-catenin alters MAP kinase and BMP-2 signaling on chondrogenesis-related gene expression. *Journal of cellular biochemistry*. 95:53-63.
Molven, A., C.V. Wright, R. Bremiller, E.M. De Robertis, and C.B. Kimmel. 1990. Expression of a homeobox gene product in normal and mutant zebrafish embryos: evolution of the tetrapod body plan. *Development*. 109:279-288.
Monteiro, R.M., S.M. de Sousa Lopes, M. Bialecka, S. de Boer, A. Zwijsen, and C.L. Mummery. 2008. Real time monitoring of BMP Smads transcriptional activity during mouse development. *Genesis*. 46:335-346.

Montero, J.A., Y. Ganan, D. Macias, J. Rodriguez-Leon, J.J. Sanz-Ezquerro, R. Merino, J. Chimal-Monroy, M.A. Nieto, and J.M. Hurle. 2001. Role of FGFs in the control of programmed cell death during limb development. *Development*. 128:2075-2084.
Montero, J.A., V. Zuzarte-Luis, V. Garcia-Martinez, and J.M. Hurle. 2007. Role of RhoC in digit morphogenesis during limb development. *Developmental biology*. 303:325-335.
Moon, A.M., and M.R. Capecchi. 2000. Fgf8 is required for outgrowth and patterning of the limbs. *Nat Genet*. 26:455-459.
Morgan, J.M., A. Wong, C.E. Yellowley, and D.C. Genetos. 2011. Regulation of tenascin expression in bone. *Journal of cellular biochemistry*. 112:3354-3363.
Morikawa, M., D. Koinuma, S. Tsutsumi, E. Vasilaki, Y. Kanki, C.H. Heldin, H. Aburatani, and K. Miyazono. 2011. ChIP-seq reveals cell type-specific binding patterns of BMP-specific Smads and a novel binding motif. *Nucleic acids research*. 39:8712-8727.
Mueller, T.D., and J. Nickel. 2012. Promiscuity and specificity in BMP receptor activation. *FEBS Lett*. 586:1846-1859.
Murakami, M., H. Kawachi, K. Ogawa, Y. Nishino, and M. Funaba. 2009. Receptor expression modulates the specificity of transforming growth factor-beta signaling pathways. *Genes to cells : devoted to molecular & cellular mechanisms*. 14:469-482.
Murakami, S., M. Kan, W.L. McKeehan, and B. de Crombrugghe. 2000. Up-regulation of the chondrogenic Sox9 gene by fibroblast growth factors is mediated by the mitogen-activated protein kinase pathway. *Proc Natl Acad Sci U S A*. 97:1113-1118.
Nagai, T., K. Ibata, E.S. Park, M. Kubota, K. Mikoshiba, and A. Miyawaki. 2002. A variant of yellow fluorescent protein with fast and efficient maturation for cell-biological applications. *Nature biotechnology*. 20:87-90.
Nagy, A., J. Rossant, R. Nagy, W. Abramow-Newerly, and J.C. Roder. 1993. Derivation of completely cell culture-derived mice from early-passage embryonic stem cells. *Proceedings of the National Academy of Sciences of the United States of America*. 90:8424-8428.
Nakashima, K., T. Takizawa, W. Ochiai, M. Yanagisawa, T. Hisatsune, M. Nakafuku, K. Miyazono, T. Kishimoto, R. Kageyama, and T. Taga. 2001. BMP2-mediated alteration in the developmental pathway of fetal mouse brain cells from neurogenesis to astrocytogenesis. *Proc Natl Acad Sci U S A*. 98:5868-5873.
Nam, H.S., and R. Benezra. 2009. High levels of Id1 expression define B1 type adult neural stem cells. *Cell stem cell*. 5:515-526.
Newman, S.A., and R. Bhat. 2007. Activator-inhibitor dynamics of vertebrate limb pattern formation. *Birth defects research. Part C, Embryo today : reviews*. 81:305-319.
Niederreither, K., V. Subbarayan, P. Dolle, and P. Chambon. 1999. Embryonic retinoic acid synthesis is essential for early mouse post-implantation development. *Nat Genet*. 21:444-448.
Niederreither, K., J. Vermot, B. Schuhbaur, P. Chambon, and P. Dolle. 2002. Embryonic retinoic acid synthesis is required for forelimb growth and anteroposterior patterning in the mouse. *Development*. 129:3563-3574.
Nissim, S., P. Allard, A. Bandyopadhyay, B.D. Harfe, and C.J. Tabin. 2007. Characterization of a novel ectodermal signaling center regulating Tbx2 and Shh in the vertebrate limb. *Dev Biol*. 304:9-21.
Nissim, S., S.M. Hasso, J.F. Fallon, and C.J. Tabin. 2006. Regulation of Gremlin expression in the posterior limb bud. *Dev Biol*. 299:12-21.
Niswander, L., C. Tickle, A. Vogel, I. Booth, and G.R. Martin. 1993. FGF-4 replaces the apical ectodermal ridge and directs outgrowth and patterning of the limb. *Cell*. 75:579-587.
Oberg, K.C. 2013. Review of the Molecular Development of the Thumb: Digit Primera. *Clinical orthopaedics and related research*.
Ogata, T., J.M. Wozney, R. Benezra, and M. Noda. 1993. Bone morphogenetic protein 2 transiently enhances expression of a gene, Id (inhibitor of differentiation),

encoding a helix-loop-helix molecule in osteoblast-like cells. *Proc Natl Acad Sci U S A*. 90:9219-9222.
Oh, S.P., and E. Li. 1997. The signaling pathway mediated by the type IIB activin receptor controls axial patterning and lateral asymmetry in the mouse. *Genes Dev*. 11:1812-1826.
Ohuchi, H., T. Nakagawa, A. Yamamoto, A. Araga, T. Ohata, Y. Ishimaru, H. Yoshioka, T. Kuwana, T. Nohno, M. Yamasaki, N. Itoh, and S. Noji. 1997. The mesenchymal factor, FGF10, initiates and maintains the outgrowth of the chick limb bud through interaction with FGF8, an apical ectodermal factor. *Development*. 124:2235-2244.
Ohuchi, H., T. Nakagawa, M. Yamauchi, T. Ohata, H. Yoshioka, T. Kuwana, T. Mima, T. Mikawa, T. Nohno, and S. Noji. 1995. An additional limb can be induced from the flank of the chick embryo by FGF4. *Biochem Biophys Res Commun*. 209:809-816.
Osterwalder, M., A. Galli, B. Rosen, W.C. Skarnes, R. Zeller, and J. Lopez-Rios. 2010. Dual RMCE for efficient re-engineering of mouse mutant alleles. *Nature methods*. 7:893-895.
Ouyang, M., S. Lu, T. Kim, C.E. Chen, J. Seong, D.E. Leckband, F. Wang, A.B. Reynolds, M.A. Schwartz, and Y. Wang. 2013. N-cadherin regulates spatially polarized signals through distinct p120ctn and beta-catenin-dependent signalling pathways. *Nature communications*. 4:1589.
Ovchinnikov, D.A., J. Selever, Y. Wang, Y.T. Chen, Y. Mishina, J.F. Martin, and R.R. Behringer. 2006. BMP receptor type IA in limb bud mesenchyme regulates distal outgrowth and patterning. *Dev Biol*. 295:103-115.
Pajni-Underwood, S., C.P. Wilson, C. Elder, Y. Mishina, and M. Lewandoski. 2007. BMP signals control limb bud interdigital programmed cell death by regulating FGF signaling. *Development*. 134:2359-2368.
Pan, Q., Y. Yu, Q. Chen, C. Li, H. Wu, Y. Wan, J. Ma, and F. Sun. 2008. Sox9, a key transcription factor of bone morphogenetic protein-2-induced chondrogenesis, is activated through BMP pathway and a CCAAT box in the proximal promoter. *Journal of cellular physiology*. 217:228-241.
Panman, L., A. Galli, N. Lagarde, O. Michos, G. Soete, A. Zuniga, and R. Zeller. 2006. Differential regulation of gene expression in the digit forming area of the mouse limb bud by SHH and gremlin 1/FGF-mediated epithelial-mesenchymal signalling. *Development (Cambridge, England)*. 133:3419-3428.
Parr, B.A., and A.P. McMahon. 1995. Dorsalizing signal Wnt-7a required for normal polarity of D-V and A-P axes of mouse limb. *Nature*. 374:350-353.
Pearse, R.V., 2nd, P.J. Scherz, J.K. Campbell, and C.J. Tabin. 2007. A cellular lineage analysis of the chick limb bud. *Dev Biol*. 310:388-400.
Perry, M.J., K.E. McDougall, S.C. Hou, and J.H. Tobias. 2008. Impaired growth plate function in bmp-6 null mice. *Bone*. 42:216-225.
Pizette, S., and L. Niswander. 1999. BMPs negatively regulate structure and function of the limb apical ectodermal ridge. *Development*. 126:883-894.
Pizette, S., and L. Niswander. 2000. BMPs are required at two steps of limb chondrogenesis: formation of prechondrogenic condensations and their differentiation into chondrocytes. *Developmental biology*. 219:237-249.
Pizette, S., and L. Niswander. 2001. Early steps in limb patterning and chondrogenesis. *Novartis Foundation symposium*. 232:23-36; discussion 36-46.
Ploger, F., P. Seemann, M. Schmidt-von Kegler, K. Lehmann, J. Seidel, K.W. Kjaer, J. Pohl, and S. Mundlos. 2008. Brachydactyly type A2 associated with a defect in proGDF5 processing. *Human molecular genetics*. 17:1222-1233.
Probst, S., C. Kraemer, P. Demougin, R. Sheth, G.R. Martin, H. Shiratori, H. Hamada, D. Iber, R. Zeller, and A. Zuniga. 2011. SHH propagates distal limb bud development by enhancing CYP26B1-mediated retinoic acid clearance via AER-FGF signalling. *Development*. 138:1913-1923.

Probst, S., R. Zeller, and A. Zuniga. 2013. The hedgehog target Vlk genetically interacts with Gli3 to regulate chondrocyte differentiation during mouse long bone development. *Differentiation; research in biological diversity*. 85:121-130.
Pryce, B.A., S.S. Watson, N.D. Murchison, J.A. Staverosky, N. Dunker, and R. Schweitzer. 2009. Recruitment and maintenance of tendon progenitors by TGFbeta signaling are essential for tendon formation. *Development*. 136:1351-1361.
Retting, K.N., B. Song, B.S. Yoon, and K.M. Lyons. 2009. BMP canonical Smad signaling through Smad1 and Smad5 is required for endochondral bone formation. *Development*. 136:1093-1104.
Riddle, R.D., R.L. Johnson, E. Laufer, and C. Tabin. 1993. Sonic hedgehog mediates the polarizing activity of the ZPA. *Cell*. 75:1401-1416.
Roark, E.F., and K. Greer. 1994. Transforming growth factor-beta and bone morphogenetic protein-2 act by distinct mechanisms to promote chick limb cartilage differentiation in vitro. *Developmental dynamics : an official publication of the American Association of Anatomists*. 200:103-116.
Rock, R., A.C. Heinrich, N. Schumacher, and M. Gessler. 2005. Fjx1: a notch-inducible secreted ligand with specific binding sites in developing mouse embryos and adult brain. *Developmental dynamics : an official publication of the American Association of Anatomists*. 234:602-612.
Ros, M.A., A. Lopez-Martinez, B.K. Simandl, C. Rodriguez, J.C. Izpisua Belmonte, R. Dahn, and J.F. Fallon. 1996. The limb field mesoderm determines initial limb bud anteroposterior asymmetry and budding independent of sonic hedgehog or apical ectodermal gene expressions. *Development*. 122:2319-2330.
Rosello-Diez, A., and M. Torres. 2011. Regulative patterning in limb bud transplants is induced by distalizing activity of apical ectodermal ridge signals on host limb cells. *Dev Dyn*. 240:1203-1211.
Rowe, D.A., and J.F. Fallon. 1982. The proximodistal determination of skeletal parts in the developing chick leg. *Journal of embryology and experimental morphology*. 68:1-7.
Rudnicki, J.A., and A.M. Brown. 1997. Inhibition of chondrogenesis by Wnt gene expression in vivo and in vitro. *Dev Biol*. 185:104-118.
Sagai, T., M. Hosoya, Y. Mizushina, M. Tamura, and T. Shiroishi. 2005. Elimination of a long-range cis-regulatory module causes complete loss of limb-specific Shh expression and truncation of the mouse limb. *Development*. 132:797-803.
Saito, D., S. Yonei-Tamura, K. Kano, H. Ide, and K. Tamura. 2002. Specification and determination of limb identity: evidence for inhibitory regulation of Tbx gene expression. *Development*. 129:211-220.
Sanchez-Adams, J., and K.A. Athanasiou. 2012. Dermis isolated adult stem cells for cartilage tissue engineering. *Biomaterials*. 33:109-119.
Sanford, L.P., I. Ormsby, A.C. Gittenberger-de Groot, H. Sariola, R. Friedman, G.P. Boivin, E.L. Cardell, and T. Doetschman. 1997. TGFbeta2 knockout mice have multiple developmental defects that are non-overlapping with other TGFbeta knockout phenotypes. *Development*. 124:2659-2670.
Sato, K., Y. Koizumi, M. Takahashi, A. Kuroiwa, and K. Tamura. 2007. Specification of cell fate along the proximal-distal axis in the developing chick limb bud. *Development*. 134:1397-1406.
Satokata, I., L. Ma, H. Ohshima, M. Bei, I. Woo, K. Nishizawa, T. Maeda, Y. Takano, M. Uchiyama, S. Heaney, H. Peters, Z. Tang, R. Maxson, and R. Maas. 2000. Msx2 deficiency in mice causes pleiotropic defects in bone growth and ectodermal organ formation. *Nat Genet*. 24:391-395.
Satokata, I., and R. Maas. 1994. Msx1 deficient mice exhibit cleft palate and abnormalities of craniofacial and tooth development. *Nat Genet*. 6:348-356.
Saunders, J.W., Jr. 1948. The proximo-distal sequence of origin of the parts of the chick wing and the role of the ectoderm. *The Journal of experimental zoology*. 108:363-403.

Saunders, J.W., Jr.; Gasseling MT. 1968. Ectoderm–mesenchymal interaction in the origins of wing symmetry. In Epithelial–mesenchymal interactions (ed. R. Fleisch- majer, R.E. Billingham), 78 – 97. Williams Wilkins, Baltimore.

Scherz, P.J., E. McGlinn, S. Nissim, and C.J. Tabin. 2007. Extended exposure to Sonic hedgehog is required for patterning the posterior digits of the vertebrate limb. *Dev Biol*. 308:343-354.

Schlake, T., and J. Bode. 1994. Use of mutated FLP recognition target (FRT) sites for the exchange of expression cassettes at defined chromosomal loci. *Biochemistry*. 33:12746-12751.

Schweitzer, R., J.H. Chyung, L.C. Murtaugh, A.E. Brent, V. Rosen, E.N. Olson, A. Lassar, and C.J. Tabin. 2001. Analysis of the tendon cell fate using Scleraxis, a specific marker for tendons and ligaments. *Development (Cambridge, England)*. 128:3855-3866.

Schwenk, F., U. Baron, and K. Rajewsky. 1995. A cre-transgenic mouse strain for the ubiquitous deletion of loxP-flanked gene segments including deletion in germ cells. *Nucleic acids research*. 23:5080-5081.

Scotti, M., and M. Kmita. 2012. Recruitment of 5' Hoxa genes in the allantois is essential for proper extra-embryonic function in placental mammals. *Development (Cambridge, England)*. 139:731-739.

Sekiya, I., K. Tsuji, P. Koopman, H. Watanabe, Y. Yamada, K. Shinomiya, A. Nifuji, and M. Noda. 2000. SOX9 enhances aggrecan gene promoter/enhancer activity and is up-regulated by retinoic acid in a cartilage-derived cell line, TC6. *J Biol Chem*. 275:10738-10744.

Selever, J., W. Liu, M.F. Lu, R.R. Behringer, and J.F. Martin. 2004. Bmp4 in limb bud mesoderm regulates digit pattern by controlling AER development. *Developmental biology*. 276:268-279.

Sharpe, J., U. Ahlgren, P. Perry, B. Hill, A. Ross, J. Hecksher-Sorensen, R. Baldock, and D. Davidson. 2002. Optical projection tomography as a tool for 3D microscopy and gene expression studies. *Science (New York, N.Y.)*. 296:541-545.

Sheth, R., L. Marcon, M.F. Bastida, M. Junco, L. Quintana, R. Dahn, M. Kmita, J. Sharpe, and M.A. Ros. 2012. Hox genes regulate digit patterning by controlling the wavelength of a Turing-type mechanism. *Science*. 338:1476-1480.

Shi, Y., Y.F. Wang, L. Jayaraman, H. Yang, J. Massague, and N.P. Pavletich. 1998. Crystal structure of a Smad MH1 domain bound to DNA: insights on DNA binding in TGF-beta signaling. *Cell*. 94:585-594.

Shu, B., M. Zhang, R. Xie, M. Wang, H. Jin, W. Hou, D. Tang, S.E. Harris, Y. Mishina, R.J. O'Keefe, M.J. Hilton, Y. Wang, and D. Chen. 2011. BMP2, but not BMP4, is crucial for chondrocyte proliferation and maturation during endochondral bone development. *Journal of cell science*. 124:3428-3440.

Solursh, M. 1984. Ectoderm as a determinant of early tissue pattern in the limb bud. *Cell differentiation*. 15:17-24.

Spagnoli, A., L. O'Rear, R.L. Chandler, F. Granero-Molto, D.P. Mortlock, A.E. Gorska, J.A. Weis, L. Longobardi, A. Chytil, K. Shimer, and H.L. Moses. 2007. TGF-beta signaling is essential for joint morphogenesis. *The Journal of cell biology*. 177:1105-1117.

Spitz, F., F. Gonzalez, and D. Duboule. 2003. A global control region defines a chromosomal regulatory landscape containing the HoxD cluster. *Cell*. 113:405-417.

Spitz, F., C. Herkenne, M.A. Morris, and D. Duboule. 2005. Inversion-induced disruption of the Hoxd cluster leads to the partition of regulatory landscapes. *Nat Genet*. 37:889-893.

St-Jacques, B., H.R. Dassule, I. Karavanova, V.A. Botchkarev, J. Li, P.S. Danielian, J.A. McMahon, P.M. Lewis, R. Paus, and A.P. McMahon. 1998. Sonic hedgehog signaling is essential for hair development. *Current biology : CB*. 8:1058-1068.

Storm, E.E., and D.M. Kingsley. 1999. GDF5 coordinates bone and joint formation during digit development. *Dev Biol*. 209:11-27.

Sugimoto, Y., A. Takimoto, H. Akiyama, R. Kist, G. Scherer, T. Nakamura, Y. Hiraki, and C. Shukunami. 2013. Scx+/Sox9+ progenitors contribute to the establishment of the junction between cartilage and tendon/ligament. *Development*. 140:2280-2288.
Summerbell, D., and J.H. Lewis. 1975. Time, place and positional value in the chick limb-bud. *Journal of embryology and experimental morphology*. 33:621-643.
Sun, X., M. Lewandoski, E.N. Meyers, Y.H. Liu, R.E. Maxson, Jr., and G.R. Martin. 2000. Conditional inactivation of Fgf4 reveals complexity of signalling during limb bud development. *Nat Genet*. 25:83-86.
Sun, X., F.V. Mariani, and G.R. Martin. 2002. Functions of FGF signalling from the apical ectodermal ridge in limb development. *Nature*. 418:501-508.
Suzuki, T., S.M. Hasso, and J.F. Fallon. 2008. Unique SMAD1/5/8 activity at the phalanx-forming region determines digit identity. *Proc Natl Acad Sci U S A*. 105:4185-4190.
Suzuki, T., J. Takeuchi, K. Koshiba-Takeuchi, and T. Ogura. 2004. Tbx Genes Specify Posterior Digit Identity through Shh and BMP Signaling. *Developmental cell*. 6:43-53.
Tabin, C., and L. Wolpert. 2007. Rethinking the proximodistal axis of the vertebrate limb in the molecular era. *Genes Dev*. 21:1433-1442.
Tanaka, M., A.K. Hadjantonakis, K. Vintersten, and A. Nagy. 2009. Aggregation chimeras: combining ES cells, diploid, and tetraploid embryos. *Methods in molecular biology (Clifton, N.J.)*. 530:287-309.
Tanaka, M., K. Tamura, S. Noji, T. Nohno, and H. Ide. 1997. Induction of additional limb at the dorsal-ventral boundary of a chick embryo. *Dev Biol*. 182:191-203.
Tarchini, B., D. Duboule, and M. Kmita. 2006. Regulatory constraints in the evolution of the tetrapod limb anterior-posterior polarity. *Nature*. 443:985-988.
Tchorz, J.S., T. Suply, I. Ksiazek, C. Giachino, D. Cloetta, C.P. Danzer, T. Doll, A. Isken, M. Lemaistre, V. Taylor, B. Bettler, B. Kinzel, and M. Mueller. 2012. A modified RMCE-compatible Rosa26 locus for the expression of transgenes from exogenous promoters. *PloS one*. 7:e30011.
te Welscher, P., M. Fernandez-Teran, M.A. Ros, and R. Zeller. 2002. Mutual genetic antagonism involving GLI3 and dHAND prepatterns the vertebrate limb bud mesenchyme prior to SHH signaling. *Genes Dev*. 16:421-426.
ten Berge, D., S.A. Brugmann, J.A. Helms, and R. Nusse. 2008. Wnt and FGF signals interact to coordinate growth with cell fate specification during limb development. *Development (Cambridge, England)*. 135:3247-3257.
Tsanov, K.M., Y. Nishi, K.A. Peterson, J. Liu, M. Baetscher, and A.P. McMahon. 2012. An embryonic stem cell-based system for rapid analysis of transcriptional enhancers. *Genesis*. 50:443-450.
Turan, S., M. Galla, E. Ernst, J. Qiao, C. Voelkel, B. Schiedlmeier, C. Zehe, and J. Bode. 2011. Recombinase-mediated cassette exchange (RMCE): traditional concepts and current challenges. *Journal of molecular biology*. 407:193-221.
Turan, S., C. Zehe, J. Kuehle, J. Qiao, and J. Bode. 2013. Recombinase-mediated cassette exchange (RMCE) - a rapidly-expanding toolbox for targeted genomic modifications. *Gene*. 515:1-27.
Urist, M.R. 1965. Bone: formation by autoinduction. *Science (New York, N.Y.)*. 150:893-899.
Vargesson, N., and E. Laufer. 2009. Negative Smad expression and regulation in the developing chick limb. *PloS one*. 4:e5173.
Verheyden, J.M., and X. Sun. 2008. An Fgf/Gremlin inhibitory feedback loop triggers termination of limb bud outgrowth. *Nature*. 454:638-641.
Vintersten, K., C. Monetti, M. Gertsenstein, P. Zhang, L. Laszlo, S. Biechele, and A. Nagy. 2004. Mouse in red: red fluorescent protein expression in mouse ES cells, embryos, and adult animals. *Genesis (New York, N.Y.: 2000)*. 40:241-246.

Walsh, D.W., C. Godson, D.P. Brazil, and F. Martin. 2010. Extracellular BMP-antagonist regulation in development and disease: tied up in knots. *Trends in cell biology*. 20:244-256.
Wang, C.K., M. Omi, D. Ferrari, H.C. Cheng, G. Lizarraga, H.J. Chin, W.B. Upholt, C.N. Dealy, and R.A. Kosher. 2004. Function of BMPs in the apical ectoderm of the developing mouse limb. *Developmental biology*. 269:109-122.
Wellik, D.M., and M.R. Capecchi. 2003. Hox10 and Hox11 genes are required to globally pattern the mammalian skeleton. *Science*. 301:363-367.
Wilkinson, D.G. 1992. The Use of in Situ Hybridisation to Study the Molecular Genetics of Mouse Development. *Development*. The Molecular Genetic Approach, Section 3:pp 409-419.
Wisotzkey, R.G., A. Mehra, D.J. Sutherland, L.L. Dobens, X. Liu, C. Dohrmann, L. Attisano, and L.A. Raftery. 1998. Medea is a Drosophila Smad4 homolog that is differentially required to potentiate DPP responses. *Development*. 125:1433-1445.
Witte, F., D. Chan, A.N. Economides, S. Mundlos, and S. Stricker. 2010. Receptor tyrosine kinase-like orphan receptor 2 (ROR2) and Indian hedgehog regulate digit outgrowth mediated by the phalanx-forming region. *Proc Natl Acad Sci U S A*. 107:14211-14216.
Woltering, J.M., and D. Duboule. 2010. The origin of digits: expression patterns versus regulatory mechanisms. *Developmental cell*. 18:526-532.
Wong, Y.L., R.R. Behringer, and K.M. Kwan. 2012. Smad1/Smad5 signaling in limb ectoderm functions redundantly and is required for interdigital programmed cell death. *Dev Biol*. 363:247-257.
Wood, S.A., N.D. Allen, J. Rossant, A. Auerbach, and A. Nagy. 1993a. Non-injection methods for the production of embryonic stem cell-embryo chimaeras. *Nature*. 365:87-89.
Wood, S.A., W.S. Pascoe, C. Schmidt, R. Kemler, M.J. Evans, and N.D. Allen. 1993b. Simple and efficient production of embryonic stem cell-embryo chimeras by coculture. *Proc Natl Acad Sci U S A*. 90:4582-4585.
Wright, E., M.R. Hargrave, J. Christiansen, L. Cooper, J. Kun, T. Evans, U. Gangadharan, A. Greenfield, and P. Koopman. 1995. The Sry-related gene Sox9 is expressed during chondrogenesis in mouse embryos. *Nat Genet*. 9:15-20.
Yang, X., L.H. Castilla, X. Xu, C. Li, J. Gotay, M. Weinstein, P.P. Liu, and C.X. Deng. 1999. Angiogenesis defects and mesenchymal apoptosis in mice lacking SMAD5. *Development*. 126:1571-1580.
Yang, X., C. Li, P.L. Herrera, and C.X. Deng. 2002. Generation of Smad4/Dpc4 conditional knockout mice. *Genesis (New York, N.Y.: 2000)*. 32:80-81.
Yang, X., C. Li, X. Xu, and C. Deng. 1998a. The tumor suppressor SMAD4/DPC4 is essential for epiblast proliferation and mesoderm induction in mice. *Proceedings of the National Academy of Sciences of the United States of America*. 95:3667-3672.
Yang, Y., P. Guillot, Y. Boyd, M.F. Lyon, and A.P. McMahon. 1998b. Evidence that preaxial polydactyly in the Doublefoot mutant is due to ectopic Indian Hedgehog signaling. *Development*. 125:3123-3132.
Yashiro, K., X. Zhao, M. Uehara, K. Yamashita, M. Nishijima, J. Nishino, Y. Saijoh, Y. Sakai, and H. Hamada. 2004. Regulation of retinoic acid distribution is required for proximodistal patterning and outgrowth of the developing mouse limb. *Dev Cell*. 6:411-422.
Yi, S.E., A. Daluiski, R. Pederson, V. Rosen, and K.M. Lyons. 2000. The type I BMP receptor BMPRIB is required for chondrogenesis in the mouse limb. *Development*. 127:621-630.
Ying, Q.L., J. Nichols, I. Chambers, and A. Smith. 2003. BMP induction of Id proteins suppresses differentiation and sustains embryonic stem cell self-renewal in collaboration with STAT3. *Cell*. 115:281-292.

Yoon, B.S., D.A. Ovchinnikov, I. Yoshii, Y. Mishina, R.R. Behringer, and K.M. Lyons. 2005. Bmpr1a and Bmpr1b have overlapping functions and are essential for chondrogenesis in vivo. *Proc Natl Acad Sci U S A*. 102:5062-5067.

Yoon, B.S., R. Pogue, D.A. Ovchinnikov, I. Yoshii, Y. Mishina, R.R. Behringer, and K.M. Lyons. 2006. BMPs regulate multiple aspects of growth-plate chondrogenesis through opposing actions on FGF pathways. *Development*. 133:4667-4678.

Yu, K., and D.M. Ornitz. 2008. FGF signaling regulates mesenchymal differentiation and skeletal patterning along the limb bud proximodistal axis. *Development*. 135:483-491.

Yu, K., J. Xu, Z. Liu, D. Sosic, J. Shao, E.N. Olson, D.A. Towler, and D.M. Ornitz. 2003. Conditional inactivation of FGF receptor 2 reveals an essential role for FGF signaling in the regulation of osteoblast function and bone growth. *Development*. 130:3063-3074.

Yvernogeau, L., G. Auda-Boucher, and J. Fontaine-Perus. 2012. Limb bud colonization by somite-derived angioblasts is a crucial step for myoblast emigration. *Development*. 139:277-287.

Zambrowicz, B.P., A. Imamoto, S. Fiering, L.A. Herzenberg, W.G. Kerr, and P. Soriano. 1997. Disruption of overlapping transcripts in the ROSA beta geo 26 gene trap strain leads to widespread expression of beta-galactosidase in mouse embryos and hematopoietic cells. *Proc Natl Acad Sci U S A*. 94:3789-3794.

Zeller, R., J. Lopez-Rios, and A. Zuniga. 2009. Vertebrate limb bud development: moving towards integrative analysis of organogenesis. *Nature reviews. Genetics*. 10:845-858.

Zeng, X., J.A. Goetz, L.M. Suber, W.J. Scott, Jr., C.M. Schreiner, and D.J. Robbins. 2001. A freely diffusible form of Sonic hedgehog mediates long-range signalling. *Nature*. 411:716-720.

Zhang, J., X. Tan, W. Li, Y. Wang, J. Wang, X. Cheng, and X. Yang. 2005. Smad4 is required for the normal organization of the cartilage growth plate. *Dev Biol*. 284:311-322.

Zhang, Y., C. Chang, D.J. Gehling, A. Hemmati-Brivanlou, and R. Derynck. 2001. Regulation of Smad degradation and activity by Smurf2, an E3 ubiquitin ligase. *Proceedings of the National Academy of Sciences of the United States of America*. 98:974-979.

Zhao, X., I.O. Sirbu, F.A. Mic, N. Molotkova, A. Molotkov, S. Kumar, and G. Duester. 2009. Retinoic acid promotes limb induction through effects on body axis extension but is unnecessary for limb patterning. *Current biology : CB*. 19:1050-1057.

Zhou, J., and D.M. Kochhar. 2004. Cellular anomalies underlying retinoid-induced phocomelia. *Reproductive toxicology*. 19:103-110.

Zhu, J., E. Nakamura, M.T. Nguyen, X. Bao, H. Akiyama, and S. Mackem. 2008. Uncoupling Sonic hedgehog control of pattern and expansion of the developing limb bud. *Developmental cell*. 14:624-632.

Zou, H., K.M. Choe, Y. Lu, J. Massague, and L. Niswander. 1997. BMP signaling and vertebrate limb development. *Cold Spring Harbor symposia on quantitative biology*. 62:269-272.

Zuniga, A., and R. Zeller. 1999. Gli3 (Xt) and formin (ld) participate in the positioning of the polarising region and control of posterior limb-bud identity. *Development*. 126:13-21.

Zuniga, A., R. Zeller, and S. Probst. 2012. The molecular basis of human congenital limb malformations. *Wiley interdisciplinary reviews. Developmental biology*. 1:803-822.

Zuzarte-Luis, V., J.A. Montero, N. Torre-Perez, J.A. Garcia-Porrero, and J.M. Hurle. 2007. Cathepsin D gene expression outlines the areas of physiological cell death during embryonic development. *Dev Dyn*. 236:880-885.

Zwilling, E. 1956. Interaction between limb bud ectoderm and mesoderm in the chick embryo. II. Experimental limb manipulation. *The Journal of experimental zoology*:173–188.

CURRICULUM VITAE

EMANUELE PIGNATTI
Florastrasse 26
4057 Basel
Switzerland
emanuele.pignatti@unibas.ch
Nationality: Italian

Current Position

PhD candidate in Developmental Genetics in the laboratory of Prof. Rolf Zeller, Basel, CH.

Qualifications

- Jan 2010 - Mar 2014, PhD, Developmental Genetics, laboratory of Prof. Dr. Rolf Zeller, University of Basel, Switzerland;
  Doctoral thesis title: 'Targeting canonical BMP signaling: SMAD4 in limb patterning and differentiation'.

- 2009 Sep-Nov, pre-doc internship, Proteomics, laboratory of Dr. Massimo Alessio, DIBIT2, Milan, Italy;

- 2004 - 2009, Master of Science, Immunology, laboratory of Prof. Dr. Angelo A. Manfredi, DIBIT, Milan, Italy.
  Master's thesis title: 'Cellular polarization rules iron metabolism in primary macrophages'.

- 2004 - 2007, Bachelor of Science, Neuroscience, laboratory of Prof. Dr. Flavia Valtorta, DIBIT, Milan, Italy;
  Bachelor's thesis title: 'The role of brain-derived neurotrophic factor in synaptogenesis'.

- 1999 - 2004, Italian high school diploma of classical studies, final mark 100/100 *magna cum laude*.

Conference talks

- 2nd European Congress of Immunology, Berlin, Germany 2009;
Iron disposal by inflammatory and alternatively activated macrophages.

- Mouse Molecular Genetics, Wellcome Trust Conference Centre, Hinxton (CA), UK 2011;
Smad4-mediated BMP Signal Transduction is Key to Maintaining Digit Cell Fate.

Abstracts and Posters

MAKING MUSCLE IN THE EMBRYO AND ADULT
Columbia University, New York, NY
28 May-2 June 2009;
From macrophage polarization to mesoangioblast stem cells differentiation: changing microenviroment strongly modifies myotube formation.

Basel Computational Biology Conference, Basel, CH, June 2011;
The role of Smad4 in initiating chondrogenesis and determination of digits in mouse limb buds.

Publications

Corna, G., L. Campana, **E. Pignatti**, A. Castiglioni, E. Tagliafico, L. Bosurgi, A. Campanella, S. Brunelli, A.A. Manfredi, P. Apostoli, L. Silvestri, C. Camaschella, and P. Rovere-Querini. 2010. Polarization dictates iron handling by inflammatory and alternatively activated macrophages. *Haematologica.* 95:1814-1822.

Benazet, J.D.*, **E. Pignatti***, A. Nugent, E. Unal, F. Laurent, and R. Zeller. 2012. Smad4 is required to induce digit ray primordia and to initiate the aggregation and differentiation of chondrogenic progenitors in mouse limb buds. *Development.* 139:4250-4260. **(*shared co-first authorship)**

E.Pignatti, R. Zeller, A. Zuniga. 2014. BMP signalling pathway in the limb bud development. *Review. Submitted to Seminars in cell and developmental biology.*

Technical skills

Cell culture, primary cell cultures and stem cells;

- Isolation of bone marrow precursors and culture of primary macrophages;
- Isolation and culture of mesenchymal pluripotent cells from embryonic limb buds;
- Maintenance of G4, R1 and V6.5 mouse ESC lines. Homologous recombination, RMCE and dual-RMCE ESC targeting and clones selection, expansion and analysis.

Mouse genetics:

- Maintenance of several mouse strains (conditional and delta alleles of *Smad4*, *Bmp4*, *Bmp2*, *Grem1*; *Prx1-Cre*, *Msx2-Cre*, *Hoxa13-Cre*, *Hoxb6-Cre* transgenes; allele crossing for generating up to triple transgenic animals).

Diploid and tetraploid complementation assay and embryo transfer;

- setting up of an in-house protocol for generation of chimeras for analysis of *cis*-regulatory sequences and/or establishment of stable mouse strains (this includes ESC maintenance, handling of vasectomized males and pseudopregnant females, embryo flushing and processing according to Nagy's protocol, embryo transfer into foster mothers).

Limb bud culture:

- *ex vivo* culture of embryonic limb buds and grafting of protein-coated beads.

Optical projection tomography (OPT):

- embedding, dehydration and clearance of embryonic tissues for OPT 3-D scanning.

Molecular cloning;

Whole-mount and section *in situ*;

Western and Southern blotting;
Immunocyto- and Immunohistochemistry;
FACS analysis;
Real-time quantitative PCR.

Awards

- October 2009, Winner of a position in the PhD Program in Cellular and Molecular Biology at San Raffaele Institute in Milan.

Certifications

LTK Module 1 : Introductory course in Laboratory Animal Science, *T&T FELASA board*, April 2010 – April 2014

Optical Projection Tomography (OPT) training course at MRC in Edinburgh, March 2011

Spoken languages

Italian: native
English: excellent
German: basic